



Contents lists available at ScienceDirect

European Journal of Medicinal Chemistry

journal homepage: <http://www.elsevier.com/locate/ejmech>

Research paper

Design, synthesis and biological evaluation of second-generation benzoylpiperidine derivatives as reversible monoacylglycerol lipase (MAGL) inhibitors



Carlotta Granchi ^a, Giulia Bononi ^a, Rebecca Ferrisi ^a, Eleonora Gori ^a, Giulia Mantini ^{g, h}, Sandra Glasmacher ^b, Giulio Poli ^a, Stefano Palazzolo ^c, Isabella Caligiuri ^c, Flavio Rizzolio ^{c, d}, Vincenzo Canzonieri ^{c, e}, Tiziana Perin ^c, Jürg Gertsch ^b, Andrea Sodi ^f, Elisa Giovannetti ^{g, h}, Marco Macchia ^a, Filippo Minutolo ^a, Tiziano Tuccinardi ^{a, *}, Andrea Chicca ^b

^a Department of Pharmacy, University of Pisa, Via Bonanno 6, 56126, Pisa, Italy^b Institute of Biochemistry and Molecular Medicine, NCCR TransCure, University of Bern, CH-3012, Bern, Switzerland^c Pathology Unit, Centro di Riferimento Oncologico di Aviano (CRO) IRCCS, 33081, Aviano, Italy^d Department of Molecular Sciences and Nanosystems, Ca' Foscari University, 30123, Venezia, Italy^e Department of Medical, Surgical and Health Sciences, Università Degli Studi di Trieste, Strada di Fiume 447, Trieste, Italy^f Department of Neurosciences, Psychology, Drug Research and Child Health Eye Clinic, University of Florence, AOU Careggi, 50139, Florence, Italy^g Department of Medical Oncology, VU University Medical Center, Cancer Center Amsterdam, DeBoelelaan 1117, 1081HV, Amsterdam, the Netherlands^h Cancer Pharmacology Lab, Fondazione Pisana per La Scienza, Via Giovannini 13, 56017, San Giuliano Terme, Pisa, Italy

ARTICLE INFO

Article history:

Received 31 August 2020

Received in revised form

16 September 2020

Accepted 17 September 2020

Keywords:

Monoacylglycerol lipase inhibitors

MAGL

Benzoylpiperidine derivatives

ABSTRACT

An interesting enzyme of the endocannabinoid system is monoacylglycerol lipase (MAGL). This enzyme, which metabolizes the endocannabinoid 2-arachidonoylglycerol (2-AG), has attracted great interest due to its involvement in several physiological and pathological processes, such as cancer progression. Experimental evidences highlighted some drawbacks associated with the use of irreversible MAGL inhibitors *in vivo*, therefore the research field concerning reversible inhibitors is rapidly growing. In the present manuscript, the class of benzoylpiperidine-based MAGL inhibitors was further expanded and optimized. Enzymatic assays identified some compounds in the low nanomolar range and steered molecular dynamics simulations predicted the dissociation itinerary of one of the best compounds from the enzyme, confirming the observed structure-activity relationship. Biological evaluation, including assays in intact U937 cells and competitive activity-based protein profiling experiments in mouse brain membranes, confirmed the selectivity of the selected compounds for MAGL versus other components of the endocannabinoid system. An antiproliferative ability in a panel of cancer cell lines highlighted their potential as potential anticancer agents. Future studies on the potential use of these compounds in the clinical setting are also supported by the inhibition of cell growth observed both in cancer organoids derived from high grade serous ovarian cancer patients and in pancreatic ductal adenocarcinoma primary cells, which showed genetic and histological features very similar to the primary tumors.

© 2020 Elsevier Masson SAS. All rights reserved.

Abbreviations: MAGL, monoacylglycerol lipase; GPCRs, G protein-coupled receptors; ECS, endocannabinoid system; eCBs, endocannabinoids; AEA, anandamide; 2-AG, 2-arachidonoylglycerol; FAAH, fatty acid amide hydrolase; ABHD6, α/β hydrolase-6; ABHD12, α/β hydrolase-12; MD, molecular dynamics; 2-OG, 2-oleoylglycerol; 4-NPA, 4-nitrophenylacetate; 4-NP, 4-nitrophenol; GAFF, General Amber force field; SMD, steered molecular dynamics; ABPP, activity-based protein profiling; PDTXs, primary patient-derived tumor xenografts.

* Corresponding author.

E-mail address: tiziano.tuccinardi@unipi.it (T. Tuccinardi).

1. Introduction

The endocannabinoid system (ECS) is composed of two seven-transmembrane G protein-coupled receptors (GPCRs) named cannabinoid receptors type-1 and type-2 (CB1R, CB2R), a family of lipophilic molecules that binds to CB receptors called endocannabinoids (eCBs) and several biosynthetic and degrading enzymes involved in the production and metabolism of eCBs. CB1R is one of

the most abundant GPCRs in mammalian brain and it is highly expressed in neuronal cells, where it regulates neurotransmitter release. CB2R is prevalently expressed in immune cells, where it controls the activation state during inflammation. Anandamide (AEA) and 2-arachidonoylglycerol (2-AG) are the most important eCBs and are biosynthesized on-demand from phospholipid precursors in the inner leaflet of the plasma membrane and released into the extracellular environment [1]. After activating CB receptors, eCBs are transported into the cytoplasm via facilitated diffusion mediated by a putative eCB membrane transporter. [2,3] Intracellular eCBs degradation is mediated by fatty acid amide hydrolase (FAAH) for AEA, and by monoacylglycerol lipase (MAGL) and α/β hydrolase-6 and -12 (ABHD6 and ABHD12) for 2-AG. MAGL is the main hydrolytic enzyme for 2-AG and it is responsible for approximately 85% of 2-AG hydrolysis in the brain, with a minor contribution of ABHD6 and ABHD12. Modulation of eCB levels represents a promising pharmacological strategy to activate the ECS without the typical side effects associated with direct CB1R agonists [4]. Several studies indicate the therapeutic potential of selective eCB reuptake inhibitors, as well as of selective FAAH and MAGL inhibitors in different animal disease models of inflammation, pain, anxiety and other neuroinflammatory diseases [3,5,6].

In the last decades, many academic research groups and pharmaceutical industries have focused their research on the discovery of new MAGL inhibitors, and some of the most representative inhibitors are reported in Fig. 1 [6,7]. MAGL inhibitors reported in the literature can be classified on the basis of their mechanism of action: 1) irreversible inhibitors, which bind covalently to the

enzyme, and usually permanently block its catalytic activity; 2) reversible inhibitors, which interact with MAGL for a limited time, and then the activity of the protein is restored. Irreversible inhibitors are usually highly potent, with inhibition activities in the low nanomolar range; however, they manifested some drawbacks when tested in *in vivo* studies. Fig. 1 shows three representative irreversible MAGL inhibitors, i.e. derivative **1** (JZL184, 4-nitrophenyl-4-[bis(1,3-benzodioxol-5-yl)(hydroxy)methyl]piperidine-1-carboxylate, Fig. 1) [8], **2** (CAY10499, benzyl(4-(5-methoxy-2-oxo-1,3,4-oxadiazol-3(2H)-yl)-2-methylphenyl)carbamate, Fig. 1) [9], and **3** (ABX-1431, 1,1,1,3,3,3-Hexafluoropropan-2-yl-4-[[2-(pyrrolidin-1-yl)-4-(trifluoromethyl)phenyl]methyl]piperazine-1-carboxylate) [10]. In detail, genetic deletion and irreversible MAGL inhibition determine the loss of CB1R-mediated biological effects and induce cross-tolerance to exogenous CB1R agonists [11–15]. These effects are provoked by prolonged pharmacological blockage or genetic inactivation of MAGL, which leads to an excessive increase of 2-AG concentration (5–10-times over basal levels), which triggers CB1R desensitization. Moreover, MAGL-deficient mice are characterized by an impaired CB1R-dependent synaptic plasticity and physical dependence [11]. These aspects may represent a serious limitation for the therapeutic use of most irreversible MAGL inhibitors, especially for chronic treatments. In the last years, MAGL inhibitors endowed with a reversible mode of action gained more interest in the scientific community as potential alternative strategy to modulate MAGL. Initially, only natural compounds, such as the terpenoid Euphol **4** (Fig. 1), a potent MAGL inhibitor with an IC_{50} value in the nanomolar range [16], and the triterpenoid β -

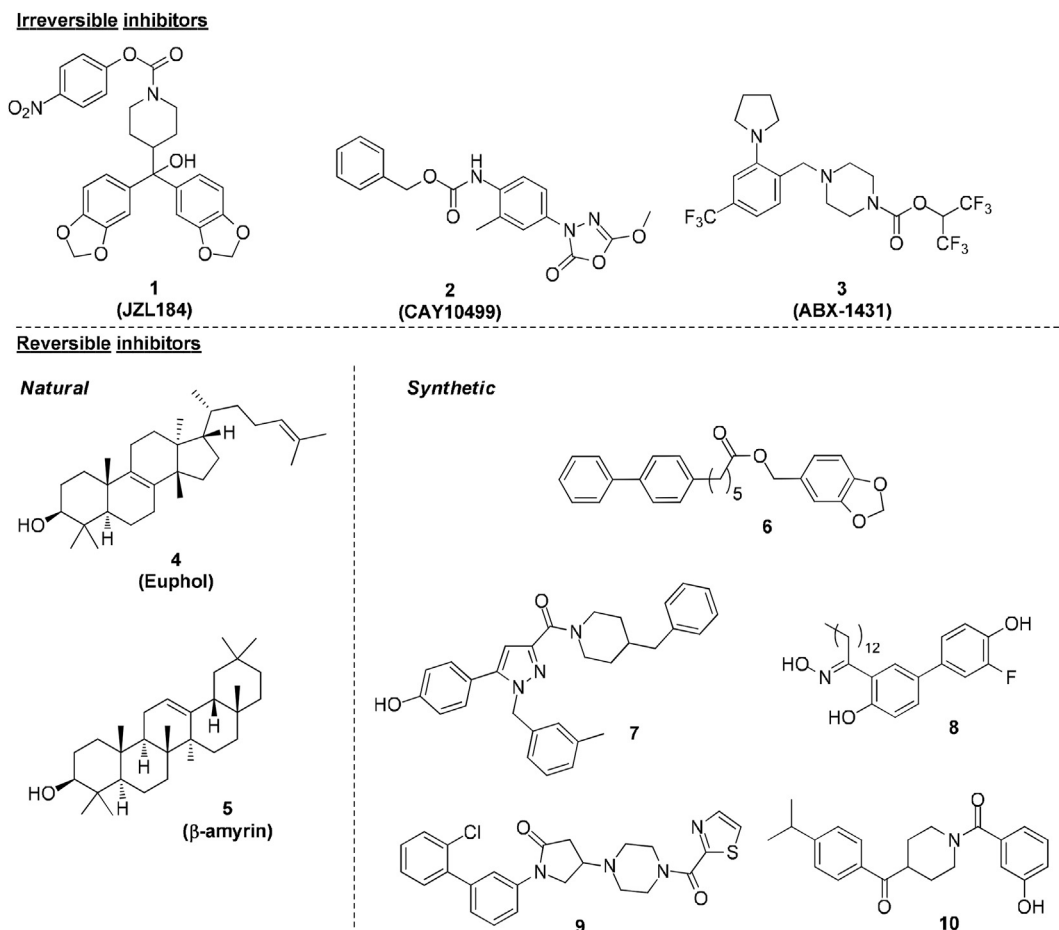


Fig. 1. Structures of some of the most representative MAGL inhibitors.

amyrin **5** (Fig. 1) [17], less potent than Euphol, were identified as reversible MAGL inhibitors. However, they are not selective for MAGL: Euphol was active on other targets, affecting the cell cycle of cancer cells [18], whereas β -amyrin inhibited ABHDs too [17]. Hernández-Torres et al. discovered the first synthetic and selective MAGL inhibitor, benzo[d][1,3]dioxol-5-ylmethyl 6-phenylhexanoate **6** (Fig. 1): this nanomolar inhibitor was able to slow down the clinical progression and to decrease the symptoms of multiple sclerosis in an experimental autoimmune encephalomyelitis mouse model, without inducing unwanted CB1-mediated side effects [19]. Tabrizi et al. disclosed the 1,5-diphenylpyrazole-3-carboxamide **7** (Fig. 1): this reversible MAGL inhibitor mitigated the neuropathic hypersensitivity induced *in vivo* by oxaliplatin [20]. A series of long-chain salicylketoxime derivatives was developed as MAGL inhibitors and, among them, **8** (Fig. 1) was the most active compound of this series. Compound **8** proved to be selective for MAGL over other targets of the ECS and to exert antiproliferative activity in a series of cancer cells [21]. Very recently, Takeda Pharmaceuticals identified a series of piperazinyl pyrrolidin-2-ones, exemplified by compound **9** (Fig. 1) [22], which showed high potency *in vitro* (IC_{50} value in the subnanomolar range). Some derivatives of this class showed promising efficacy *in vivo*, decreasing arachidonic acid level and increasing 2-AG level in mouse brain. Compound **10** (Fig. 1) belongs to the class of the benzoylpiperidine-based MAGL inhibitors [23–25], developed by our group since 2014. This compound derives from an optimization process of this scaffold, possessing a phenolic amidic moiety and a 4-isopropylbenzoyl ring, and these portions are both necessary to reach a nanomolar affinity for MAGL.

2. Results and discussion

2.1. Design

In the last years, a series of benzoylpiperidine-based compounds was identified and developed as reversible and selective MAGL inhibitors, reaching inhibition values in the nanomolar range. In the present manuscript, the most potent inhibitor so far discovered within this series of compounds (**11**, Fig. 2) [24] was further optimized, to find more potent MAGL inhibitors belonging to this

chemical class. The structural optimization was focused mainly on the phenolic ring (in blue, Fig. 2) as well as on the benzoyl moiety (in red, Fig. 2). All the newly synthesized compounds were designed keeping in mind that the *meta*-hydroxyl group on the amidic phenolic ring should not be changed, since it proved to be fundamental for the inhibition activity of the enzyme, establishing a strategic hydrogen bond network with two active site residues, E53 and H272 [23]. As the first modification we added a second fluorine atom on the phenolic ring of **11**, maintaining the other part of the molecule fixed, thus obtaining compound **12** (Fig. 3). This choice was determined by considering that the presence of a fluorine atom in *para* to the phenolic hydroxyl group (as in compound **11**, IC_{50} = 80 nM) and in *para* position to the amide carbonyl group (the analogue compound of **11** bearing the fluorine atom in this position showed an IC_{50} value of 110 nM) [24], proved to be fundamental for the improvement of the enzyme inhibition potency. As the second modification, the fluorine atom of compound **11** was substituted by other groups. Considering that modeling studies suggested that this part of the molecule is located in a small polar pocket of the enzyme, normally hosting the glycerol portion of the substrate 2-AG, the groups suitable to be introduced in this position should not be too bulky, to maintain the same binding disposition of the parent molecule [23]. The groups were chosen among those characterized by electron-withdrawing properties, such as trifluoromethyl and nitro groups, as in compounds **13a** and **13b** (Fig. 3) or electron-donating properties, such as amine and methyl groups, as in compounds **13c** and **13d** (Fig. 3), to determine if a variation of the electronic density on the amidic part could influence the activity of the enzyme. The last modification concerning the phenolic ring was the introduction of hydroxy-pyridine rings, in which the relative position between the pyridine nitrogen and the hydroxyl group is diversified, thus originating compounds **14–17** (Fig. 3). In the second part of our structural optimization, the benzoyl moiety of the reference compound **11** was varied, although the modifications concerning this part of the scaffold were introduced maintaining the phenolic ring of the amide moiety, but without the fluorine atom of compound **11**. This choice was guided by the easy accessibility and the low cost of the 3-methoxybenzoic acid, used for the synthesis of the compounds bearing the 3-hydroxy-phenyl substitution pattern, compared to the 2-fluoro-5-

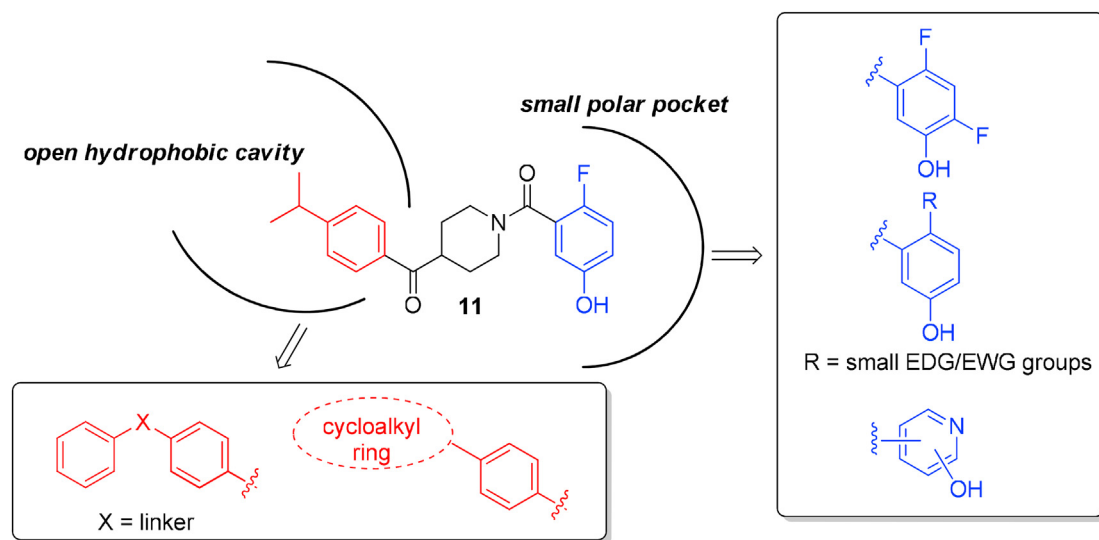


Fig. 2. Design of new benzoylpiperidine derivatives. Previously published reference compound **11** was schematically represented as located in the MAGL binding site. The planned modifications of the benzoyl part and of the amidic moiety are represented in red and blue, respectively. (For interpretation of the references to color in this figure legend, the reader is referred to the Web version of this article.)

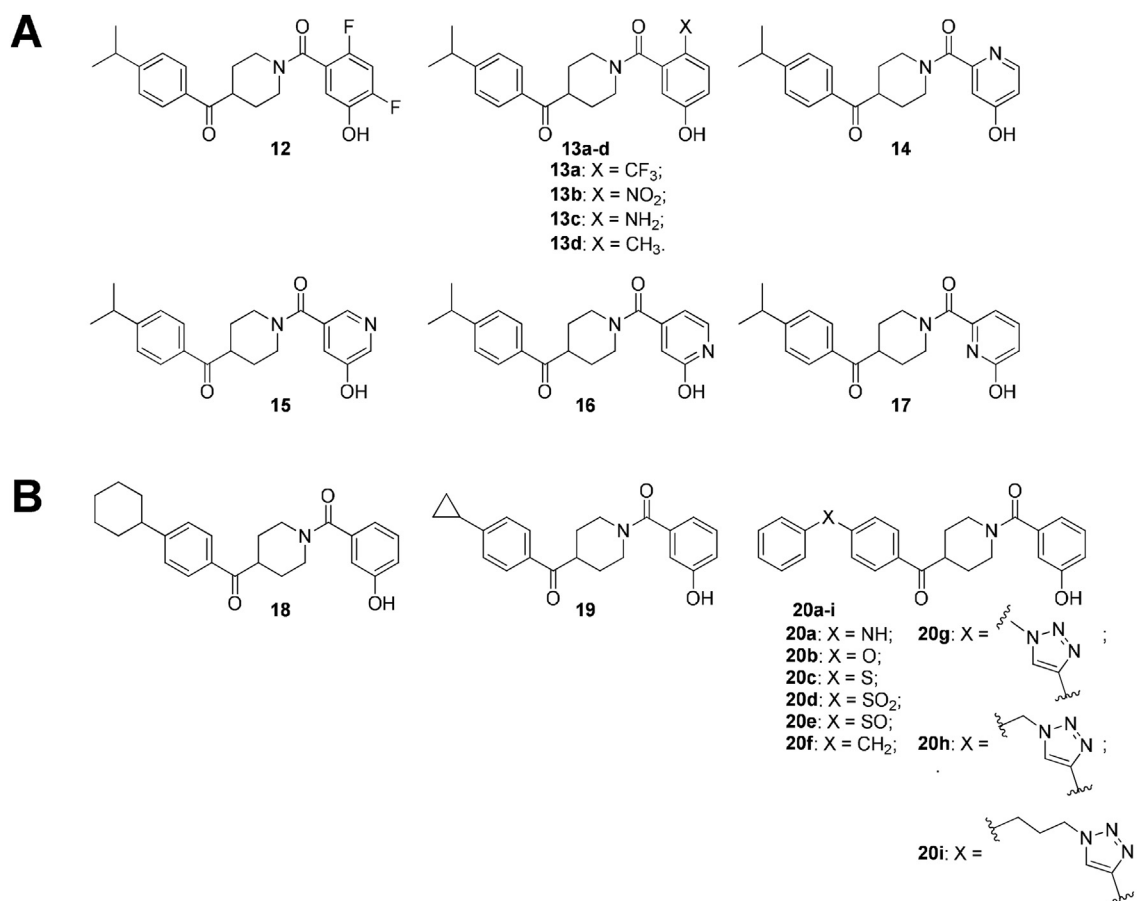


Fig. 3. New series of benzoylpiperidine derivatives. Upper panel (A): newly synthesized compounds with different phenolic moieties (**12**, **13a-d**, **14–17**). Lower panel (B): newly synthesized compounds bearing new substituents in the benzoyl portion (**18**, **19**, **20a-i**).

methoxy benzoic acid necessary for the synthesis of compound **11**. The isopropyl group of compound **11** demonstrated to be beneficial for the inhibition potency, however, we considered the possibility to introduce bulkier and lipophilic moieties in this position, since modeling studies revealed that the benzoyl part extends in the wide lipophilic channel pointing outwards, in which the long unsaturated chain of 2-AG accommodates. A first modification involved the replacement of the isopropyl group by some cycloalkyl rings, such as cyclohexyl or cyclopropyl rings (compounds **18** and **19**, Fig. 3). Moreover, we considered that the previously obtained analogue of **11**, where the isopropyl group was replaced by a second phenyl ring, showed a moderately good activity (IC₅₀ value of 460 nM) [23], therefore we hypothesized that a more flexible portion could be better accommodated into the lipophilic channel of the protein. Therefore, the second phenyl ring was connected to the benzoyl moiety by means of a linker, which could be oxygen or sulphur atoms (compounds **20b** and **20c**, respectively, Fig. 3), NH, sulfone, sulfoxide or methylene groups (compounds **20a**, **20d**, **20e** and **20f**, respectively, Fig. 3). In addition, in some cases the triazole ring was used as the spacer, alone or in combination with a short alkyl chain (1 or 3 carbon atoms), thus obtaining compounds **20g-i** (Fig. 3). Finally, the inhibition potencies shown by the first two groups of new MAGL inhibitors (panel A and panel B of Fig. 3) prompted us to investigate the combinations of chemical modifications on both sides of the benzoylpiperidine scaffold (compounds **21a,b** and **22a,b**, Fig. 4). In particular, the newly optimized compounds possess a fluorine atom in *para* to the phenolic hydroxyl group (compounds **21a,b**), as in compound **11**, or the simultaneous

presence of two fluorine atoms in *para* and in *ortho* positions to the phenolic OH, as in compound **12**, together with the presence of a sulphur atom or a methylene group as linkers between the benzoyl ring and the second phenyl, as in compounds **20c** and **20f**.

2.2. Chemistry

The synthesis of compounds **12**, **13a** and **13b** started from an amide condensation between amine **23** [24] and the corresponding commercially available substituted benzoic acids, which are 2,4-difluoro-5-methoxybenzoic acid **24**, 5-methoxy-2-(trifluoromethyl)benzoic acid **26** and 5-methoxy-2-nitrobenzoic acid **28**, as shown in Scheme 1. The amide formation was performed in the presence of 1-[bis(dimethylamino)methylene]-1*H*-1,2,3-triazolo[4,5-*b*]pyridinium 3-oxide hexafluorophosphate (HATU) as the condensing agent, DIPEA as the base and dry *N,N*-dimethylformamide as the solvent, as previously reported [24]. Finally, the methoxy groups of these intermediates were deprotected by boron tribromide in dichloromethane to yield the final hydroxy-substituted compounds.

For the preparation of amino- and methyl-substituted derivatives **13c** and **13d**, the corresponding methoxylated benzoic acids bearing the proper moiety in position *para* to the methoxy group were not commercially available, therefore they were prepared starting from appropriate precursors. In order to obtain compound **32**, 5-methoxy-2-nitrobenzoic acid **28** was converted to methyl ester **30**, to facilitate the isolation and purification procedures of the subsequent intermediates. Nitro group of compound **30**

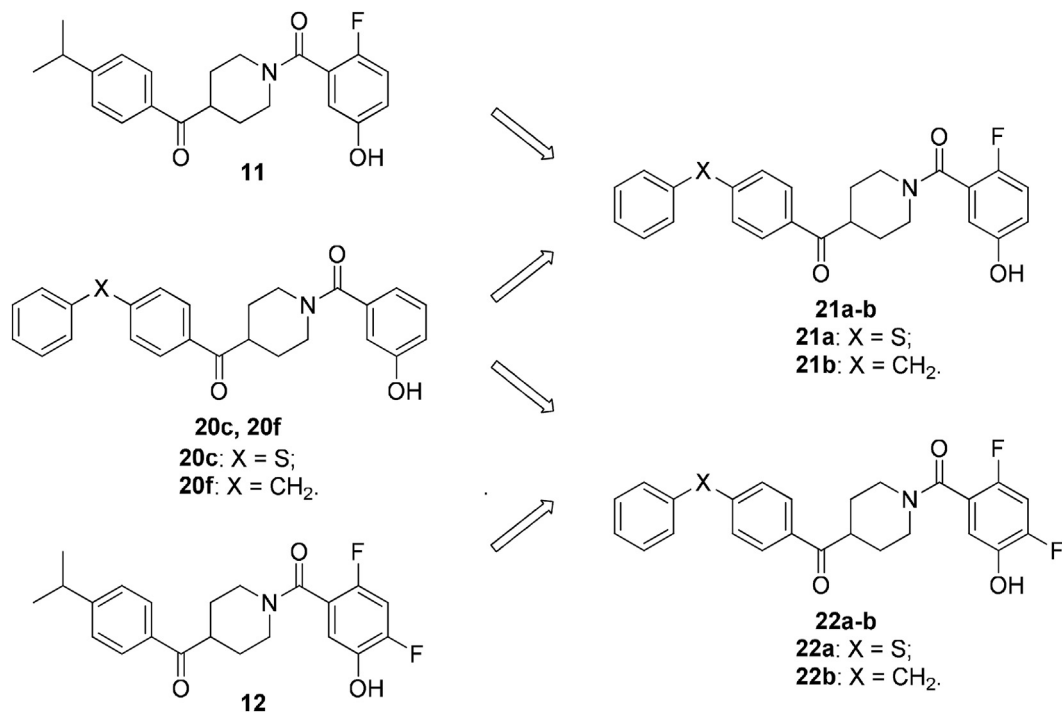
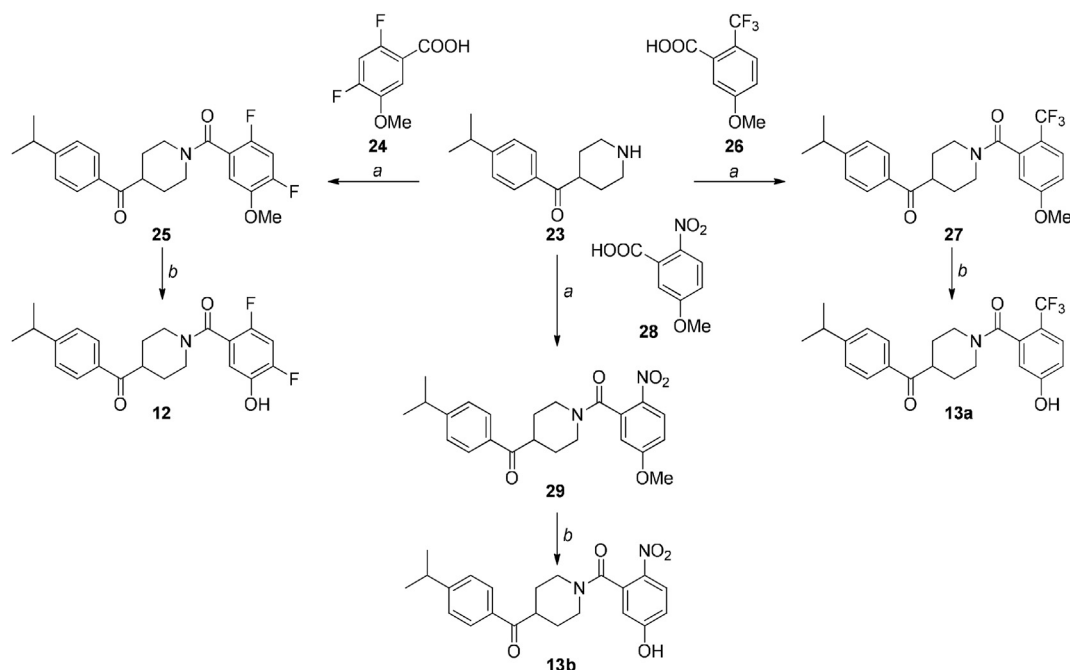


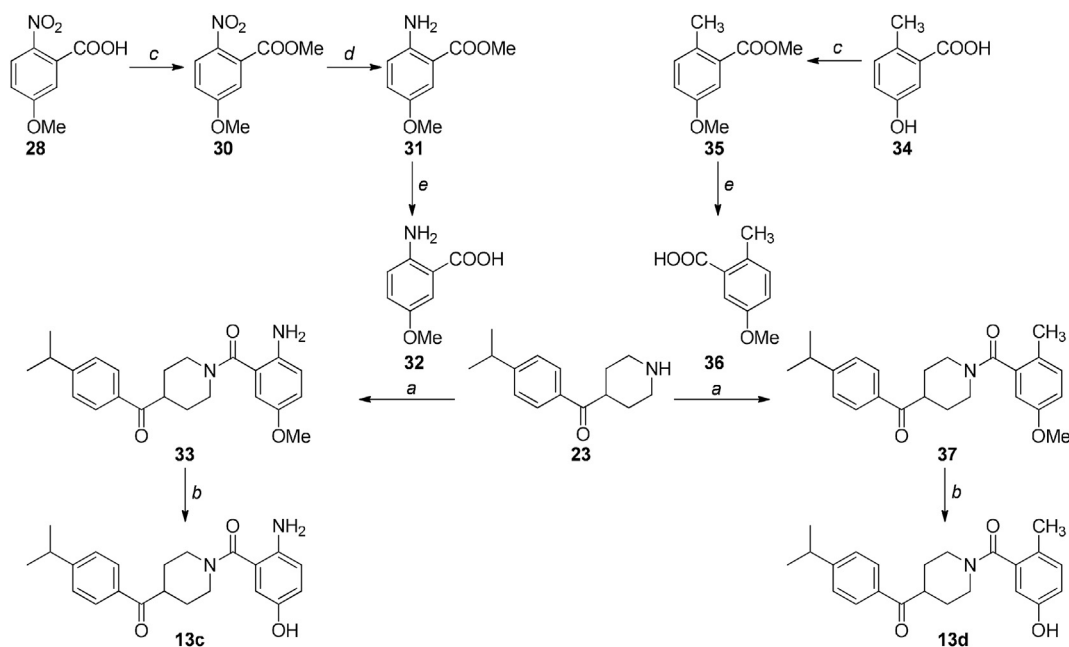
Fig. 4. New series of benzoylpiperidine derivatives, deriving from the combinations of compounds **11** and **20c, f** (compounds **21a,b**) and of compounds **12** and **20c,f** (compounds **22a,b**).



Scheme 1. Synthesis of compounds **12**, **13a** and **13b**. Reagents and conditions: (a) HATU, DIPEA, dry DMF, RT, 2–3 h [59–84%]; (b) 1 M BBr₃, dry CH₂Cl₂, –10 to 0 °C, then RT, 1.5–4 h [6–60%].

was reduced to an amine by using stannous chloride dihydrate in a mixture of chloroform and methanol as the solvent. Then, the methyl ester of compound **31** was hydrolyzed under basic conditions to obtain 2-amino-5-methoxybenzoic acid **32** (Scheme 2). For the synthesis of compound **36**, commercially available 5-hydroxy-2-methylbenzoic acid **34** was subjected to a reaction with methyl iodide by using potassium carbonate in DMF and in these

conditions both the phenolic and the carboxylic acid were methylated. The methyl ester of intermediate **35** was hydrolyzed to generate the free carboxylic group of 5-methoxy-2-methylbenzoic acid **36** (Scheme 2). At this point, the previously adopted reaction conditions were followed, which consisted in the amide condensation with amine **23** and the subsequent BBr₃-promoted deprotection of intermediates **33** and **27** to obtain final compounds **13c**

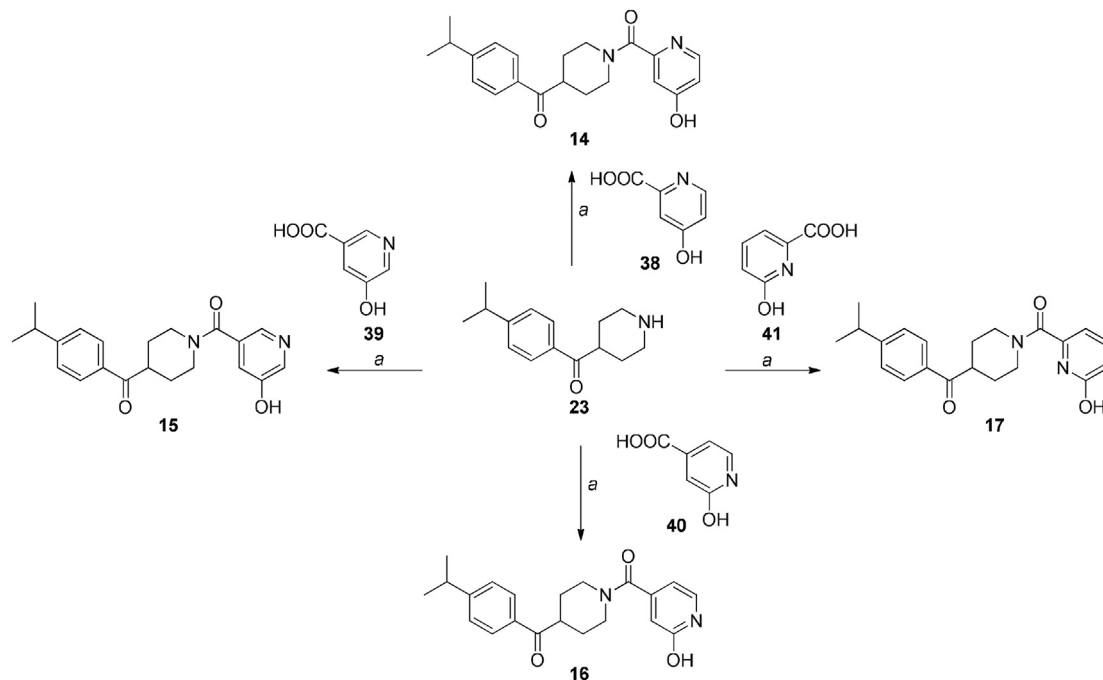


Scheme 2. Synthesis of compounds **13c** and **13d**. Reagents and conditions: (a) HATU, DIPEA, dry DMF, RT, 1.5–2 h [54–70%]; (b) 1 M BBr₃, dry CH₂Cl₂, –10 to 0 °C, then RT, 1–6.5 h [48–59%]; (c) MeI, K₂CO₃, DMF, RT, 4–5 h [85–91%]; (d) SnCl₂·2H₂O, CHCl₃/MeOH, 65 °C, 1 h [85%]; (e) aq. 2 N LiOH, THF/MeOH 1:1 v/v, RT, overnight [77–99%].

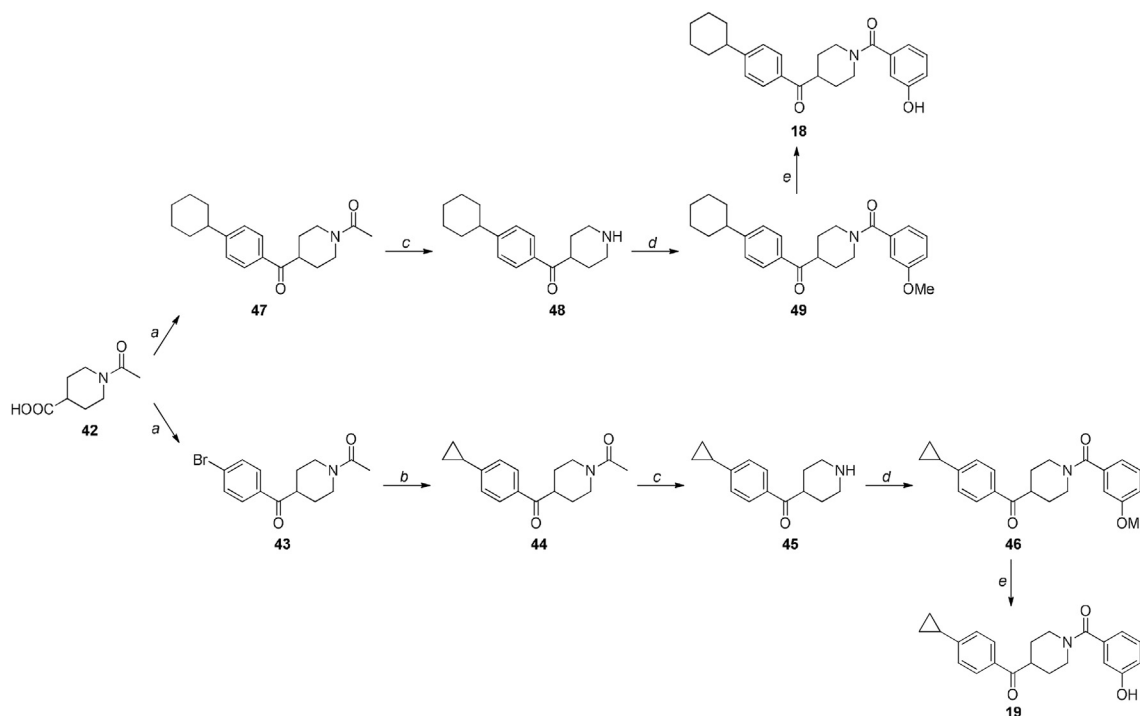
and **13d**, respectively (Scheme 2).

The synthesis of hydroxy-pyridine derivatives **14**–**17** was performed in one step (Scheme 3), since in these cases the use of commercially available hydroxy-substituted pyridine-carboxylic acids was preferred to their methoxylated counterparts. Therefore, amine **23** was condensed with 4-hydroxypyridine-2-carboxylic acid **38**, 5-hydroxynicotinic acid **39**, 2-hydroxypyridine-4-carboxylic acid **40** or 6-hydroxypyridine-2-carboxylic acid **41** to obtain final compounds **14**, **15**, **16** or **17**, respectively, in moderate yields (Scheme 3).

Compounds **18** and **19** bearing cycloalkyl rings, such as cyclopropyl or cyclohexyl groups, on the benzoyl ring were prepared starting from the same precursor, acetylated isonipecotic acid **42** [24]. The synthetic pathway is reported in Scheme 4: common intermediate **42** was refluxed with thionyl chloride in dichloroethane to convert it to the corresponding acyl chloride and then reacted in a Friedel-Crafts reaction with phenylcyclohexane in the presence of aluminum chloride in dichloroethane to obtain compound **47**, or with bromobenzene under the same conditions to give compound **43**. For the introduction of the cyclopropyl ring, a palladium



Scheme 3. Synthesis of compounds **14**–**17**. Reagents and conditions: (a) HATU, DIPEA, dry DMF, RT, 3–4 h [50–57%].



Scheme 4. Synthesis of compounds **18–19**. Reagents and conditions: (a) i. SOCl_2 , dry 1,2-DCE, 60°C , 4 h; ii. bromobenzene (for **43**) or phenylcyclohexane (for **47**), AlCl_3 , dry 1,2-DCE, 90°C , overnight [40–64%]; (b) cyclopropylboronic acid, $\text{Pd}(\text{OAc})_2$, Cy_3P 20% toluene, K_3PO_4 , toluene, 100°C , 24 h [92%]; (c) NaOH 1 N, EtOH, 90°C , overnight [81–86%]; (d) 3-methoxybenzoic acid, HATU, DIPEA, dry DMF, RT, 3 h [68–75%]; (e) 1 M BBr_3 , dry CH_2Cl_2 , -10 to 0°C , then RT, 2 h [28–59%].

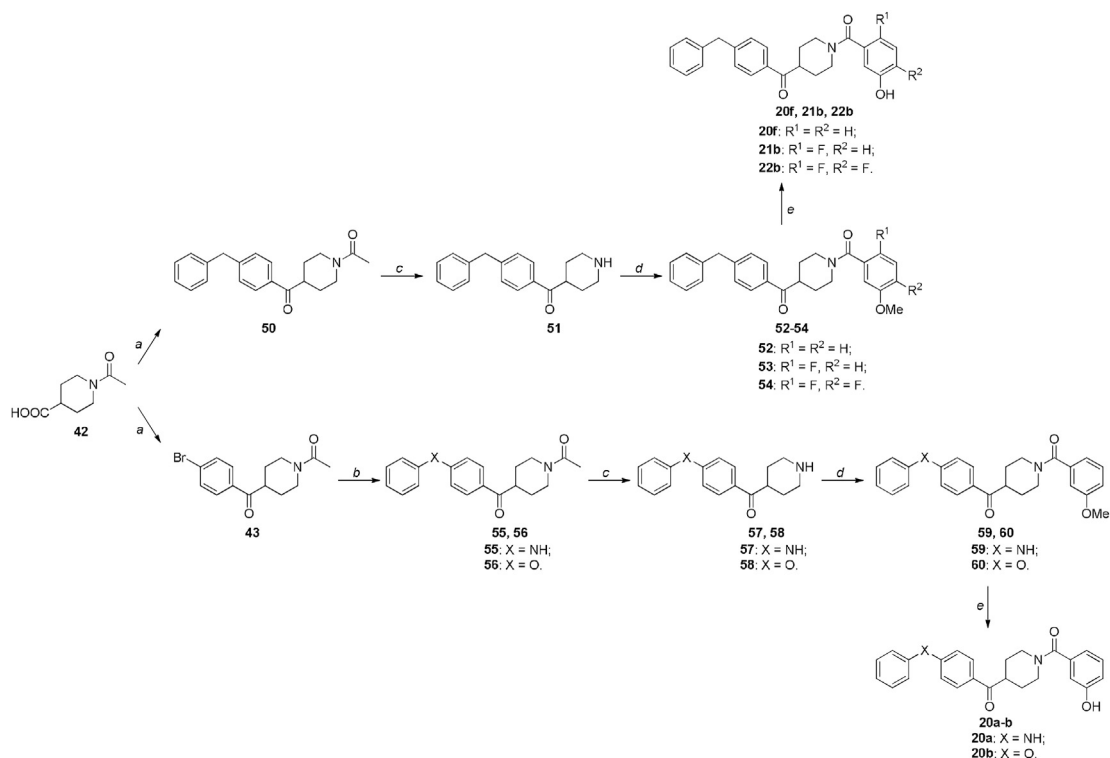
catalyzed cross-coupling reaction with cyclopropylboronic acid, using the catalytic system comprised of palladium acetate, together with tricyclohexylphosphine as the catalyst ligand and potassium phosphate as the base, allowed the insertion of the desired group, thus giving compound **44**. After the different functionalization of the benzoyl ring, hydrolysis under aqueous basic conditions and heating removed the acetyl group of the piperidine nitrogen, thus obtaining amines **45** and **48**, which were then submitted to amidic condensation with 3-methoxybenzoic acid to obtain amides **46** and **49**. The final demethylation step afforded compounds **18** and **19**.

Compounds **20a** and **20b**, bearing a benzoyl moiety with two phenyl rings connected through a nitrogen (**20a**) or an oxygen atom (**20b**), were prepared starting from the previously described bromo-substituted intermediate **43** (Scheme 5). Two different palladium-catalyzed cross-coupling reactions under suitable reaction conditions gave the desired compounds (Scheme 5): a) with aniline, using tris(dibenzylideneacetone)dipalladium as the catalyst, XPhos as the ligand and potassium *tert*-butoxide as the base, in toluene, for compound **55** or b) with phenol, using palladium acetate as the catalyst, tetramethyl di-*tert*-butylXPhos as the ligand and potassium phosphate as the base, in toluene, for compound **56**. Compounds **55** and **56** were then subjected to the same sequence of reactions, consisting in basic aqueous hydrolysis of the *N*-acetyl group of the piperidine, amidic condensation with 3-methoxybenzoic acid and, finally, deprotection of the methoxy group to produce phenolic derivatives **20a–b**. Compounds **20f**, **21b** and **22b** have in common the methylene group as the linker between the two phenyl rings, and they were prepared following a common synthetic strategy (Scheme 5). *N*-Acetylated isonipecotic acid **42** was transformed to the corresponding acyl chloride and then reacted in a Friedel-Crafts reaction with diphenylmethane in the presence of aluminum chloride in dichloroethane. Hydrolysis of the *N*-acetyl group furnished free amine **51**, which was reacted with the proper benzoic acid: 3-methoxybenzoic acid to obtain amide

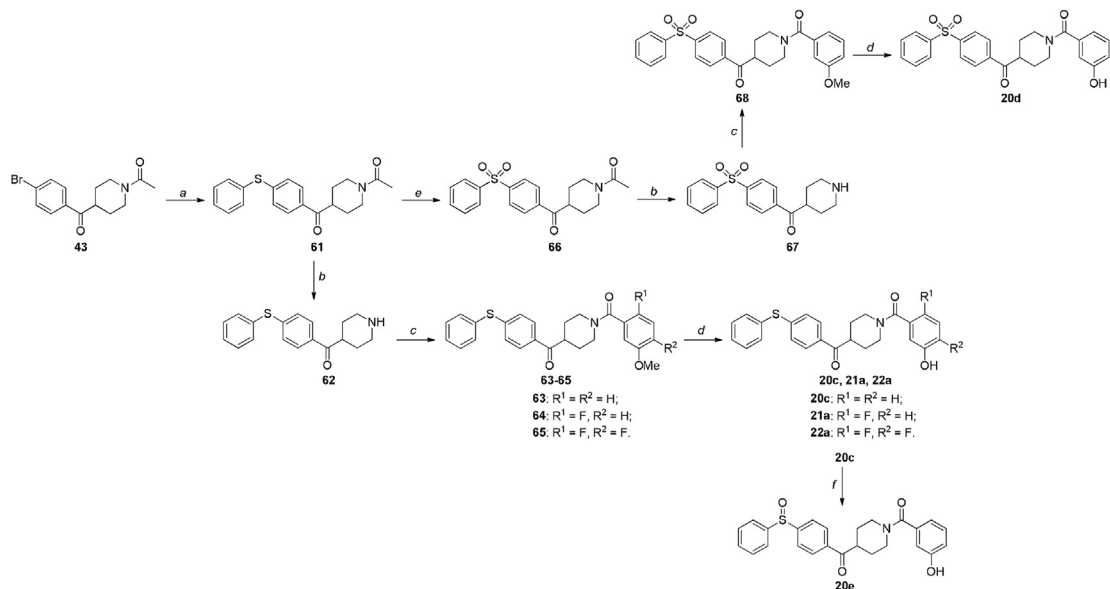
52, 2-fluoro-5-methoxybenzoic acid to obtain amide **53** or 2,4-difluoro-5-methoxybenzoic acid for amide **54**. The final step, common for all these intermediates, is the deprotection of the methoxy group promoted by boron tribromide (Scheme 5).

Scheme 6 displays the synthetic pathways for the sulphur-based compounds **20c,d,e**, **21a** and **22a**, starting from the previously described bromo-substituted derivative **43**. Compound **43** was subjected to a cross-coupling reaction with thiophenol, using tris(dibenzylideneacetone)dipalladium as the catalyst, XanthPhos as the ligand and potassium carbonate as the base, in toluene, to obtain aryl sulfide derivative **61**. This intermediate was subjected to the same sequence of reactions, that are the hydrolysis of *N*-acetyl piperidine group (compound **62**), amide formation with the proper unsubstituted or fluoro-substituted benzoic acids (compounds **63–65**) and deprotection of the methoxy group, thus finally obtaining compounds **20c**, **21a** and **22a**. Alternatively, intermediate **61** was oxidized by using oxone® in a mixture water/1,4-dioxane to obtain the corresponding sulfone **66**. Similarly, compound **66** followed the usual synthetic sequence to get compound **20d**, which is the sulfone analogue of derivative **20c**. We also synthesized the sulfoxide analogue of **20c**, compound **20e**: in this case compound **20c** was oxidized in the presence of a mild oxidizing system composed of hydrogen peroxide and 1,3,5-triazo-2,4,6-triphosphorine-2,2,4,4,6,6-tetrachloride (TAPC) in acetic acid as the solvent.

Some of the newly synthesized compounds, such as derivatives **20g–i**, contain 1,2,3-triazole portions in their structures. The triazole ring acts as a linker between the benzoyl phenyl ring and the second phenyl ring. In some cases, a short linear carbon chain (1 or 3 carbon chain, in compounds **20h** or **20i**, respectively) was also added between the triazole and the peripheral phenyl ring (Scheme 7). These compounds were prepared starting from compound **43**, which is a common intermediate for the synthesis of other compounds shown in the previously described schemes,



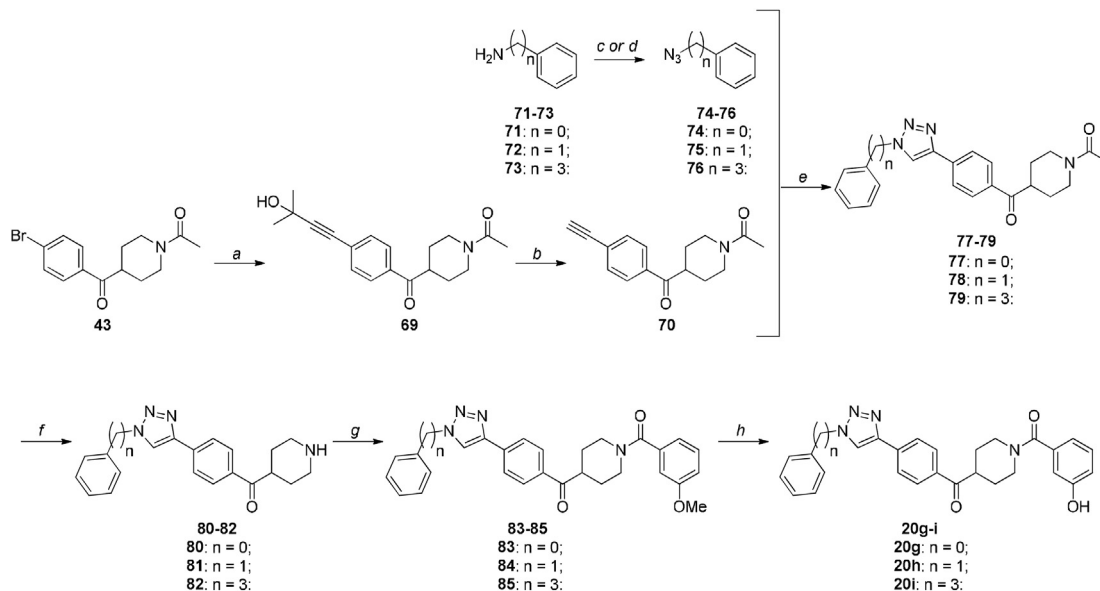
Scheme 5. Synthesis of compounds **20a,b,f**, **21b** and **22b**. *Reagents and conditions:* (a) i. $SOCl_2$, dry 1,2-DCE, 60 °C, 4 h; ii. bromobenzene (for **43**) or diphenylmethane (for **50**), $AlCl_3$, dry 1,2-DCE, 90 °C, overnight [49–64%]; (b) if $X = NH$ (**55**): aniline, $Pd_2(dba)_3$, XPhos, $KOtBu$, toluene, 100 °C, 24 h [99%], if $X = O$ (**56**): phenol, $Pd(OAc)_2$, $Me_4tBuXPhos$, K_3PO_4 , toluene, 100 °C, 24 h [84%]; (c) $NaOH$ 1 N, EtOH, 90 °C, overnight [91–99%]; (d) 3-methoxybenzoic acid (for **52**, **59** and **60**), or 2-fluoro-5-methoxybenzoic acid (for **53**) or 2,4-difluoro-5-methoxybenzoic acid **24** (for **54**), HATU, DIPEA, dry DMF, RT, 3–4 h [65–85%]; (e) 1 M BBr_3 , dry CH_2Cl_2 , –10 to 0 °C, then RT, 1–5 h [25–90%].



Scheme 6. Synthesis of compounds **20c-e**, **21a** and **22a**. *Reagents and conditions:* (a) thiophenol, $Pd_2(dba)_3$, XantPhos, K_2CO_3 , toluene, 120 °C, 24 h [97%]; (b) $NaOH$ 1 N, EtOH, 90 °C, overnight [81–99%]; (c) 3-methoxybenzoic acid (for **63** and **68**), or 2-fluoro-5-methoxybenzoic acid (for **64**) or 2,4-difluoro-5-methoxybenzoic acid **24** (for **65**), HATU, DIPEA, dry DMF, RT, 3 h [49–85%]; (d) 1 M BBr_3 , dry CH_2Cl_2 , –10 to 0 °C, then RT, 1–3 h [45–78%]; (e) oxone®, $H_2O/1,4$ -dioxane, 0 °C, then RT, overnight [99%]; (f) 35% H_2O_2 , TAPC, AcOH, RT, 48 h [78%].

which was subjected to a copper-catalyzed Sonogashira reaction with alkyne 2-methyl-3-butyn-2-ol (MEBYNOL), in the presence of palladium acetate, triphenylphosphine, with triethylamine as the base and DMF as the solvent [26]. After 4 h the desired

compound **69** was obtained, then removal of the 2-hydroxypropyl group was achieved under basic conditions, reacting **69** with potassium phosphate and potassium hydroxide in refluxing toluene for 24 h, thus obtaining compound **70** bearing the terminal alkyne



Scheme 7. Synthesis of compounds **20g-i**. Reagents and conditions: (a) MEBYNOL, Pd(OAc)₂, PPh₃, K₂CO₃, CuI, Et₃N, dry DMF, 90 °C, 4 h [99%]; (b) K₃PO₄, KOH, toluene, 115 °C, 24 h [82%]; (c) for **71**: NaNO₂, NaN₃, HCl aq, H₂O, 0 °C for 1 h, then RT, overnight [70%]; (d) for **72**, **73**: imidazole-1-sulfonyl azide hydrochloride, K₂CO₃, CuSO₄·5H₂O, MeOH, RT, 2.5 h [61–77%]; (e) CuSO₄·5H₂O, sodium ascorbate, H₂O/tBuOH 1:1 v/v, 80 °C, overnight [66–97%]; (f) NaOH 1 N, EtOH, 90 °C, overnight [69–88%]; (g) 3-methoxybenzoic acid, HATU, DIPEA, dry DMF, RT, 3 h [87–99%]; (h) 1 M BBr₃, dry CH₂Cl₂, –10 to 0 °C, then RT, 1–3.5 h [8–61%].

moiety. At this point, compound **70** was subjected to a Cu(I)-catalyzed 1,3-dipolar cycloaddition also known as “Huisgen cycloaddition” or “click-reaction” [27] leading to the formation of triazole-substituted intermediates **77–79**. Azides **74–76** were prepared from the corresponding amines, following two different procedures, according to the type of amine, either aliphatic or aromatic: 1) aniline **71** was converted to the corresponding azide **74** by using sodium nitrite and sodium azide in aqueous hydrochloric acid (condition c, Scheme 7); 2) differently, benzylamine **72** and 3-phenyl-1-propylamine **73** were subjected to a reaction with a suitable diazotransfer reagent, imidazole-1-sulfonyl azide hydrochloride, which was prepared as previously reported [28], in a copper-catalyzed reaction in the presence of potassium carbonate in methanol, thus obtaining azides **75** and **76** (condition d, Scheme 7). After the formation of the triazole ring, compounds **77–79** followed the usual sequence of reactions to obtain compounds **20g-i**.

Analysis of ¹H and ¹³C NMR spectra of the newly synthesized benzoylpiperidine derivatives revealed that in two cases, in particular in compounds **13a** and **13d** bearing bulky groups in *ortho* position to the amidic carbonyl group (trifluoromethyl for **13a** and methyl group for **13d**), it was possible to identify two rotational conformers generated by the hindered rotation around the C–C bond between the amidic phenyl ring and the carbonyl group nearby, as previously observed by us for similar compounds [23]. The splitting of NMR signals was not observed for other compounds bearing nitro (**13b**) or amino group (**13c**) in the same position, since the presence of the *ortho*-NH₂ moiety allowed the formation of an intramolecular H-bond between the hydrogen atom of the amino group and the amide carbonyl oxygen atom, thus inducing stabilization of only one conformer. Similarly, the *ortho*-NO₂ substituted derivative **13b** was visible as a single conformer by NMR analysis, because the repulsion between the partially negatively charged oxygen of the amide carbonyl group and the negatively charged oxygen of the NO₂ group induces a block of rotation, stabilizing only the conformer in which these two portions are distant.

2.3. Enzymatic assays

The herein reported compounds were evaluated for their inhibition activity on human MAGL by using 4-nitrophenylacetate as the substrate [25], comparing the inhibition data with those of some reference compounds, which are the previously published benzoylpiperidine derivatives (1-(3-hydroxybenzoyl)piperidin-4-yl)(4-isopropylphenyl)methanone (**10**) and (1-(2-fluoro-5-hydroxybenzoyl)piperidin-4-yl)(4-isopropylphenyl)methanone (**11**) and the irreversible MAGL inhibitor CAY10499 (**2**). In Table 1, the activity results related to the modification of the phenolic fragment of compound **11** are reported. It is evident that the addition of a second fluorine atom in *para* position to the amide moiety led to an evident increase of the inhibition potency. In fact, compound **12** was about 2.6-fold more active than mono-fluoro substituted derivative **11**. All the other modifications of the phenolic portion, such as the substitution with different groups as well as the presence of a pyridine ring, were detrimental for the inhibition activity, since compounds **13a-d** and **14–17** showed higher IC₅₀ values that fall in the micromolar range, at best.

Once the best substituted phenolic fragment for an optimal interaction with human MAGL was identified, we evaluated the modifications of the benzoyl moiety, considering the larger dimensions of the binding site cavity in which this fragment is supposed to be located. As reported above, in order to speed up the synthesis of the new compounds and reduce the costs, we preferred to maintain in first instance the simple phenolic ring of compound **10** at this stage of the optimization process. As shown in Table 2, among the two cycloalkyl rings introduced in the *para* position to the benzoyl ring, the cyclohexyl group of compound **18** was preferred compared to the smaller cyclopropyl ring of compound **19**, reaching a good IC₅₀ value, slightly lower than that of reference compound **10** (IC₅₀ value of 129 nM compared to 142 nM). In the group of compounds in which the benzoyl ring and a terminal phenyl ring are connected by different moieties, the most promising results were achieved by the introduction of a sulphur atom (compound **20c**) or a methylene moiety (compound **20f**). The IC₅₀ values of **20c** and **20f** (74 and 78 nM, respectively)

Table 1*In vitro* inhibitory activity on MAGL (IC₅₀, nM)^a of derivatives **12**, **13a–d**, **14–17**.^a Enzymatic values are the mean of three or more independent experiments, performed in duplicate.

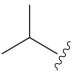
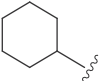

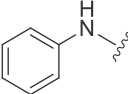
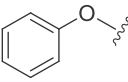
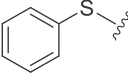
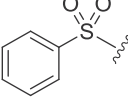
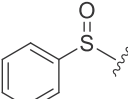
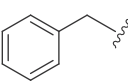
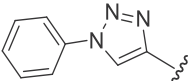
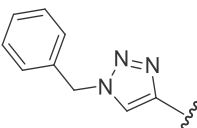
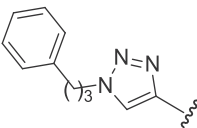
Compounds		Ar	IC ₅₀ (nM)
11			81 ± 10
12			31 ± 2
13	a		X = CF ₃ 8200 ± 900
	b		X = NO ₂ 4500 ± 600
	c		X = NH ₂ > 10000
	d		X = CH ₃ 2300 ± 200
14			> 10000
15			2000 ± 200
16			> 10000
17			> 10000
CAY10499 (2)			130 ± 13

were about two-fold lower than that of compound **10**. Unfortunately, when the spacer is an NH group (**20a**) or an oxygen atom (**20b**), the inhibition activities decreased (IC₅₀ = 758 and 258 nM, respectively). The inhibition potency was negatively affected by the presence of more polar groups, such as a sulfoxide or a sulphone spacer between the two aromatic portions (**20e** and **20d**). Likewise, the triazole moiety present in compounds **20g–i** led to high IC₅₀ values in the micromolar range.

The results shown in Tables 1 and 2 demonstrated that the best inhibition activity of MAGL was obtained when: a) the phenolic moiety is substituted with one or two fluorine atoms in appropriate positions, and b) on the opposite side of the benzoylpiperidine

scaffold, the benzoyl ring and the peripheral phenyl ring are spaced by means of a sulphur atom or a methylene moiety. Therefore, these features were simultaneously combined to obtain compounds **21a,b** and **22a,b**, and their inhibitory activities were tested on MAGL. As shown in Table 3, mono-fluoro-substituted compounds **21a** and **21b** exhibited IC₅₀ values 2.7-fold or 1.6-fold lower, respectively, than their isopropyl parent compound **11** (Table 1), confirming that the diphenylmethane and diphenyl sulphide moieties are optimal lipophilic moieties that nicely fit in the open channel of the MAGL active site. Difluoro-substituted compound **22b** showed similar potency to that of compound **21a**, whereas the best result was obtained with compound **22a**, in which the difluoro

Table 2
In vitro inhibitory activity on MAGL (IC₅₀, nM)^a of derivatives **18**, **19**, **20a–i**.

Compounds	R	IC ₅₀ (nM)
10		142 ± 8
18		129 ± 4
19		368 ± 16
20a		758 ± 88
20b		278 ± 12
20c		74 ± 6
20d		3400 ± 400
20e		4300 ± 500
20f		78 ± 6
20g		1000 ± 100
20h		4400 ± 400
20i		3300 ± 300
CAY10499 (2)		130 ± 13

^a Enzymatic values are the mean of three or more independent experiments, performed in duplicate.

Table 3
In vitro inhibitory activity on MAGL (IC₅₀ and K_i, nM)^a of derivatives **21a,b**, **22a,b**.

Compounds	R	X	IC ₅₀ (nM)	K _i (nM)
21a	H	S	30 ± 2	27 ± 3
21b	H	CH ₂	49 ± 3	37 ± 3
22a	F	S	18 ± 1	11 ± 1
22b	F	CH ₂	36 ± 1	30 ± 2

^a Enzymatic values are the mean of three or more independent experiments, performed in duplicate.

substitution was combined with the diphenyl sulphide moiety, showing an IC₅₀ value of 18 nM, thus reaching the highest potency of this series of MAGL inhibitors.

With the aim to confirm the reversible mechanism of inhibition, already proved for other members of this chemical class [23,24], the four derivatives **21a,b**, **22a,b** were subjected to preincubation and dilution assays. With regards to the preincubation assay, a higher potency after longer incubation times should be produced by an irreversible inhibition, whereas for a reversible inhibitor a constant inhibition potency over all the different incubation times should be observed. The four compounds were thus preincubated with the enzyme for 0, 30 and 60 min before adding the substrate to start the enzymatic reaction. As shown in Fig. 5A, the test suggests a reversible binding mode for all compounds, as they showed very similar activities at all the three different incubation times. As a second test, we studied the effect of dilution on the inhibitory activity of these four compounds. In this test, the potency of an irreversible mechanism of inhibition should not decrease after dilution, whereas for a reversible inhibitor, the potency should be strongly reduced after dilution. Therefore, the inhibition produced by incubation with a 50 nM concentration of compounds **21a,b** and **22a,b** was measured after a 40x dilution and compared to the potency observed by a 2000 nM and a 50 nM concentration of the same compounds. As shown in Fig. 5B, for all compounds, the inhibition produced at a concentration of 50 nM was similar to that obtained after a 40x dilution and was considerably lower than that produced by the same compound at a concentration of 2000 nM, thus supporting a reversible mechanism of inhibition.

The inhibition mode of the four best compounds was then evaluated by measuring Michaelis–Menten kinetics at various inhibitor concentrations. The datasets were plotted as substrate concentration versus enzyme activity and analyzed by applying the mixed-model inhibition fit of GraphPad Prism 5.0, which includes competitive, uncompetitive, and noncompetitive inhibition terms. The model evaluates the V_{max}, K_m and the α parameter, which is indicative of the inhibition mechanism. When α corresponds to one, the inhibitor does not alter the binding of the substrate to the enzyme, and the mixed-model can be considered as a noncompetitive inhibition. When α is a very large value, the inhibitor interaction prevents the substrate binding and the mixed-model corresponds to competitive inhibition. Finally, when α is a very small value, the binding of the inhibitor increases the binding of the substrate and the mixed model corresponds to an uncompetitive model. Kinetic studies indicate for **21a,b** and **22a,b** an α value greater than 10 000, thus supporting a competitive behavior for these compounds (Fig. S1) and as shown in Table 3, the K_i values measured for **21a,b** and **22a,b** ranged from 11 to 37 nM.

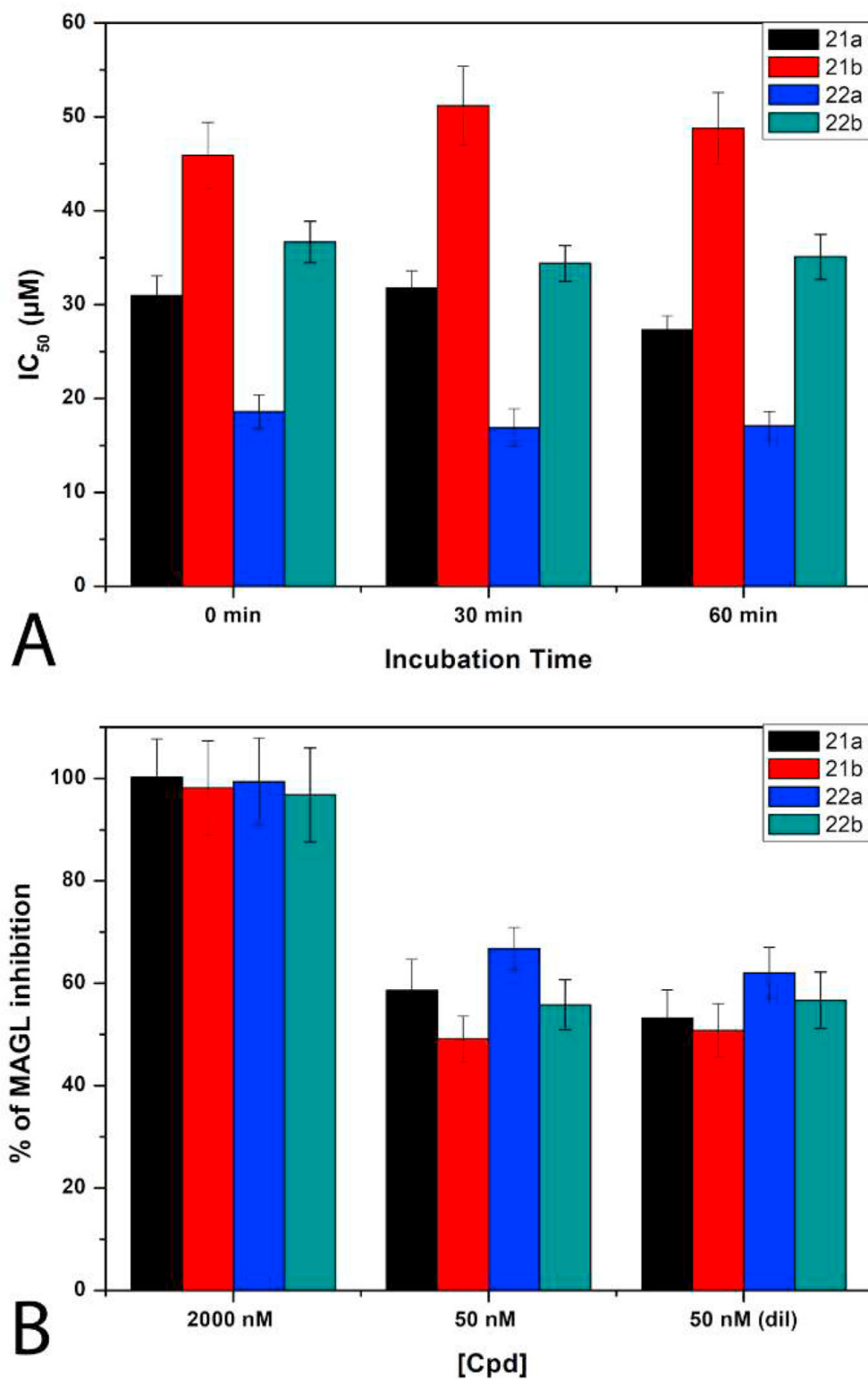


Fig. 5. Analysis of the mechanism of MAGL inhibition of compounds **21a,b** and **22a,b**. A) IC_{50} (nM) values at different preincubation times with MAGL (0 min, 30 min and 60 min). B) Dilution assay: the first two columns indicate the inhibition percentage of the compounds at a concentration of 2000 nM and 50 nM. The third column indicates the inhibition percentage of the compounds after dilution (final concentration = 50 nM).

2.4. Molecular modeling studies

Compound **22a**, which is one of the most promising MAGL inhibitors among the synthesized derivatives, was used as the

reference ligand for molecular modeling studies. A thorough docking procedure performed with AUTODOCK 4.2, aimed at predicting its potential binding mode, was initially performed (See Experimental Section for details). The docking calculations

confirmed the general binding disposition of this series of ligands that guided the structure-based optimization of this class of compounds [23]. In fact, the phenol moiety of compound **22a** was located into the terminal portion of MAGL binding site, showing the key H-bond network with H272 and E53. As expected, the diphenyl sulphide moiety was placed into the lipophilic channel at the entrance of the catalytic site, while the central carbonyl group of the ligand formed H-bonds interactions with A51 and M123 within the oxyanion hole (Fig. S2). The binding mode generated by docking for compound **22a** was then refined and further studied by running molecular dynamics (MD) simulation analysis, followed by ligand-protein binding energy evaluations. The predicted **22a**-MAGL complex was subjected to an MD protocol consisting in 250 ns of simulation, which confirmed the reliability of both the disposition of the ligand into MAGL binding site (with an average RMSD of 1.9 Å during the MD simulation) and the ligand-protein interactions predicted by docking (Table S1). Fig. 6 shows the minimized average structure of **22a** within the MAGL catalytic site generated from the last 200 ns of MD simulation. The ligand slightly adjusted its binding conformation during the MD simulation, especially at the level of the terminal phenyl ring of the diphenyl sulphide moiety, which showed to be highly mobile and able to establish multiple hydrophobic interactions with the residues located at the entrance of the binding pocket, such as A151, A156, F159, L205, L213, and L241. The central phenyl ring of the ligand is sandwiched between A51 and L213 from one side and L241 from the other, forming lipophilic interactions with these residues, while the adjacent carbonyl group establishes stable H-bonds with the backbone nitrogen of both A51 and M123, which were maintained for most of the MD simulation (Table S1). The difluorophenolic moiety of **22a** showed the π - π stacking with Y194 and the H-bond network with E53 and H272, already predicted for reference compound **11** and other phenolic derivatives of this series [24]. However, while the charged H-bond with E53 showed to be firmly maintained during the whole simulation, the H-bond with H272 was found to be less stable, being maintained for about 64% of the MD simulation. Nevertheless, a further H-bond, that was not initially predicted by docking, was observed between the fluorine atom in *ortho* position to the hydroxyl group of the ligand and the guanidine moiety of R57; this additional interaction, which was

maintained for 77% of the simulation, could well compensate the reduced strength of the H-bond with H272.

With the aim to evaluate the reliability of the binding mode predicted for compound **22a** from a quantitative point of view, the last 200 ns of MD simulation of the **22a**-MAGL complex were employed to perform ligand-protein binding energy evaluations, using the MM-GBSA method. Notably, the binding affinity estimated for the complex (-71.9 kcal/mol) was found to outperform of 7 kcal/mol the affinity previously predicted for the parent compound **11** (-64.9 kcal/mol) [24]. This result is consistent with the higher inhibitory activity of compound **22a** with respect to **11**, and could thus confirm the reliability of the binding mode and the ligand-protein interactions predicted for **22a**.

The **22a**-MAGL complex was then subjected to steered molecular dynamics (SMD) simulations aimed at predicting the potential dissociation process of this class of inhibitors from their complex with the enzyme. The simulation of the putative ligand unbinding process was motivated by the attempt of obtaining a deeper insight of the inhibition mechanism of this class of compounds in terms of ligand-protein interactions, analyzing the importance of the key structural moieties of these ligands from a different point of view and also providing a first hint about the ligand-binding process. In view of this last purpose, we aimed at simulating the exit of the ligand through the lipophilic channel at the entrance of the MAGL catalytic site, which should constitute the access gate to MAGL substrates and inhibitors. In particular, three different SMD simulations were performed following three different unbinding pathways (P1-3), each defined based on the α carbon of a specific protein residue: S48, M123 and A126, respectively (Fig. S3A). In each simulation, the distance between the terminal phenyl ring of the ligand and the residue α carbon was progressively increased by a total 30 Å, to allow the dissociation of the ligand from the protein through the desired direction (see Experimental section for details). Importantly, in each SMD the ligand was moved at a constant velocity of 0.1 Å/ns, which required to perform 300 ns of simulation for each unbinding pathway, for a total of 0.9 μ s of SMD. This approach allowed us to consider the simulated ligand dissociation process as reversible, and the work associated with it as the free energy variation of the process [29,30]. As shown in Fig. S3B, the unbinding pathway P2 demonstrated to be the most energetically

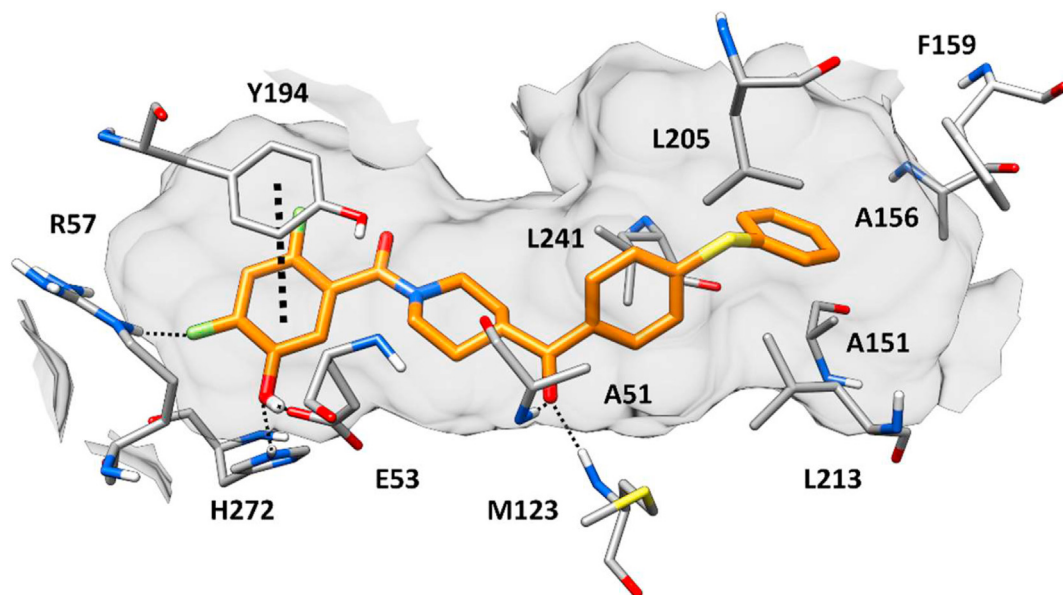


Fig. 6. Minimized average structure of compound **22a** within the MAGL catalytic site (PDB code 3PE6).

favoured one since its corresponding total free energy (48.6 kcal/mol) was found to be significantly lower than those associated with P1 (70.8 kcal/mol) and P3 (64.7 kcal/mol). Therefore, P2 was considered as a likely unbinding pathway of compound **22a** and was thus further analyzed from both the quantitative and qualitative point of view. The MM-GBSA method was used to perform a per-frame ligand-protein binding energy evaluation, to monitor the free energy of binding during the simulation. In parallel, the SMD trajectory showing the whole ligand unbinding process was inspected in relation to the binding energy profile, to correlate the change in ligand disposition with the change in the corresponding binding free energy. Fig. 7 shows different snapshots of the SMD simulation that illustrate the evolution of the **22a**-MAGL complex during the different stages of the ligand unbinding process.

Right after the first few nanoseconds of simulation, the ligand loses some of the interactions with the protein, such as the H-bond with R57 and even the H-bond with M123. Nevertheless, similarly to what observed in the predicted binding mode of the parent compound **11** [24], the loss of the key interaction with the oxyanion hole is compensated by the formation of a stable H-bond with the hydroxyl group of S181. Therefore, for about the first 55 ns of simulation, the ligand globally maintains its binding mode (Fig. 7A), which is only slightly weakened, since the ΔG of binding is still around -60 kcal/mol (Fig. S4). Subsequently, the central carbonyl group of **22a** is slowly pulled away from the oxyanion hole, thus losing the H-bond with A51 (Fig. 7B). Moreover, the H-bond between the phenolic OH group of the ligand and H272 is also lost in this stage (between 55 and 85 ns of SMD), in which the binding energy continuously decreases up to about -40 kcal/mol. However, both the H-bond with E53 and S181 are still maintained. During the following 40 ns, the diphenyl sulphide moiety of the ligand moves outside the entrance of the lipophilic channel, while its phenol ring is dragged out the polar pocket of MAGL binding site (Fig. 7C), with the consequent disruption of the H-bond with E53 and the further drop of the ΔG of binding to about -30 kcal/mol. During this stage, even the loss of the H-bond with S181 is eventually observed, although this interaction is maintained for almost the first 110 ns of SMD. After about 130 ns from the beginning of the SMD, compound **22a** further slides out MAGL catalytic site, reaching a sort of intermediate, half-unbound state (Fig. 7D) that is maintained for about

30 ns of simulation (between 155 and 185 ns of SMD). In this time-lapse, the binding free energy of the complex fluctuates steadily around -26 kcal/mol. The ligand then moves completely out of the binding pocket; after about 200 ns from the beginning of the simulation, **22a** only interacts with the residue at the entrance of the lipophilic channel from the outside region of the protein (Fig. 7E), with a binding energy around -10 kcal/mol. After that, the ligand moves away from MAGL catalytic site, forming only transient and very weak interactions (with average ΔG_{bind} around -6 kcal/mol) with the protein surface residues until about 245 ns of SMD. A complete detachment of compound **22a** from MAGL is then observed (Fig. 7F), consistently with the total drop of the binding free energy, which remains to zero until the end of the simulation, except for few frames in which the ligand forms transient occasional interactions with the protein surface. For a deeper analysis of the ligand unbinding process, we focused our attention on the simulation interval ranging from about 100 to 185 ns, which was found to be associated with a quite stable ΔG of binding (Fig. S4). By carefully inspecting the SMD trajectory in this time-lapse, we identified two different ligand conformations that are stably maintained for a considerable time. In particular, when compound **22a** starts crossing the entrance of the MAGL catalytic site, it assumes for about 18 ns (110–127 ns of SMD) a binding pose in which it interacts predominantly with H269 (and secondarily with S122) through its OH group. The phenolic ring also shows van der Waals contacts with A51, Y194 and L184, while the piperidine core and the diphenyl sulphide moiety of **22a** form extensive hydrophobic interactions with F159, P178, I179, L241 and L205, placed at the entrance of the lipophilic channel (Fig. S5A). Subsequently, as mentioned above, the ligand reaches a stable conformation that is maintained for a quite long time-lapse (between 155 and 185 ns of SMD) with respect to the whole unbinding process. Although a major portion of the ligand is already outside MAGL binding pocket, the compound is anchored to the protein through two H-bonds with the backbone nitrogen of D178 and L205. Additionally, the hydroxyl group of **22a** forms a water bridged interaction with S122 (Fig. S5B). Taken together, these results highlight the key role of the ligand phenolic moiety, which is not only necessary for achieving a high MAGL inhibitory activity, but may also be important for the ligand recognition and binding process. Indeed, the interaction

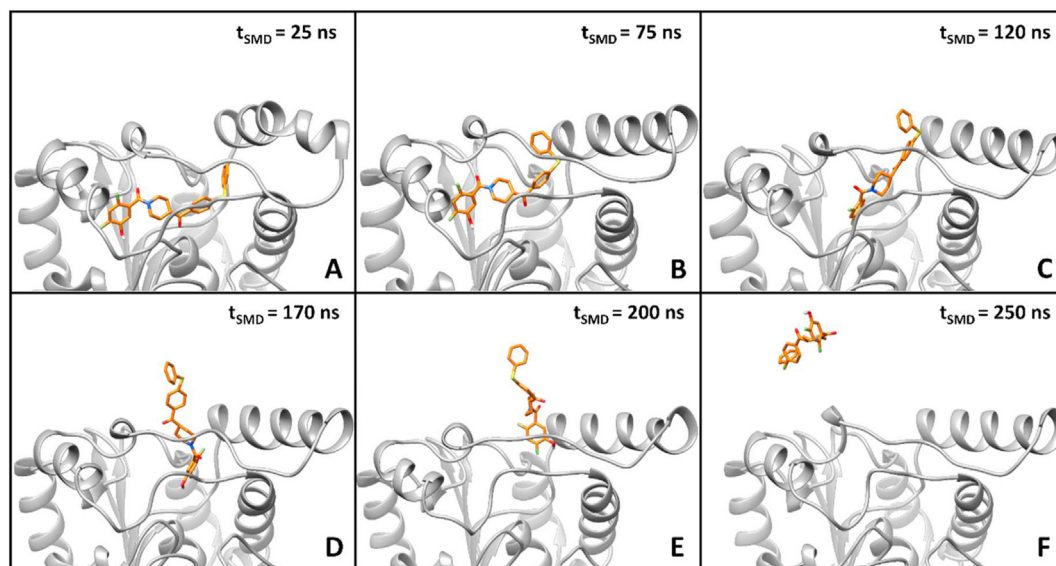


Fig. 7. Evolution of the **22a**-MAGL complex during the SMD simulation. Six different SMD snapshots, obtained after A) 25, B) 75, C) 120, D) 170, E) 200 and F) 250 ns from the beginning of the simulation, are shown.

with E53 is maintained for the first 30% of the SMD; when this is disrupted, multiple additional H-bonds established by the ligand OH group were observed during the dissociation process. For the same reason, the two carbonyl groups of **22a** could also play a role in the first stages of ligand binding to MAGL. Finally, the interactions observed with D178 and L205 highlight two potential pharmacophore interactions that might be exploited in the design of more potent MAGL inhibitors.

2.5. Selectivity

Compounds **21a,b** and **22a,b** were profiled for their selectivity towards the other components of the ECS. As shown in Table 4, at the concentration of 10 μ M none of the compounds significantly bound to CB1R and CB2R or inhibited ABHD6 and ABHD12; only compound **21a** showed a weak inhibition of ABHD6 (40% at 10 μ M). Importantly, the four MAGL inhibitors showed high selectivity over FAAH, with no significant inhibition at 10 μ M (Table 4).

2.6. Cell-based assays of MAGL inhibition

In order to confirm the MAGL inhibition in a more physiological system, **21a,b** and **22a,b** were tested in intact U937 cells as previously described [24]. As shown in Fig. 8, all four compounds showed an IC₅₀ value in the nanomolar range; in particular, compound **22a** was the most potent inhibitor with an IC₅₀ value of 568 nM.

2.7. Activity-based protein profiling experiments

With the aim to assess the selectivity of the four MAGL inhibitors in a broader context of serine hydrolase family, we performed competitive activity-based protein profiling (ABPP) experiments for compounds **21a,b** and **22a,b** using mouse brain membrane preparations. ABPP is a functional proteomic technology, which exploits chemical probes that react with mechanistically related classes of enzymes [31]. TAMRA-fluorophosphonate (TAMRA-FP) is used to visualize serine hydrolases, which include the major eCB degrading enzymes [32]. An important advantage of ABPP relative to other approaches is that it can detect changes in the activity of very low-abundance enzymes in highly complex samples and can simultaneously assess the potency and selectivity of an inhibitor towards the entire family of serine hydrolases in a specific tissue.

As shown in Fig. 9, at the concentration of 10 μ M the four compounds significantly inhibited the two bands associated to MAGL (doublet band 3 and 4 as MAGL migrates as double band in the ABPP) [33]. In agreement with the data obtained in intact cells, compounds **21a**, **21b**, **22a** and **22b** showed a concentration-dependent inhibition of MAGL (Fig. S6, band 3 and 4) without affecting FAAH (Fig. S6, band 1), ABHD6 (Fig. S6, band 5) and ABHD12 (Fig. S6, band 2) up to 30 μ M, indicating a high MAGL

selectivity over other relevant enzymes in the ECS. Compounds **21a** and **21b** showed high selectivity also towards other serine hydrolases up to 30 μ M (Fig. S6, Table S2), while compound **22a** and **22b** exhibited a partial inhibition of two non-identified bands (approximately 50 and 55 kDa) at 10 and 30 μ M (Fig. S6, Table S2).

2.8. Cell viability assays

The four compounds **21a,b** and **22a,b** were selected for further *in vitro* experiments to evaluate their anticancer potency against a series of cancer cells. Compound CAY10499 (**2**) was used as the reference compound. Due to the key role that MAGL plays in the tumor progression of breast, colon and ovarian cancers, five tumor cell lines were chosen: human breast MDA-MB-231, colorectal HCT116 and ovarian CAOV3, OVCAR3 and SKOV3 cancer cells (Table 6) [34–36]. With the exception of OVCAR3, all compounds produced an appreciable inhibition of cell viability in tested cancer cell lines. With respect to the covalent reference inhibitor **2**, compounds **21a,b** and **22a,b** showed more potent cytotoxic activities on HCT116, MDA-MB-231, CAOV3 and SKOV3, whereas the proliferation of the OVCAR3 tumor cells was most significantly affected only by compound **21b**.

2.9. Human cancer organoids

Beyond the cancer cell lines, human cancer models include the use of primary patient-derived tumor xenografts (PDXs) that can mimic the biological characteristics of the tumor better than *in vitro* culture models. However, limitations of PDXs include the use of animals and limited engraftment efficiencies for subsets of patient tumors. Moreover, the approach is expensive, time-consuming, resource-consuming, and PDXs may undergo mouse-specific tumor evolution [37]. In this scenario, cancer organoids represent an emerging approach for creating patient-derived *in vitro* cancer models that closely recapitulate the pathophysiological features of natural tumorigenesis and metastasis [38]. Cancer-derived organoids are three-dimensional tissue-resembling cellular clusters derived from tumor-specific stem cells that mimic the *in vivo* tumor characteristics, as well as tumor cell heterogeneity. Organoids have been demonstrated to closely recapitulate the drug response in clinical setting and could be utilized to measure the efficacy and toxicity of small molecules [39–42]. Furthermore, the generation of cancer organoids is inexpensive, easy to use, and can be accomplished in 1–2 months.

On these bases, the abilities of the four compounds **21a,b** and **22a,b** to inhibit the growth of cancer cells prompted us to investigate their activities directly on cancer organoids derived from human tumor tissues. In our study, the high grade serous ovarian cancer (HGSOC) was selected, since it is one of the most aggressive cancer types with a lethality/incidence ratio of more than 60% [43]. Cancer organoids derived from three HGSOC patients were treated with 100 μ M of **21a,b**, **22a,b** and carboplatin as the positive control. Carboplatin turned out to be the most effective agent with a range of values of inhibition from 50% to 67%. Compound **22b** was the least effective inhibitor with a percentage of inhibition ranging from 18% to 35%. Compounds **21a,b** and **22a** inhibited the growth of cancer organoids in the range of 42%–63%, thus moving near the values shown by carboplatin (Fig. 10). Considering the targeting nature of MAGL inhibitors, the results obtained for compounds **21a,b** and **22a** are comparable to that of carboplatin and therefore open up to an in-depth analysis by considering a higher number of patients.

Table 4

Pharmacological characterization of compounds **21a,b**, **22a,b** towards the other components of the ECS. Data represent IC₅₀ values (μ M, mean \pm SD) and the % of receptor binding/enzyme inhibition at the concentration of 10 μ M (in brackets).

Compound	IC ₅₀ values (μ M, mean \pm SD)				
	CB1	CB2	FAAH	ABHD6	ABHD12
21a	>10 (<10%)	>10 (<10%)	>10 (<10%)	>10 (40%)	>10 (26%)
21b	>10 (<10%)	>10 (<10%)	>10 (<10%)	>10 (21%)	>10 (20%)
22a	>10 (<10%)	>10 (<10%)	>10 (22%)	>10 (18%)	>10 (27%)
22b	>10 (<10%)	>10 (<10%)	>10 (21%)	>10 (10%)	>10 (28%)

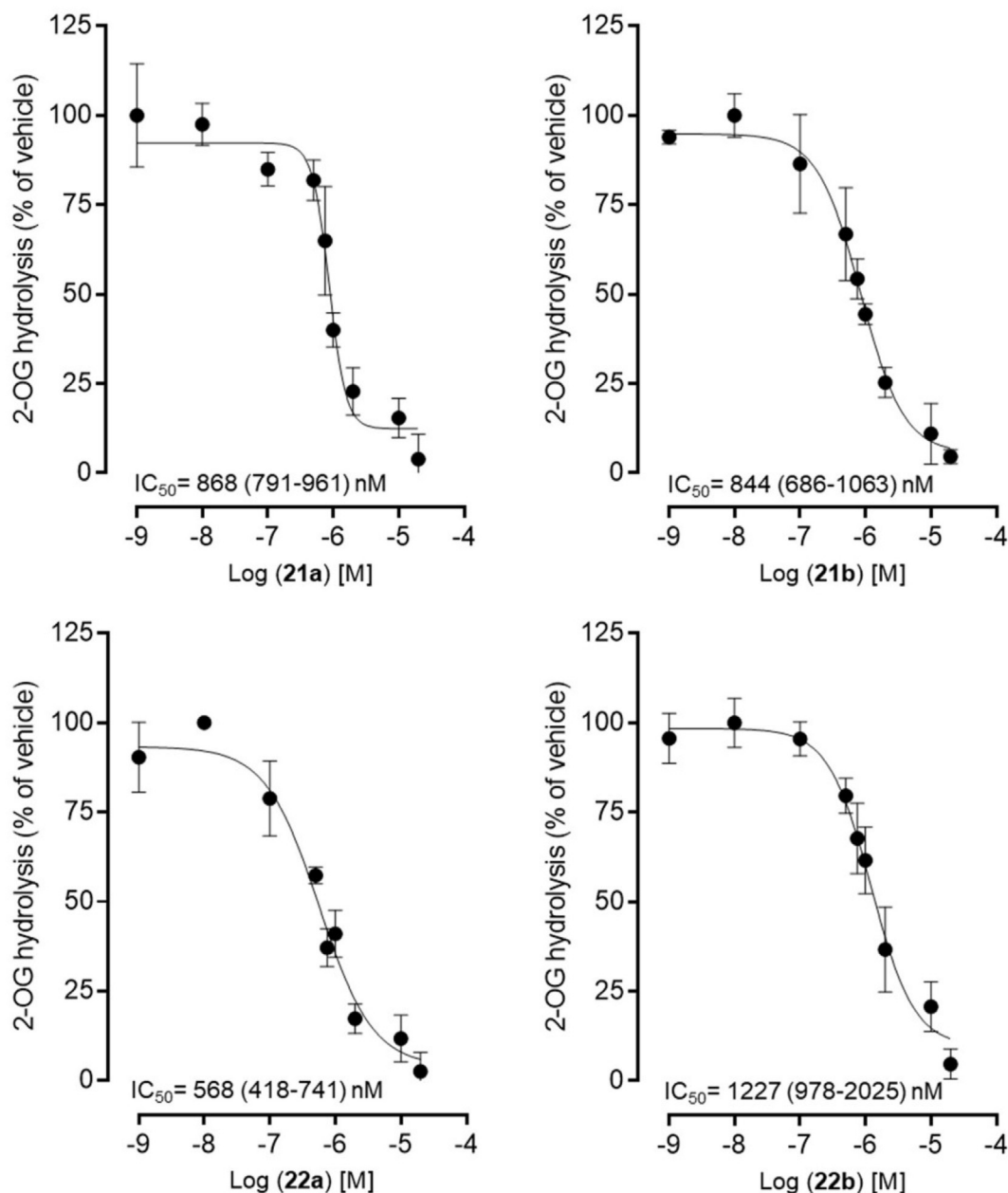


Fig. 8. Concentration-dependent inhibition of 2-OG hydrolysis in intact U937 cells for compounds **21a,b** and **22a,b**. Cells were pre-incubated for 30 min with the compounds and then with 2-OG/[3H]2-OG (final concentration 10 μ M) for additional 15 min at 37 °C. JZL184 **1** (1 μ M) was used as a positive control for full inhibition of MAGL. Data represent mean \pm SD of two independent experiments in triplicate. IC_{50} values are expressed as mean (95% CI). Data were normalized (residual 2-OG hydrolysis of 30%).

2.10. PDAC cells viability assay

Compounds **21a,b** and **22a,b** were also subjected to Sulforhodamine-B (SRB) assay in order to evaluate their anti-proliferative activity on a pancreatic ductal adenocarcinoma (PDAC) model: PDAC-3 primary cell culture. Gemcitabine was used as reference compound because it is a drug of choice in the treatment of PDAC, but chemoresistance to this drug is common and should prompt the development of new therapeutic approaches. PDAC is an extremely lethal cancer with a 5-year survival rate of approximately 10% in the USA [44], and because of its increasing incidence and mortality rates it is expected to become the second leading cause of cancer-related deaths before 2030 [45]. Despite the recent improvements in the molecular knowledge about this type of

pancreatic neoplasm, the later disease diagnosis and the low effectiveness of available chemotherapeutic agents are the main causes of PDAC poor prognosis [46]. Thus, developing new and more effective drugs to treat PDAC represents an urgent and unmet medical need.

The use of preclinical models which do not take into account the complex molecular and histopathologic features of PDAC may be one of the reasons of the limited effects shown by most of the anticancer agents developed so far in clinical trials. The use of patient-derived primary cell cultures which are *ex vivo* cell populations recovered directly from fresh surgically resected tissue samples has the advantage of preserving the most important original tumor features. Therefore, the primary patient-derived PDAC-3 cell culture was chosen as cellular model in the present

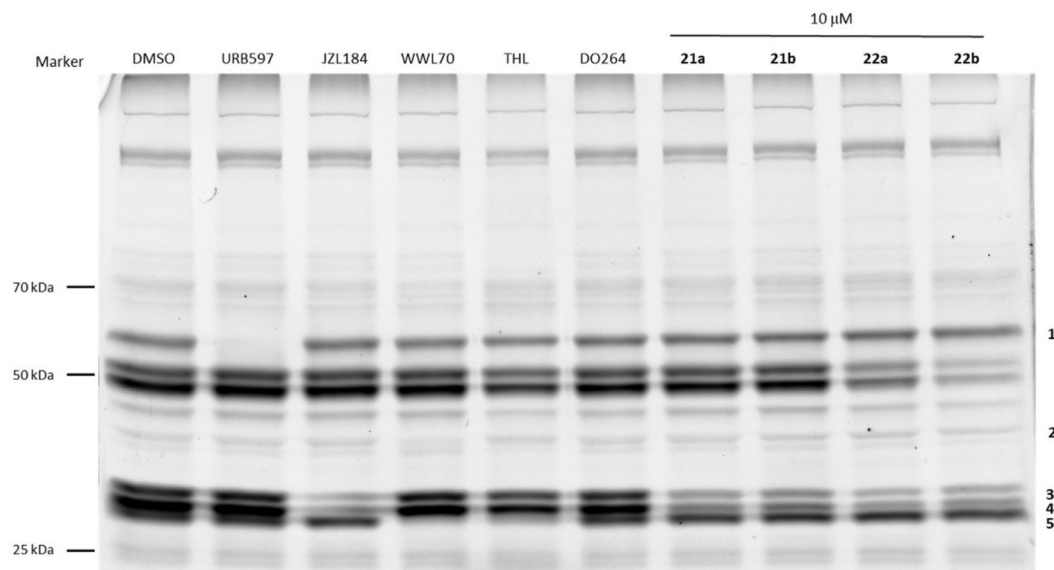


Fig. 9. ABPP fluorescent screen of mouse brain membrane preparations (4 mg/mL) with TAMRA-Fluorophosphonate serine hydrolase probe (TAMRA-FP). The proteome was preincubated for 25 min with either DMSO, URB597 (FAAH inhibitor, 4 μ M), JZL184 (MAGL inhibitor, 1 μ M), WWL70 (ABHD6 inhibitor, 10 μ M), THL (ABHD6 and 12 inhibitor, 20 μ M), DO264 (ABHD12 inhibitor, 5 μ M) or compounds **21a,b** and **22a,b** at 10 μ M followed by 5 min labeling with TAMRA-FP (125 nM final concentration). Band 1 = FAAH, band 2 = ABDH12, band 3 and 4 = doublet of MAGL, band 5 = ABHD6.

Table 6

Cell growth inhibitory activities (IC_{50} values) of CAY10499 (**2**) and compounds **21a**, **21b**, **22a** and **22b**.

IC_{50} (μ M, mean \pm SD)					
Compound	HCT116	MDA-MB-231	CAOV3	OVCAR3	SKOV3
CAY10499 (2)	38 \pm 4	83 \pm 5	95 \pm 4	53 \pm 4	33 \pm 2
21a	5.1 \pm 0.8	43 \pm 5	34 \pm 4	>100	4.6 \pm 0.7
21b	17 \pm 2	25 \pm 3	70 \pm 2	20.7	8 \pm 1
22a	15 \pm 1	63 \pm 5	42 \pm 5	>100	11 \pm 2
22b	5.3 \pm 0.9	65 \pm 4	44 \pm 4	>100	12 \pm 1

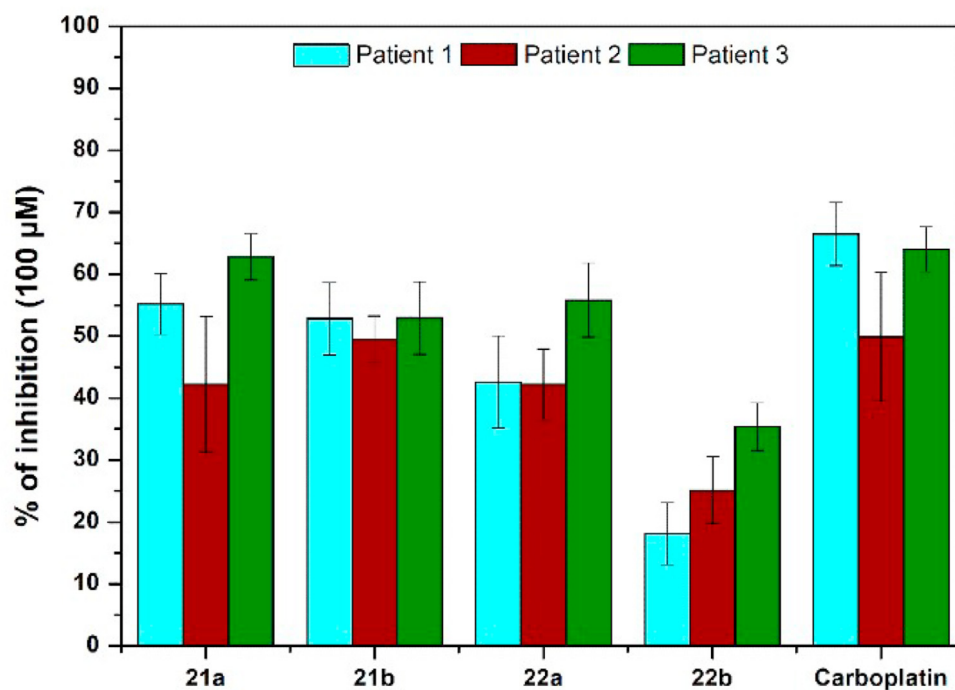


Fig. 10. Growth inhibition of cancer-derived human organoids derived from three HGSOC patients. The activity of compounds **21a,b** and **22a,b** was compared to carboplatin standard chemotherapeutic drug. The % of inhibition is shown at 100 μ M dilution.

study, considering that its genetic, metastatic and histopathological characteristics are comparable to the originator tumor [47]. These cells were cultured *in vitro* only for a few passages (less than 20) to maintain the genetic hallmarks of the primary tumor and before entering into senescence. Moreover, PDAC-3 cell culture was chosen as cellular model since showed an over-expression of MAGL respect to the normal cell line HPDE (fold change = 2.7). Compounds **21a,b** and **22a,b** were tested on PDAC-3 primary cell culture at 8 different concentrations (from 156.25 to 20 000 nM) showing a remarkable antiproliferative activity, with IC₅₀ values in the range of 9.28–14.6 μ M (Table 7).

3. Conclusions

In the present work, the class of benzoylpiperidine-based MAGL inhibitors was expanded and optimized, leading to the identification of compounds **21a,b** and **22a,b**, which are characterized by a potent MAGL inhibition activity, with K_i values ranging from 11 to 37 nM, a reversible mode of action, as well as a high selectivity for MAGL vs. CB1R, CB2R, FAAH, ABHD6 and ABHD12 (IC₅₀ value > 10 μ M in all cases). These four derivatives were also tested in intact human monocytic cell line U937, where they inhibited 2-OG hydrolysis, and showed antiproliferative activities in human breast MDA-MB-231, colorectal HCT116, ovarian CAOV3 and SKOV3 cancer cells at micromolar concentrations. ABPP gels confirmed a broad selectivity towards other serine hydrolases for compound **21a,b**, while compound **22a,b** showed potential off-target inhibition of two non-identified bands at 50–55 KDa. The potential applicability to the clinical setting was supported by the results obtained in additional preclinical models that better mimic the molecular and histopathological complexity of the tumors, such as primary PDAC cells and cancer organoids derived from high grade serous ovarian cancer patients. These models have the advantage of maintaining the original genotype and phenotype of the tumors and represent an important tool for the experimental testing of anticancer agents, that could directly counsel individualized decisions in future clinical trials. Taken together, these results suggest that these derivatives are among the most active and selective reversible MAGL inhibitors reported in the literature so far and may therefore open up new perspectives for studying the therapeutic potential of reversible MAGL inhibition. Finally, the applicability in clinical setting was demonstrated in cancer organoids derived from high grade serous ovarian cancer patients.

4. Experimental section

4.1. Synthesis. General procedures and materials

All solvents and chemicals were used as purchased without further purification. Chromatographic separations were performed on silica gel columns by flash chromatography (Kieselgel 40, 0.040–0.063 mm; Merck). Reactions were followed by thin layer chromatography (TLC) on Merck aluminum silica gel (60 F254)

sheets that were visualized under a UV lamp. Evaporation was performed *in vacuo* (rotating evaporator). Sodium sulfate was always used as the drying agent. Proton (¹H) and carbon (¹³C) NMR spectra were obtained with a Bruker Avance III 400 MHz spectrometer using the indicated deuterated solvents. Chemical shifts are given in parts per million (ppm) (δ relative to residual solvent peak for ¹H and ¹³C). ¹H NMR spectra are reported in this order: multiplicity and number of protons. Standard abbreviation indicating the multiplicity were used as follows: s = singlet, d = doublet, dd = doublet of doublets, ddd = doublet of doublet of doublets, t = triplet, tt = triplet of triplets, dt = doublet of triplets, td = triplet of doublets, quint = quintet, sept = septet, m = multiplet, bm = broad multiplet and bs = broad singlet. HPLC analysis was used to determine purity: all target compounds (i.e., assessed in biological assays) were \geq 95% pure by HPLC, as confirmed via UV detection (λ = 254 nm). Analytical reversed-phase HPLC was conducted using a Kinetex EVO C18 column (5 μ m, 150 \times 4.6 mm, Phenomenex, Inc.); eluent A, water; eluent B, CH₃CN; after 5 min at 25% B, a gradient was formed from 25% to 75% of B in 5 min and held at 75% of B for 10 min; flow rate was 1 mL/min. HPLC analyses were performed at 254 nm. Elemental analysis was used to further characterize the final compounds; analytical results are within \pm 0.4% of the theoretical value. Yields refer to isolated and purified products derived from non-optimized procedures. Compound **2** was purchased from Cayman Chemical and compounds **10**, **11**, **23** and **42** were synthesized as previously reported [24].

4.1.1. General procedure for the synthesis of amide derivatives 25, 27, 29, 33, 37, 14–17, 46, 49, 52–54, 59, 60, 63–65, 68, 83–85

HATU (1.05 equiv) was added to a solution of the appropriate benzoic acid (1 equiv) in dry DMF (2.1 mL), then DIPEA (4 equiv) was added dropwise. The resulting mixture was stirred at room temperature for 30 min and then the proper amine (100 mg, 1 equiv) was added and left under stirring at room temperature until consumption of starting material (TLC). After this time, the residue was diluted with water and extracted with EtOAc. The organic layer was repeatedly washed with brine, dried over Na₂SO₄ and the solvent was removed under reduced pressure. The residue was purified with a flash column chromatography (silica gel, an appropriate mixture of *n*-hexane or petroleum ether/ethyl acetate or CHCl₃/MeOH) and pure fractions containing the desired compound were evaporated to dryness affording the amides.

4.1.2. General procedure for the synthesis of O-deprotected benzoylpiperidines 12, 13a–d, 18, 19, 20a–d, 20f–i, 21a,b, 22a,b

A solution of pure O-methylated amides (0.23 mmol) in anhydrous CH₂Cl₂ (2.7 mL) was cooled to –10 °C and treated dropwise with a 1.0 M solution of BBr₃ in CH₂Cl₂ (0.73 mL) under argon. The mixture was left under stirring at the same temperature for 5 min and then at 0 °C for 1 h and finally at RT until starting material was consumed (TLC). The mixture was then diluted with water and extracted with ethyl acetate. The organic phase was washed with

Table 7
Cell growth inhibitory activities (IC₅₀ values) of Gemcitabine and compounds **21a,b** and **22a,b**.

IC ₅₀ (μ M) \pm SEM	
Compound	PDAC-3
Gemcitabine	0.00554 \pm 0.00044
21a	9.28 \pm 0.91
21b	12.5 \pm 0.1
22a	14.6 \pm 1.3
22b	12.0 \pm 0.6

brine, dried and concentrated. The crude product was purified by flash chromatography over silica gel. Elution with *n*-hexane/EtOAc or CHCl₃/MeOH mixtures afforded the desired compounds.

4.1.3. Procedure for the synthesis of sulfoxide derivative 20e

To the mixture of sulfide **20c** (27 mg, 1 equiv) in acetic acid (4 mL), TAPC (0.22 equiv) and 30% H₂O₂ (2.2 equiv) were added at room temperature with continuous stirring overnight. The progress of the reaction was monitored by TLC and TAPC (0.22 equiv) and 30% H₂O₂ (2.2 equiv) were added to consume the starting material. After the completion of the reaction, H₂O was added to the reaction mixture and the residue was then extracted with EtOAc and the combined extracts were dried (Na₂SO₄). The filtrate was evaporated and the corresponding sulfoxide was obtained after purification by flash chromatography.

4.1.4. General procedure for the synthesis of methyl 3-methoxybenzoates 30 and 35

A solution of commercially available 5-methoxy-2-nitrobenzoic acid **28** or 5-hydroxy-2-methylbenzoic acid **34** (500 mg, 1 equiv) in 10 mL of DMF was treated with anhydrous K₂CO₃ (2.2 equiv) and iodomethane (3 equiv) and the reaction mixture was stirred at room temperature for 4–5 h. The mixture was diluted with water and extracted with ethyl acetate. The organic extract was washed with brine, dried over Na₂SO₄ and the organic solvent was removed under vacuum on a rotary evaporator. The crude product afforded the pure desired compounds **30** and **35**, that were used in the next step without further purification.

4.1.5. Procedure for the synthesis of compound 31

Nitro-substituted derivative **30** (240 mg, 1.14 mmol, 1 equiv) was dissolved in 1:1 *v/v* CHCl₃/MeOH mixture (6.2 mL), then SnCl₂·2H₂O (8 equiv) was added and the mixture was heated at 65 °C for 1 h. Upon consumption of starting material, the mixture was concentrated, diluted with water, neutralized with 1 N aqueous NaOH, extracted with EtOAc and the organic phase was washed with brine. The combined organic phase was dried over anhydrous sodium sulfate, filtered and evaporated, affording a crude residue which was used in the next step without further purification.

4.1.6. General procedure for the synthesis of 3-methoxybenzoic acids 32 and 36

Methyl esters **31** or **35** (190 mg, 1 equiv) were dissolved in a 1:1 *v/v* mixture of THF/methanol (10.6 mL) and treated with 3.2 mL of 2 N aqueous solution of LiOH. The reaction was stirred until consumption of starting material, then the solvents were evaporated, and the residue was treated with 1 N aqueous HCl and extracted with EtOAc. The organic phase was dried and evaporated to afford the pure desired carboxylic acid derivatives.

4.1.7. General procedure for the synthesis of compounds 43, 47, 50

To a cooled suspension of 1-acetylpiperidine-4-carboxylic acid **42** (500 mg, 1 equiv) in 2.7 mL of anhydrous 1,2-dichloroethane was slowly added SOCl₂ (2.3 equiv). The mixture was stirred at 60 °C for 4 h (the mixture turned from white to orange) and then evaporated under vacuum. Under argon atmosphere, the residue acyl chloride was dissolved in 2.2 mL of anhydrous 1,2-dichloroethane, then the reddish solution was cooled at 0 °C and AlCl₃ (2 equiv) was slowly added. Finally, a solution of the aromatic reagent (1 equiv; bromobenzene for **43**, phenylcyclohexane for **47**, diphenylmethane for **50**) in anhydrous 1,2-dichloroethane (1.3 mL) was added dropwise. The mixture was stirred at 90 °C overnight. The solution was cooled to room temperature and poured into ice. The water layer was extracted with EtOAc, the combined organic phase was washed with brine, dried over anhydrous sodium sulfate and concentrated

in vacuo. The residue was purified by silica gel chromatography using appropriate *n*-hexane or petroleum ether/EtOAc mixtures.

4.1.8. Procedure for the synthesis of compound 44

Substituted bromobenzene **43** (96 mg, 0.31 mmol, 1 equiv), cyclopropylboronic acid (1.3 equiv), and K₃PO₄ (3.5 equiv) were added to a sealed vial under argon atmosphere. Toluene (1.4 mL), 20 wt % solution of P(Cy)₃ in toluene (0.1 equiv, 0.05 mL) and Pd(OAc)₂ (0.05 equiv) were added to the reaction mixture. The reaction mixture was heated to 100 °C and stirred for 24 h. After removing from heat, the reaction mixture was diluted with EtOAc, filtered through Celite, and concentrated. The crude product was purified by flash column chromatography to obtain the desired compound.

4.1.9. General procedure for the synthesis of piperidine derivatives 45, 48, 51, 57, 58, 62, 67, 80–82

To a solution of *N*-acetylated intermediates **44**, **47**, **50**, **55**, **56**, **61**, **66**, **77–79** (400 mg) in 17 mL of EtOH, 1 N aqueous solution of NaOH was added (17 mL). The reaction mixture was heated at 90 °C overnight. The solution was cooled to room temperature, then concentrated under reduced pressure, diluted with water and extracted with EtOAc. The organic layer was washed with brine, dried over Na₂SO₄ and concentrated to dryness to obtain the pure desired compounds that were used in the next step without further purification.

4.1.10. Procedure for the synthesis of compound 55

A solution of Pd₂dba₃ (0.02 equiv), XPhos (0.08 equiv), potassium *tert*-butoxide (1.4 equiv), commercially available aniline (1.2 equiv) and intermediate **43** (100 mg, 1 equiv) in toluene (0.6 mL) was stirred at 100 °C under inert atmosphere in a sealed vial for 24 h. The reaction mixture was allowed to cool to room temperature, then filtered through a small pad of Celite, washed with ethyl acetate and concentrated under vacuum. The obtained crude residue was purified by flash column chromatography (eluent mixture *n*-hexane/EtOAc) to give intermediate **55**.

4.1.11. Procedure for the synthesis of compound 56

A sealed vial was charged with Me₄tBuXPhos (0.03 equiv), Pd(OAc)₂ (0.02 equiv), K₃PO₄ (2 equiv), intermediate **43** (100 mg, 1 equiv), commercially available phenol (1.2 equiv) and toluene (0.6 mL) under a positive pressure of argon. The resulting mixture was heated at 100 °C for 24 h. Then the mixture was allowed to cool to room temperature and then filtered through a small pad of Celite, washed several times with ethyl acetate and the filtrate was concentrated under reduced pressure. The crude product was purified by flash chromatography on silica gel (*n*-hexane/EtOAc mixture) to afford compound **56**.

4.1.12. Procedure for the synthesis of compound 61

A sealed vial was charged with K₂CO₃ (1 equiv), compound **43** (200 mg, 1 equiv), Pd₂(dba)₃ (0.1 equiv), Xantphos (0.11 equiv), toluene (9.7 mL), and commercially available thiophenol (1.25 equiv). After purging with argon, the resulting mixture was then heated at 120 °C for 24 h. After cooling to room temperature, the mixture was diluted with EtOAc and water, the organic phase was washed with brine, dried over Na₂SO₄ and concentrated under reduced pressure. The crude product was then purified by silica gel chromatography to afford the expected product.

4.1.13. Procedure for the synthesis of sulfone derivative 66

An aqueous solution (1.1 mL) of Oxone® (50% w/v, 3 equiv) was added dropwise to a stirred solution of the sulfide derivative **61** (100 mg, 1 equiv) in 1,4-dioxane (3.0 mL) at 0 °C, and the reaction

was allowed to proceed with stirring at RT for 12 h. The reaction mixture was diluted with water, extracted with EtOAc, the organic phase was washed successively with water and brine, and dried over anhydrous sodium sulfate. After filtration, the solvent from the organic fraction was evaporated to give the desired crude product which was used in the next reaction without any further purification.

4.1.14. Procedure for the synthesis of compound 69

A solution of Pd(OAc)₂ (0.05 equiv) and triphenylphosphine (0.25 equiv) in dry DMF (0.2 mL) was stirred at RT under argon for 10 min. After that period, aryl-bromide **43** (100 mg, 1 equiv), copper iodide (0.05 equiv), 2-methyl-3-butyne-2-ol (1.2 equiv) and Et₃N (1.0 mL) were sequentially added. The mixture was stirred at 90 °C for 4 h. After being cooled to RT, the mixture was diluted with water and extracted several times with EtOAc. The combined organic phase was washed with brine, dried over anhydrous sodium sulfate and concentrated. The crude product was purified by flash chromatography to yield the product.

4.1.15. Procedure for the synthesis of compound 70

Compound **69** (130 mg, 1 equiv) was suspended in toluene (16.5 mL), then potassium hydroxide (1 equiv) and potassium phosphate (1 equiv) were added and the mixture was refluxed at 115 °C for 24 h. The reaction mixture was cooled to RT, filtered through a small pad of Celite and washed several times with ethyl acetate. Evaporation under vacuum of the filtrate afforded compound **70**.

4.1.16. General procedure for the synthesis of azides 74-76

To a solution of aniline **71** (500 mg, 5.37 mmol, 1 equiv) in aqueous 4 N HCl (7.8 mL) cooled to −5 °C was added dropwise a solution of sodium nitrite (1.2 equiv) in water (1.4 mL) and the mixture was stirred at the same temperature for 30 min. Then, another solution of sodium azide (1.2 equiv) in water (1.7 mL) was added dropwise, keeping the temperature below 0 °C. Stirring was continued for 1 h at 0 °C and overnight at room temperature. The reaction mixture was then extracted with EtOAc and the combined organic phase was washed with a saturated solution of NaHCO₃ and brine, then dried and concentrated under vacuum, to obtain pure **74** without any further purification. In the case of aliphatic azides **75** and **76**, imidazole-1-sulfonyl azide hydrochloride (0.86 g, 4.9 mmol, 1.2 equiv) [28] was added to the commercially available amine (benzylamine **72** or 3-phenyl-1-propylamine **73**, 1 equiv), K₂CO₃ (1.7 equiv) and CuSO₄·5H₂O (0.01 equiv) in MeOH (20.6 mL) and the mixture was stirred at room temperature for 2.5 h. The mixture was concentrated, diluted with H₂O, acidified with conc. HCl and extracted with EtOAc. The combined organic layers were dried, filtered and concentrated. The crude product was purified by flash chromatography to give the desired azides.

4.1.17. General procedure for the synthesis of triazole-substituted derivatives 77-79

Alkyne **70** (287 mg, 1 equiv) and azides **74**, **75** or **76** (1 equiv) were suspended in a 1:1 mixture of water and tert-butyl alcohol (4.5 mL). A freshly prepared sodium ascorbate aqueous solution (0.1 equiv, 1.1 mL of water) was added, followed by copper (II) sulfate pentahydrate aqueous solution (0.01 equiv, 0.04 mL of water). The heterogeneous mixture was stirred vigorously at 80 °C in a sealed vial until consumption of the starting materials. The reaction mixture was cooled, diluted with water, extracted with EtOAc. The combined organic extracts were washed with brine, dried with anhydrous Na₂SO₄, filtered and concentrated. The crude product was purified by flash column chromatography to obtain the title triazole-substituted compounds.

4.1.17.1. (1-(2,4-Difluoro-5-hydroxybenzoyl)piperidin-4-yl)(4-isopropylphenyl)methanone (**12**). White solid; 60% yield from **25**, eluent *n*-hexane/EtOAc 6:4. ¹H NMR (DMSO-*d*₆) δ (ppm): 1.22 (d, 6H, *J* = 6.9 Hz), 1.38–1.54 (bm, 2H), 1.70–1.79 (bm, 1H), 1.84–1.93 (bm, 1H), 2.91–3.04 (m, 2H), 3.17–3.28 (m, 1H), 3.44–3.54 (m, 1H), 3.68–3.79 (m, 1H), 4.43–4.53 (m, 1H), 6.89 (dd, 1H, *J* = 9.5, 6.6 Hz), 7.29 (dd, 1H, *J* = 11.1, 9.3 Hz), 7.41 (d, 2H, *J* = 8.2 Hz), 7.93 (d, 2H, *J* = 8.4 Hz), 10.13 (exchangeable bs, 1H). ¹³C NMR (DMSO-*d*₆) δ (ppm): 23.46 (2C), 28.27, 28.62, 33.47, 40.74, 42.09, 45.96, 105.00 (dd, *J*_{CF} = 27.4, 23.0 Hz), 116.00 (t, *J*_{CF} = 4.5 Hz), 120.07 (dd, *J*_{CF} = 19.7, 4.2 Hz), 126.78 (2C), 128.51 (2C), 133.31, 141.85 (dd, *J*_{CF} = 12.3, 2.9 Hz), 149.05 (dd, *J*_{CF} = 104.0, 11.4 Hz), 151.46 (dd, *J*_{CF} = 112.0, 11.4 Hz), 154.19, 163.13, 201.30. HPLC analysis: retention time = 12.486 min; peak area, 97% (254 nm). Elemental analysis for C₂₂H₂₃F₂NO₃, calculated: % C, 68.20; % H, 5.98; % N, 3.62; found: % C, 68.02; % H, 6.30; % N, 3.35.

4.1.17.2. (1-(5-Hydroxy-2-(trifluoromethyl)benzoyl)piperidin-4-yl)(4-isopropylphenyl)methanone (**13a**). Light yellow solid; 6% yield from **27**, eluent *n*-hexane/EtOAc 6:4. ¹H NMR (DMSO-*d*₆; asterisk denotes isomer peaks) δ (ppm): 1.22 (d, 6H, *J* = 6.9 Hz), 1.34–1.58 (bm, 2H), 1.62–1.77 (m, 1H), 1.83–1.95 (bm, 1H), 2.90–3.29 (m, 4H), 3.64–3.80 (bm, 1H), 4.45–4.55 (m, 1H), 6.70* (d, 1H, *J* = 2.2 Hz), 6.75 (d, 1H, *J* = 2.4 Hz), 6.91–6.99 (m, 1H), 7.41 (d, 2H, *J* = 7.8 Hz), 7.59 (d, 1H, *J* = 8.8 Hz), 7.90–7.98 (m, 2H), 10.59 (exchangeable s, 1H). ¹³C NMR (DMSO-*d*₆; asterisk denotes isomer peaks) δ (ppm): 23.40 (2C), 23.42* (2C), 27.64*, 27.89, 28.09, 28.22*, 33.42, 40.17, 40.31*, 41.90*, 42.08, 45.86*, 45.92, 113.33, 113.52*, 115.51*, 115.74, 124.23 (q, *J*_{CF} = 281.7 Hz), 126.74 (2C), 128.46 (2C), 128.57, 133.24, 136.88, 154.13*, 154.16, 160.52*, 160.63, 165.71*, 165.86, 201.27. HPLC analysis: retention time = 12.898; peak area, 96% (254 nm). Elemental analysis for C₂₃H₂₄F₃NO₃, calculated: % C, 65.86; % H, 5.77; % N, 3.34; found: % C, 65.50; % H, 5.92; % N, 3.71.

4.1.17.3. (1-(5-Hydroxy-2-nitrobenzoyl)piperidin-4-yl)(4-isopropylphenyl)methanone (**13b**). Light yellow solid; 22% yield from **29**, eluent EtOAc/MeOH 95:5. ¹H NMR (DMSO-*d*₆) δ (ppm): 1.22 (d, 6H, *J* = 6.9 Hz), 1.41–1.61 (bm, 2H), 1.61–1.75 (bm, 1H), 1.84–1.97 (bm, 1H), 2.91–3.07 (m, 2H), 3.07–3.18 (bm, 1H), 3.35–3.47 (m, 1H), 3.65–3.80 (m, 1H), 4.40–4.57 (m, 1H), 6.68–6.78 (m, 1H), 6.95 (dd, 1H, *J* = 9.1, 2.6 Hz), 7.41 (d, 2H, *J* = 8.2 Hz), 7.88–8.00 (m, 2H), 8.12 (d, 1H, *J* = 8.3 Hz), 11.29 (exchangeable bs, 1H). ¹³C NMR (DMSO-*d*₆) δ (ppm): 23.45 (2C), 28.09, 33.46, 40.40, 113.66, 116.16, 126.45, 126.77 (2C), 127.69, 128.50 (2C), 129.90, 133.31, 135.73, 149.20, 154.20, 163.46.

HPLC analysis: retention time = 12.279 min; peak area, 98% (254 nm). Elemental analysis for C₂₂H₂₄N₂O₅, calculated: % C, 66.65; % H, 6.10; % N, 7.07; found: % C, 66.99; % H, 6.12; % N, 7.01.

4.1.17.4. (1-(2-Amino-5-hydroxybenzoyl)piperidin-4-yl)(4-isopropylphenyl)methanone (**13c**). Light yellow solid; 59% yield from **33**, eluent *n*-hexane/EtOAc 3:7. ¹H NMR (DMSO-*d*₆) δ (ppm): 1.22 (d, 6H, *J* = 6.9 Hz), 1.45–1.58 (m, 2H), 1.74–1.85 (m, 2H), 2.97 (sept, 1H, *J* = 6.7 Hz), 3.02–3.14 (m, 2H), 3.70 (tt, 1H, *J* = 11.4, 3.6 Hz), 3.95–4.10 (bm, 2H), 4.48 (s, 2H), 6.43 (t, 1H, *J* = 1.6 Hz), 6.57 (d, 2H, *J* = 1.6 Hz), 7.41 (d, 2H, *J* = 8.2 Hz), 7.93 (d, 2H, *J* = 8.4 Hz), 8.62 (exchangeable s, 1H). ¹³C NMR (DMSO-*d*₆) δ (ppm): 23.44 (2C), 28.52, 33.44, 42.36, 113.27, 117.08, 117.33, 120.93, 126.74 (2C), 128.46 (2C), 133.37, 137.81, 147.87, 154.09, 168.42, 201.45. HPLC analysis: retention time = 11.174 min; peak area, 95% (254 nm). Elemental analysis for C₂₂H₂₆N₂O₃, calculated: % C, 72.11; % H, 7.15; % N, 7.64; found: % C, 71.84; % H, 7.29; % N, 7.31.

4.1.17.5. (1-(5-Hydroxy-2-methylbenzoyl)piperidin-4-yl)(4-isopropylphenyl)methanone (**13d**). White solid; 48% yield from **37**,

eluent *n*-hexane/EtOAc 55:45. ^1H NMR (DMSO- d_6 ; asterisk denotes isomer peaks) δ (ppm): 1.22 (d, 6H, J = 6.9 Hz), 1.34–1.55 (bm, 2H), 1.64–1.77 (bm, 1H), 1.85–1.94 (bm, 1H), 2.07 (s, 3H), 2.10* (s, 3H), 2.90–3.05 (bm, 1H), 2.97 (sept, 1H, J = 7.0 Hz), 3.08–3.20 (m, 1H), 3.35–3.45 (bm, 1H), 3.65–3.77 (bm, 1H), 4.48–4.59 (bm, 1H), 6.51* (bs, 1H), 6.54 (bs, 1H), 6.68 (dd, 1H, J = 8.2, 2.6 Hz), 7.04 (d, 1H, J = 8.2 Hz), 7.41 (d, 2H, J = 8.2 Hz), 7.93 (d, 2H, J = 8.4 Hz), 9.39 (exchangeable s, 1H). ^{13}C NMR (DMSO- d_6) δ (ppm): 17.49, 23.43 (2C), 28.39, 28.82, 33.44, 42.21, 45.30, 45.81, 112.01, 115.48, 123.17, 126.76 (2C), 128.47 (2C), 131.13, 133.27, 137.32, 154.15, 155.13, 168.34, 201.34. HPLC analysis: retention time = 12.215 min; peak area, 98% (254 nm). Elemental analysis for $\text{C}_{23}\text{H}_{27}\text{NO}_3$, calculated: % C, 75.59; % H, 7.45; % N, 3.83; found: % C, 75.68; % H, 7.40; % N, 3.69.

4.1.17.6. (1-(4-Hydroxypicolinoyl)piperidin-4-yl)(4-isopropylphenyl) methanone (14). White solid; 56% yield from **23** and 4-hydroxypyridine-2-carboxylic acid **38**, eluent $\text{CHCl}_3/\text{MeOH}$ 95:5. ^1H NMR (DMSO- d_6) δ (ppm): 1.22 (d, 6H, J = 6.9 Hz), 1.43–1.60 (bm, 2H), 1.67–1.77 (bm, 1H), 1.83–1.93 (bm, 1H), 2.91–3.05 (m, 2H), 3.14–3.26 (bm, 1H), 3.66–3.80 (bm, 2H), 4.41–4.52 (bm, 1H), 6.70–6.94 (bm, 2H), 7.41 (d, 2H, J = 8.3 Hz), 7.94 (d, 2H, J = 8.4 Hz), 8.16–8.30 (bm, 1H), 10.94 (exchangeable bs, 1H). ^{13}C NMR (acetone- d_6) δ (ppm): 23.93 (2C), 34.88, 42.23 (2C), 43.68, 47.25 (2C), 112.72, 114.11, 127.62 (2C), 129.45 (2C), 129.64, 131.96, 134.81, 147.92, 155.25, 166.92, 201.83. HPLC analysis: retention time = 9.940 min; peak area, 99% (254 nm). Elemental analysis for $\text{C}_{21}\text{H}_{24}\text{N}_2\text{O}_3$, calculated: % C, 71.57; % H, 6.86; % N, 7.95; found: % C, 71.60; % H, 6.93; % N, 8.01.

4.1.17.7. (1-(5-Hydroxynicotinoyl)piperidin-4-yl)(4-isopropylphenyl) methanone (15). Light yellow solid; 57% yield from **23** and 5-hydroxynicotinic acid **39**, eluent $\text{CHCl}_3/\text{MeOH}$ 95:5. ^1H NMR (DMSO- d_6) δ (ppm): 1.22 (d, 6H, J = 6.9 Hz), 1.45–1.58 (m, 2H), 1.68–1.96 (bm, 2H), 2.93–3.09 (bm, 1H), 2.97 (sept, 1H, J = 6.9 Hz), 3.18–3.37 (m, 1H), 3.55–3.68 (bm, 1H), 3.73 (tt, 1H, J = 11.3, 3.5 Hz), 4.39–4.54 (bm, 1H), 7.14 (dd, 1H, J = 2.7, 1.8 Hz), 7.41 (d, 2H, J = 8.2 Hz), 7.94 (d, 2H, J = 8.4 Hz), 8.04 (d, 1H, J = 1.7 Hz), 8.18 (d, 1H, J = 2.8 Hz), 10.25 (exchangeable bs, 1H). ^{13}C NMR (DMSO- d_6) δ (ppm): 23.44 (2C), 28.22, 28.59, 33.46, 40.99, 42.15, 46.51, 120.10, 126.76 (2C), 128.50 (2C), 132.50, 133.30, 137.81, 138.83, 153.32, 154.14, 166.51, 201.28. HPLC analysis: retention time = 11.049 min; peak area, 98% (254 nm). Elemental analysis for $\text{C}_{21}\text{H}_{24}\text{N}_2\text{O}_3$, calculated: % C, 71.57; % H, 6.86; % N, 7.95; found: % C, 71.66; % H, 7.02; % N, 8.14.

4.1.17.8. (1-(2-Hydroxyisonicotinoyl)piperidin-4-yl)(4-isopropylphenyl) methanone (16). Amber solid; 50% yield from **23** and 2-hydroxypyridine-4-carboxylic acid **40**, eluent $\text{CHCl}_3/\text{MeOH}$ 95:5. ^1H NMR (DMSO- d_6) δ (ppm): 1.22 (d, 6H, J = 6.9 Hz), 1.42–1.55 (m, 2H), 1.71–1.81 (bm, 1H), 1.82–1.92 (bm, 1H), 2.90–3.03 (m, 2H), 3.14–3.29 (m, 1H), 3.56–3.66 (m, 1H), 3.72 (tt, 1H, J = 11.0, 3.1 Hz), 4.36–4.45 (m, 1H), 6.12 (dd, 1H, J = 6.6, 1.6 Hz), 6.23 (d, 1H, J = 0.8 Hz), 7.41 (d, 2H, J = 8.2 Hz), 7.44 (d, 1H, J = 6.8 Hz), 7.93 (d, 2H, J = 8.3 Hz), 11.74 (exchangeable bs, 1H). ^{13}C NMR (DMSO- d_6) δ (ppm): 23.46 (2C), 28.07, 28.55, 33.47, 40.50, 42.12, 45.99, 102.88, 116.45, 126.77 (2C), 128.51 (2C), 133.29, 136.50, 148.57, 154.14, 161.99, 166.25, 201.24. HPLC analysis: retention time = 10.364 min; peak area, 97% (254 nm). Elemental analysis for $\text{C}_{21}\text{H}_{24}\text{N}_2\text{O}_3$, calculated: % C, 71.57; % H, 6.86; % N, 7.95; found: % C, 71.45; % H, 6.99; % N, 7.90.

4.1.17.9. (1-(6-Hydroxypicolinoyl)piperidin-4-yl)(4-isopropylphenyl) methanone (17). White solid; 53% yield from **23** and 6-hydroxypyridine-2-carboxylic acid **41**, eluent $\text{CHCl}_3/\text{MeOH}$ 98:2. ^1H NMR (DMSO- d_6) δ (ppm): 1.22 (d, 6H, J = 6.9 Hz), 1.45–1.68

(bm, 2H), 1.70–1.95 (bm, 2H), 2.90–3.07 (m, 2H), 3.14–3.30 (bm, 1H), 3.53–3.68 (bm, 1H), 3.69–3.80 (m, 1H), 4.32–4.50 (bm, 1H), 6.35–6.52 (bm, 2H), 7.41 (d, 2H, J = 8.2 Hz), 7.46–7.57 (bm, 1H), 7.94 (d, 2H, J = 8.3 Hz), 11.65 (exchangeable bs, 1H). ^{13}C NMR (DMSO- d_6) δ (ppm): 23.48 (2C), 27.92, 28.40, 33.49, 40.81, 42.15, 46.04, 126.80 (2C), 128.53 (2C), 133.32, 140.43, 154.20 (2C), 162.31, 163.45, 201.34. HPLC analysis: retention time = 10.682 min; peak area, 99% (254 nm). Elemental analysis for $\text{C}_{21}\text{H}_{24}\text{N}_2\text{O}_3$, calculated: % C, 71.57; % H, 6.86; % N, 7.95; found: % C, 71.88; % H, 6.89; % N, 8.04.

4.1.17.10. (4-(4-Cyclohexylbenzoyl)piperidin-1-yl)(3-hydroxyphenyl) methanone (18). Light yellow solid; 28% yield from **49**, eluent *n*-hexane/EtOAc 6:4. ^1H NMR (DMSO- d_6) δ (ppm): 1.30–1.55 (bm, 5H), 1.66–1.94 (bm, 8H), 2.53–2.64 (bm, 1H), 2.86–3.27 (bm, 3H), 3.56–3.80 (bm, 2H), 4.36–4.53 (bm, 1H), 6.71–6.75 (m, 1H), 6.77 (dt, 1H, J = 7.7, 1.2 Hz), 6.81 (ddd, 1H, J = 8.2, 2.5, 0.9 Hz), 7.22 (t, 1H, J = 7.8 Hz), 7.38 (d, 2H, J = 8.3 Hz), 7.93 (d, 2H, J = 8.4 Hz), 9.67 (exchangeable s, 1H). ^{13}C NMR (DMSO- d_6) δ (ppm): 25.46, 26.18 (2C), 28.50 (2C), 33.51 (2C), 42.24, 43.76, 46.43 (2C), 113.36, 116.27, 117.04, 127.15 (2C), 128.48 (2C), 129.58, 133.31, 137.49, 153.26, 157.25, 168.90, 201.37. HPLC analysis: retention time = 13.220 min; peak area, 96% (254 nm). Elemental analysis for $\text{C}_{25}\text{H}_{29}\text{NO}_3$, calculated: % C, 76.70; % H, 7.47; % N, 3.58; found: % C, 77.05; % H, 7.80; % N, 3.86.

4.1.17.11. (4-(4-Cyclopropylbenzoyl)piperidin-1-yl)(3-hydroxyphenyl) methanone (19). White solid; 59% yield from **46**, eluent *n*-hexane/EtOAc 5:5. ^1H NMR (DMSO- d_6) δ (ppm): 0.74–0.80 (m, 2H), 1.01–1.09 (m, 2H), 1.41–1.55 (m, 2H), 1.63–1.94 (bm, 2H), 1.96–2.05 (m, 1H), 2.87–3.05 (bm, 1H), 3.07–3.25 (bm, 1H), 3.58–3.77 (bm, 2H), 4.40–4.52 (bm, 1H), 6.72–6.75 (m, 1H), 6.76 (dt, 1H, J = 7.6, 1.2 Hz), 6.81 (ddd, 1H, J = 8.1, 2.4, 0.9 Hz), 7.19–7.26 (m, 3H), 7.88 (d, 2H, J = 8.4 Hz), 9.67 (exchangeable s, 1H). ^{13}C NMR (DMSO- d_6) δ (ppm): 10.49 (2C), 15.33, 28.49 (2C), 42.17, 46.44 (2C), 113.35, 116.27, 117.04, 125.49 (2C), 128.41 (2C), 129.58, 132.64, 137.48, 150.19, 157.24, 168.90, 201.16. HPLC analysis: retention time = 11.559 min; peak area, 99% (254 nm). Elemental analysis for $\text{C}_{22}\text{H}_{23}\text{NO}_3$, calculated: % C, 75.62; % H, 6.63; % N, 4.01; found: % C, 75.83; % H, 6.59; % N, 4.00.

4.1.17.12. (1-(3-Hydroxybenzoyl)piperidin-4-yl)(4-(phenylamino) phenyl) methanone (20a). Yellow solid; 25% yield from **59**, eluent $\text{CHCl}_3/\text{MeOH}$ 98:2. ^1H NMR (DMSO- d_6) δ (ppm): 1.40–1.90 (m, 5H), 2.83–3.06 (bm, 1H), 3.55–3.72 (m, 2H), 4.37–4.55 (bm, 1H), 6.72–6.79 (m, 2H), 6.81 (ddd, 1H, J = 8.2, 2.4, 0.9 Hz), 7.00 (t, 1H, J = 7.3 Hz), 7.07 (d, 2H, J = 8.9 Hz), 7.17–7.21 (m, 2H), 7.23 (t, 1H, J = 7.8 Hz), 7.29–7.36 (m, 2H), 7.89 (d, 2H, J = 8.9 Hz), 8.85 (exchangeable s, 1H), 9.67 (exchangeable s, 1H). ^{13}C NMR (DMSO- d_6) δ (ppm): 28.81, 41.08, 41.72, 46.56, 113.37, 113.96 (2C), 116.29, 117.07, 119.52 (3C), 122.07, 125.84, 129.36 (2C), 129.62, 130.54, 137.54, 141.14, 148.72, 157.29, 168.93, 199.27. HPLC analysis: retention time = 11.606 min; peak area, 96% (254 nm). Elemental analysis for $\text{C}_{25}\text{H}_{24}\text{N}_2\text{O}_3$, calculated: % C, 74.98; % H, 6.04; % N, 7.00; found: % C, 74.70; % H, 5.87; % N, 7.12.

4.1.17.13. (1-(3-Hydroxybenzoyl)piperidin-4-yl)(4-phenoxyphenyl) methanone (20b). White solid; 78% yield from **60**, *n*-hexane/EtOAc 5:5. ^1H NMR (DMSO- d_6) δ (ppm): 1.43–1.55 (m, 2H), 1.67–1.94 (bm, 2H), 2.89–3.26 (bm, 2H), 3.59–3.77 (m, 2H), 4.39–4.53 (bm, 1H), 6.72–6.75 (m, 1H), 6.77 (dt, 1H, J = 7.4, 1.2 Hz), 6.82 (ddd, 1H, J = 8.1, 2.4, 0.9 Hz), 7.06 (AA'XX', 2H, J_{AX} = 8.9 Hz, $J_{\text{AA'}/\text{XX'}}$ = 2.4 Hz), 7.11–7.16 (m, 2H), 7.19–7.28 (m, 2H), 7.42–7.50 (m, 2H), 8.04 (AA'XX', 2H, J_{AX} = 8.9 Hz, $J_{\text{AA'}/\text{XX'}}$ = 2.4 Hz), 9.67 (exchangeable s, 1H). ^{13}C NMR (DMSO- d_6) δ (ppm): 28.47 (2C), 40.94, 42.20, 46.42, 113.38, 116.29, 117.07, 117.30 (2C), 120.01 (2C), 124.80, 129.60, 130.16,

130.35 (2C), 130.87 (2C), 137.49, 154.95, 157.27, 161.31, 168.91, 200.37. HPLC analysis: retention time = 12.218 min; peak area, 95% (254 nm). Elemental analysis for $C_{25}H_{23}NO_4$, calculated: % C, 74.79; % H, 5.77; % N, 3.49; found: % C, 74.89; % H, 5.86; % N, 3.70.

4.1.17.14. (1-(3-Hydroxybenzoyl)piperidin-4-yl)(4-(phenylthio)phenyl)methanone (20c). White solid; 65% yield from **63**, *n*-hexane/EtOAc 6:4. 1H NMR (DMSO- d_6) δ (ppm): 1.40–1.53 (m, 2H), 1.65–1.92 (bm, 2H), 2.86–3.24 (bm, 2H), 3.58–3.73 (m, 2H), 4.37–4.52 (bm, 1H), 6.71–6.74 (m, 1H), 6.76 (dt, 1H, $J = 7.5, 1.3$ Hz), 6.81 (ddd, 1H, $J = 8.1, 2.4, 1.0$ Hz), 7.22 (t, 1H, $J = 7.8$ Hz), 7.26 (AA'XX', 2H, $J_{AX} = 8.7$ Hz, $J_{AA'/XX'} = 2.0$ Hz), 7.46–7.55 (m, 5H), 7.94 (AA'XX', 2H, $J_{AX} = 8.7$ Hz, $J_{AA'/XX'} = 2.0$ Hz), 9.66 (exchangeable s, 1H). ^{13}C NMR (DMSO- d_6) δ (ppm): 28.37 (2C), 40.97, 42.32, 46.32, 113.37, 116.29, 117.06, 126.68, 127.44, 128.42, 129.13, 129.23, 129.60, 130.06 (2C), 131.19, 132.94, 133.56 (2C), 137.47, 143.68, 157.26, 168.91, 200.86. HPLC analysis: retention time = 12.659 min; peak area, 95% (254 nm). Elemental analysis for $C_{25}H_{23}NO_3S$, calculated: % C, 71.92; % H, 5.55; % N, 3.35; found: % C, 72.20; % H, 5.40; % N, 2.99.

4.1.17.15. (1-(3-Hydroxybenzoyl)piperidin-4-yl)(4-(phenylsulfonyl)phenyl)methanone (20d). Off-white solid; 75% yield from **68**, *n*-hexane/EtOAc 3:7. 1H NMR (DMSO- d_6) δ (ppm): 1.39–1.52 (m, 2H), 1.72–1.90 (bm, 2H), 2.89–3.22 (bm, 2H), 3.58–3.70 (bm, 1H), 3.74 (tt, 1H, $J = 11.0, 3.5$ Hz), 4.34–4.50 (bm, 1H), 6.71–6.73 (m, 1H), 6.76 (dt, 1H, $J = 7.4, 1.2$ Hz), 6.81 (ddd, 1H, $J = 8.1, 2.4, 1.0$ Hz), 7.21 (t, 1H, $J = 7.8$ Hz), 7.62–7.68 (m, 2H), 7.73 (tt, 1H, $J = 7.4, 1.6$ Hz), 7.98–8.03 (m, 2H), 8.10 (d, 2H, $J = 8.7$ Hz), 8.17 (d, 2H, $J = 8.7$ Hz), 9.64 (exchangeable s, 1H). ^{13}C NMR (DMSO- d_6) δ (ppm): 28.07, 42.88, 113.36, 116.28, 117.02, 127.57 (2C), 127.85 (2C), 129.48 (2C), 129.54, 129.88 (2C), 134.10, 137.41, 139.30, 140.33, 144.58, 157.23, 168.90, 201.28. HPLC analysis: retention time = 11.233 min; peak area, 99% (254 nm). Elemental analysis for $C_{25}H_{23}NO_5S$, calculated: % C, 66.80; % H, 5.16; % N, 3.12; found: % C, 66.87; % H, 5.15; % N, 3.01.

4.1.17.16. (1-(3-Hydroxybenzoyl)piperidin-4-yl)(4-(phenylsulfinyl)phenyl)methanone (20e). Light yellow solid; 78% yield from **20c**, *n*-hexane/EtOAc 2:8. 1H NMR (DMSO- d_6) δ (ppm): 1.38–1.52 (m, 2H), 1.63–1.92 (bm, 2H), 2.84–3.25 (bm, 2H), 3.54–3.80 (m, 2H), 4.31–4.53 (bm, 1H), 6.69–6.84 (m, 3H), 7.22 (t, 1H, $J = 7.8$ Hz), 7.48–7.59 (m, 3H), 7.72–7.80 (m, 2H), 7.88 (d, 2H, $J = 8.4$ Hz), 8.13 (d, 2H, $J = 8.3$ Hz), 9.67 (exchangeable bs, 1H). ^{13}C NMR (DMSO- d_6) δ (ppm): 28.22 (2C), 42.65, 46.40, 113.36, 116.28, 117.05, 124.28 (2C), 124.32 (2C), 129.30 (2C), 129.57, 129.68 (2C), 131.45, 137.35, 137.43, 145.31, 150.77, 157.24, 168.89, 201.33. HPLC analysis: retention time = 10.290 min; peak area, 99% (254 nm). Elemental analysis for $C_{25}H_{23}NO_4S$, calculated: % C, 69.26; % H, 5.35; % N, 3.23; found: % C, 69.34; % H, 5.26; % N, 2.88.

4.1.17.17. (4-(4-Benzylbenzoyl)piperidin-1-yl)(3-hydroxyphenyl)methanone (20f). White solid; 79% yield from **52**, eluent *n*-hexane/EtOAc 5:5. 1H NMR (DMSO- d_6) δ (ppm): 1.40–1.53 (m, 2H), 1.67–1.91 (bm, 2H), 2.89–3.24 (bm, 2H), 3.60–3.76 (m, 2H), 4.02 (s, 2H), 4.37–4.52 (bm, 1H), 6.71–6.74 (m, 1H), 6.76 (dt, 1H, $J = 7.8, 1.2$ Hz), 6.81 (ddd, 1H, $J = 8.2, 2.5, 1.0$ Hz), 7.16–7.33 (m, 6H), 7.39 (d, 2H, $J = 8.4$ Hz), 7.93 (d, 2H, $J = 8.4$ Hz), 9.66 (exchangeable s, 1H). ^{13}C NMR (DMSO- d_6) δ (ppm): 28.41 (2C), 40.89, 42.28, 46.29 (2C), 113.34, 116.25, 117.02, 126.16, 128.50 (2C), 128.55 (2C), 128.75 (2C), 129.09 (2C), 129.55, 133.39, 137.46, 140.40, 147.02, 157.23, 168.88, 201.39. HPLC analysis: retention time = 12.325 min; peak area, 98% (254 nm). Elemental analysis for $C_{26}H_{25}NO_3$, calculated: % C, 78.17; % H, 6.31; % N, 3.51; found: % C, 77.81; % H, 6.15; % N, 3.28.

4.1.17.18. (1-(3-Hydroxybenzoyl)piperidin-4-yl)(4-(1-phenyl-1H-1,2,3-triazol-4-yl)phenyl)methanone (20g). White solid; 61% yield from **83**, $CHCl_3/MeOH$ 97:3. 1H NMR (DMSO- d_6) δ (ppm): 1.46–1.60 (m, 2H), 1.75–1.98 (bm, 2H), 2.92–3.35 (bm, 2H), 3.62–3.76 (bm, 1H), 3.81 (tt, 1H, $J = 11.2, 3.4$ Hz), 4.42–4.55 (bm, 1H), 6.75–6.85 (m, 3H), 7.23 (t, 1H, $J = 7.8$ Hz), 7.54 (t, 1H, $J = 7.3$ Hz), 7.62–7.69 (m, 2H), 7.95–8.00 (m, 2H), 8.08–8.18 (m, 4H), 9.48 (s, 1H), 9.67 (exchangeable s, 1H). ^{13}C NMR (DMSO- d_6) δ (ppm): 28.46 (2C), 42.38, 113.37, 116.28, 117.05, 120.12 (2C), 120.93, 125.48 (2C), 128.90, 129.17 (2C), 129.57, 129.95 (2C), 134.66, 134.83, 136.50, 137.48, 146.26, 157.24, 168.92, 201.27. HPLC analysis: retention time = 11.670 min; peak area, 98% (254 nm). Elemental analysis for $C_{27}H_{24}N_4O_3$, calculated: % C, 71.67; % H, 5.35; % N, 12.38; found: % C, 72.04; % H, 5.51; % N, 12.60.

4.1.17.19. (4-(4-(1-Benzyl-1H-1,2,3-triazol-4-yl)benzoyl)piperidin-1-yl)(3-hydroxyphenyl)methanone (20h). Light yellow solid; 8% yield from **84**, $CHCl_3/MeOH$ 98:2. 1H NMR (DMSO- d_6) δ (ppm): 1.45–1.60 (m, 2H), 1.70–1.98 (bm, 2H), 2.90–3.24 (bm, 2H), 3.55–3.83 (bm, 2H), 4.35–4.60 (bm, 1H), 5.67 (s, 2H), 6.73–6.80 (m, 2H), 6.81 (ddd, 1H, $J = 8.2, 2.3, 0.9$ Hz), 7.23 (t, 1H, $J = 7.8$ Hz), 7.32–7.43 (m, 5H), 8.01 (d, 2H, $J = 8.6$ Hz), 8.08 (d, 2H, $J = 8.5$ Hz), 8.80 (s, 1H), 9.67 (exchangeable bs, 1H). ^{13}C NMR (DMSO- d_6) δ (ppm): 28.71 (2C), 38.20, 42.31, 53.11, 79.13, 113.34, 116.26, 117.03, 122.83, 125.28, 127.90 (5C), 128.19, 128.80, 129.07, 129.55, 134.50, 135.06, 135.80, 137.46, 145.60, 157.23, 168.89, 201.21. HPLC analysis: retention time = 11.351 min; peak area, 99% (254 nm). Elemental analysis for $C_{28}H_{26}N_4O_3$, calculated: % C, 72.09; % H, 5.62; % N, 12.01; found: % C, 72.10; % H, 5.68; % N, 11.83.

4.1.17.20. (1-(3-Hydroxybenzoyl)piperidin-4-yl)(4-(1-(3-phenylpropyl)-1H-1,2,3-triazol-4-yl)phenyl)methanone (20i). White solid; 12% yield from **85**, $CHCl_3/MeOH$ 98:2. 1H NMR (DMSO- d_6) δ (ppm): 1.43–1.60 (m, 2H), 1.70–1.98 (bm, 2H), 2.20 (quint, 2H, $J = 7.2$ Hz), 2.62 (t, 2H, $J = 7.8$ Hz), 2.90–3.25 (bm, 2H), 3.54–3.85 (bm, 2H), 4.39–4.53 (bm, 1H), 4.44 (t, 2H, $J = 7.2$ Hz), 6.73–6.85 (m, 3H), 7.16–7.26 (m, 4H), 7.27–7.33 (m, 2H), 8.01 (d, 2H, $J = 8.6$ Hz), 8.10 (d, 2H, $J = 8.5$ Hz), 8.79 (s, 1H), 9.67 (exchangeable bs, 1H). ^{13}C NMR (DMSO- d_6) δ (ppm): 28.43 (2C), 31.18, 31.87, 40.14, 42.34, 46.53, 49.19, 113.37, 116.28, 117.06, 122.60, 125.24, 126.00, 128.33, 128.38 (5C), 129.10, 129.58, 134.44, 135.30, 137.48, 140.69, 145.31, 157.25, 168.92, 201.23. HPLC analysis: retention time = 11.959 min; peak area, 97% (254 nm). Elemental analysis for $C_{30}H_{30}N_4O_3$, calculated: % C, 72.85; % H, 6.11; % N, 11.33; found: % C, 72.95; % H, 6.44; % N, 11.20.

4.1.17.21. (1-(4-Fluoro-3-hydroxybenzoyl)piperidin-4-yl)(4-(phenylthio)phenyl)methanone (21a). White solid; 78% yield from **64**, *n*-hexane/EtOAc 5:5. 1H NMR (DMSO- d_6) δ (ppm): 1.37–1.53 (m, 2H), 1.68–1.78 (bm, 1H), 1.83–1.92 (bm, 1H), 2.90–3.11 (m, 1H), 3.12–3.26 (bm, 1H), 3.43–3.51 (m, 1H), 3.63–3.73 (m, 1H), 4.45–4.53 (bm, 1H), 6.63–6.69 (m, 1H), 6.77–6.83 (m, 1H), 7.08 (t, 1H, $J = 9.1$ Hz), 7.26 (AA'XX', 2H, $J_{AX} = 8.7$ Hz, $J_{AA'/XX'} = 1.9$ Hz), 7.46–7.55 (m, 5H), 7.93 (AA'XX', 2H, $J_{AX} = 8.7$ Hz, $J_{AA'/XX'} = 2.0$ Hz), 9.65 (exchangeable s, 1H). ^{13}C NMR (DMSO- d_6) δ (ppm): 28.23, 28.53, 40.57, 42.16, 45.90, 113.96, 116.42 (d, $J_{CF} = 23.2$ Hz), 117.20 (d, $J_{CF} = 7.9$ Hz), 124.66 (d, $J_{CF} = 20.2$ Hz), 127.43 (2C), 129.13, 129.23 (2C), 130.06 (2C), 131.18, 132.90, 133.55 (2C), 143.71, 150.71 (d, $J_{CF} = 235.2$ Hz), 153.74 (d, $J_{CF} = 1.5$ Hz), 163.78, 200.77. HPLC analysis: retention time = 12.853 min; peak area, 96% (254 nm). Elemental analysis for $C_{25}H_{22}FNO_3S$, calculated: % C, 68.95; % H, 5.09; % N, 3.22; found: % C, 68.85; % H, 5.13; % N, 3.39.

4.1.17.22. (4-(4-Benzylbenzoyl)piperidin-1-yl)(2-fluoro-5-hydroxyphenyl)methanone (21b). White solid; 90% yield from **53**,

eluent *n*-hexane/EtOAc 6:4. ^1H NMR (DMSO- d_6) δ (ppm): 1.39–1.52 (bm, 2H), 1.69–1.77 (m, 1H), 1.84–1.91 (bm, 1H), 2.93–3.02 (bm, 1H), 3.15–3.26 (bm, 1H), 3.43–3.51 (bm, 1H), 3.67–3.76 (bm, 1H), 4.02 (s, 2H), 4.44–4.54 (m, 1H), 6.59–6.69 (m, 1H), 6.77–6.83 (m, 1H), 7.07 (t, 1H, $J = 9.0$ Hz), 7.20 (tt, 1H, $J = 7.1, 1.6$ Hz), 7.23–7.32 (m, 4H), 7.39 (d, 2H, $J = 8.4$ Hz), 7.93 (d, 2H, $J = 8.4$ Hz), 9.66 (exchangeable s, 1H). ^{13}C NMR (DMSO- d_6) δ (ppm): 28.22, 28.55, 40.55, 40.89, 42.12, 45.85, 113.92 (d, $J_{\text{CF}} = 3.9$ Hz), 116.38 (d, $J_{\text{CF}} = 23.1$ Hz), 117.17 (d, $J_{\text{CF}} = 7.7$ Hz), 124.66 (d, $J_{\text{CF}} = 20.1$ Hz), 126.15, 128.49 (2C), 128.55 (2C), 128.74 (2C), 129.09 (2C), 133.35, 140.39, 147.04, 150.69 (d, $J_{\text{CF}} = 235.2$ Hz), 153.72, 163.76, 201.30. HPLC analysis: retention time = 12.537 min; peak area, 97% (254 nm). Elemental analysis for $\text{C}_{26}\text{H}_{24}\text{FNO}_3$, calculated: % C, 74.80; % H, 5.79; % N, 3.36; found: % C, 74.99; % H, 5.48; % N, 3.03.

4.1.17.23. (1-(2,4-Difluoro-5-hydroxybenzoyl)piperidin-4-yl)(4-(phenylthio)phenyl)methanone (22a). White solid; 45% yield from **65**, *n*-hexane/EtOAc 5:5. ^1H NMR (DMSO- d_6) δ (ppm): 1.37–1.52 (m, 2H), 1.68–1.79 (bm, 1H), 1.82–1.93 (bm, 1H), 2.91–3.02 (m, 1H), 3.13–3.25 (bm, 1H), 3.43–3.53 (bm, 1H), 3.63–3.74 (m, 1H), 4.42–4.52 (m, 1H), 6.88 (dd, 1H, $J = 9.5, 6.9$ Hz), 7.23–7.33 (m, 3H), 7.44–7.58 (m, 5H), 7.93 (d, 2H, $J = 8.6$ Hz), 10.14 (exchangeable bs, 1H). ^{13}C NMR (DMSO- d_6) δ (ppm): 28.18, 28.52, 40.69, 42.11, 45.92, 104.98 (dd, $J_{\text{CF}} = 27.4, 23.0$ Hz), 116.00 (t, $J_{\text{CF}} = 4.9$ Hz), 120.00 (dd, $J_{\text{CF}} = 19.5, 4.1$ Hz), 127.41 (2C), 129.09, 129.20 (2C), 130.02 (2C), 131.17, 132.89, 133.52 (2C), 141.89 (d, $J_{\text{CF}} = 15.1$ Hz), 143.68, 149.01 (dd, $J_{\text{CF}} = 109.0, 11.3$ Hz), 151.42 (dd, $J_{\text{CF}} = 117.2, 11.3$ Hz), 163.10, 200.74. HPLC analysis: retention time = 13.036 min; peak area, 95% (254 nm). Elemental analysis for $\text{C}_{25}\text{H}_{21}\text{F}_2\text{NO}_3\text{S}$, calculated: % C, 66.21; % H, 4.67; % N, 3.09; found: % C, 65.84; % H, 4.96; % N, 2.80.

4.1.17.24. (4-(4-Benzylbenzoyl)piperidin-1-yl)(2,4-difluoro-5-hydroxyphenyl)methanone (22b). White solid; 78% yield from **54**, eluent *n*-hexane/EtOAc 5:5. ^1H NMR (DMSO- d_6) δ (ppm): 1.38–1.52 (bm, 2H), 1.69–1.78 (bm, 1H), 1.83–1.92 (bm, 1H), 2.92–3.03 (m, 1H), 3.14–3.27 (bm, 1H), 3.43–3.53 (bm, 1H), 3.67–3.77 (bm, 1H), 4.02 (s, 2H), 4.42–4.52 (m, 1H), 6.89 (dd, 1H, $J = 9.5, 6.7$ Hz), 7.20 (tt, 1H, $J = 7.0, 1.8$ Hz), 7.22–7.34 (m, 5H), 7.39 (d, 2H, $J = 8.4$ Hz), 7.93 (d, 2H, $J = 8.4$ Hz), 10.14 (exchangeable s, 1H). ^{13}C NMR (DMSO- d_6) δ (ppm): 28.22, 28.58, 40.71, 40.90, 42.11, 45.93, 105.00 (dd, $J_{\text{CF}} = 27.4, 23.0$ Hz), 115.96 (t, $J_{\text{CF}} = 4.6$ Hz), 120.03 (dd, $J_{\text{CF}} = 19.6, 4.0$ Hz), 126.17, 128.51 (2C), 128.57 (2C), 128.75 (2C), 129.10 (2C), 133.33, 140.41, 141.84 (dd, $J_{\text{CF}} = 12.4, 2.9$ Hz), 147.08, 149.02 (dd, $J_{\text{CF}} = 104.3, 11.2$ Hz), 151.99 (dd, $J_{\text{CF}} = 111.3, 11.2$ Hz), 163.10, 201.30. HPLC analysis: retention time = 12.712 min; peak area, 98% (254 nm). Elemental analysis for $\text{C}_{26}\text{H}_{23}\text{F}_2\text{NO}_3$, calculated: % C, 71.71; % H, 5.32; % N, 3.22; found: % C, 72.10; % H, 5.16; % N, 3.24.

4.1.17.25. (1-(2,4-Difluoro-5-methoxybenzoyl)piperidin-4-yl)(4-isopropylphenyl)methanone (25). 84% yield from **23** to 2,4-difluoro-5-methoxybenzoic acid **24**. ^1H NMR (CDCl_3) δ (ppm): 1.27 (d, 6H, $J = 6.9$ Hz), 1.75–1.88 (bm, 3H), 1.98–2.06 (bm, 1H), 2.97 (sept, 1H, $J = 7.0$ Hz), 3.03–3.14 (bm, 1H), 3.16–3.31 (bm, 1H), 3.48–3.59 (bm, 1H), 3.65–3.75 (bm, 1H), 3.89 (s, 3H), 4.64–4.73 (bm, 1H), 6.88 (dd, 1H, $J = 10.7, 8.8$ Hz), 6.99 (dd, 1H, $J = 9.1, 6.1$ Hz), 7.33 (d, 2H, $J = 8.2$ Hz), 7.88 (d, 2H, $J = 8.4$ Hz).

4.1.17.26. (4-(4-Isopropylbenzoyl)piperidin-1-yl)(5-methoxy-2-(trifluoromethyl)phenyl)methanone (27). 75% yield from **23** and 5-methoxy-2-(trifluoromethyl)benzoic acid **26**. ^1H NMR (CDCl_3 ; asterisk denotes isomer peaks) δ (ppm): 1.27 (d, 6H, $J = 6.9$ Hz), 1.66–1.87 (bm, 3H), 1.98–2.10 (bm, 1H), 2.90–3.05 (bm, 1H), 3.05–3.18 (bm, 2H), 3.43–3.58 (bm, 2H), 3.86* (s, 3H), 3.87 (s, 3H), 4.65–4.74 (bm, 1H), 6.79* (d, 1H, $J = 2.2$ Hz), 6.84 (d, 1H, $J = 2.4$ Hz), 6.95–7.01 (m, 1H), 7.29–7.36 (m, 2H), 7.58–7.64 (m, 1H), 7.83–7.91

(m, 2H).

4.1.17.27. (4-(4-Isopropylbenzoyl)piperidin-1-yl)(5-methoxy-2-nitrophenyl)methanone (29). 59% yield from **23** and 5-methoxy-2-nitrobenzoic acid **28**. ^1H NMR (CDCl_3 ; asterisk denotes isomer peaks) δ (ppm): 1.27 (d, 6H, $J = 6.9$ Hz), 1.69–1.88 (bm, 3H), 2.06–2.15 (bm, 1H), 2.99 (sept, 1H, $J = 6.9$ Hz), 3.09–3.25 (bm, 2H), 3.43–3.60 (bm, 2H), 3.92 (s, 3H), 4.58–4.75 (m, 1H), 6.78–6.82* (m, 1H), 6.83 (d, 1H, $J = 2.6$ Hz), 6.98 (dd, 1H, $J = 9.3, 2.7$ Hz), 7.29–7.32* (m, 1H), 7.34 (d, 2H, $J = 8.1$ Hz), 7.83–7.86* (m, 1H), 7.88 (d, 2H, $J = 8.4$ Hz), 8.21 (d, 1H, $J = 9.2$ Hz).

4.1.17.28. Methyl 5-methoxy-2-nitrobenzoate (30). 91% yield from 5-methoxy-2-nitrobenzoic acid **28**. ^1H NMR (CDCl_3) δ (ppm): 3.92 (s, 3H), 3.94 (s, 3H), 7.02 (dd, 1H, $J = 9.0, 2.8$ Hz), 7.05 (d, 1H, $J = 2.6$ Hz), 8.04 (d, 1H, $J = 9.0$ Hz).

4.1.17.29. Methyl 2-amino-5-methoxybenzoate (31). 85% yield from **30**. ^1H NMR (CDCl_3) δ (ppm): 3.77 (s, 3H), 3.88 (s, 3H), 6.68 (d, 1H, $J = 8.9$ Hz), 6.96 (dd, 1H, $J = 8.9, 3.0$ Hz), 7.36 (d, 1H, $J = 3.0$ Hz).

4.1.17.30. 2-Amino-5-methoxybenzoic acid (32). 99% yield from **31**. ^1H NMR (DMSO- d_6) δ (ppm): 3.65 (s, 3H), 6.70 (d, 1H, $J = 9.0$ Hz), 6.94 (dd, 1H, $J = 9.0, 3.1$ Hz), 7.18 (d, 1H, $J = 3.1$ Hz), 8.35 (bs, 2H).

4.1.17.31. (1-(2-Amino-5-methoxybenzoyl)piperidin-4-yl)(4-isopropylphenyl)methanone (33). 54% yield from **23** and **32**. ^1H NMR (CDCl_3) δ (ppm): 1.27 (d, 6H, $J = 6.9$ Hz), 1.76–1.98 (bm, 4H), 2.50–2.86 (bm, 3H), 2.97 (sept, 1H, $J = 6.9$ Hz), 3.06–3.20 (m, 2H), 3.53 (tt, 1H, $J = 10.7, 4.0$ Hz), 3.74 (s, 3H), 4.15–4.50 (bm, 1H), 6.69 (d, 1H, $J = 2.7$ Hz), 6.75 (d, 1H, $J = 8.8$ Hz), 6.80 (dd, 1H, $J = 8.7, 2.7$ Hz), 7.33 (d, 2H, $J = 8.2$ Hz), 7.88 (d, 2H, $J = 8.3$ Hz).

4.1.17.32. Methyl 5-methoxy-2-methylbenzoate (35). 85% yield from 5-hydroxy-2-methylbenzoic acid **34**. ^1H NMR (CDCl_3) δ (ppm): 2.52 (s, 3H), 3.82 (s, 3H), 3.89 (s, 3H), 6.96 (dd, 1H, $J = 8.4, 2.8$ Hz), 7.15 (d, 1H, $J = 8.4$ Hz), 7.44 (d, 1H, $J = 2.9$ Hz).

4.1.17.33. 5-Methoxy-2-methylbenzoic acid (36). 77% yield from **35**. ^1H NMR (acetone- d_6) δ (ppm): 2.50 (s, 3H), 3.82 (s, 3H), 7.03 (dd, 1H, $J = 8.4, 2.8$ Hz), 7.21 (d, 1H, $J = 8.5$ Hz), 7.48 (d, 1H, $J = 2.9$ Hz), 11.14 (bs, 1H).

4.1.17.34. (4-(4-Isopropylbenzoyl)piperidin-1-yl)(5-methoxy-2-methylphenyl)methanone (37). 70% yield from amine **23** and **36**. ^1H NMR (CDCl_3 ; asterisk denotes isomer peaks) δ (ppm): 1.27 (d, 6H, $J = 6.9$ Hz), 1.68–1.86 (bm, 3H), 1.98–2.09 (bm, 1H), 2.22 (s, 3H), 2.26* (s, 3H), 2.97 (sept, 1H, $J = 6.9$ Hz), 3.02–3.17 (bm, 2H), 3.45–3.56 (bm, 1H), 3.56–3.66 (m, 1H), 3.78 (s, 3H), 4.67–4.82 (bm, 1H), 6.67–6.77 (m, 1H), 6.82 (dd, 1H, $J = 8.5, 2.7$ Hz), 7.08–7.16 (m, 1H), 7.33 (d, 2H, $J = 8.2$ Hz), 7.88 (d, 2H, $J = 8.3$ Hz).

4.1.17.35. 1-(4-(4-Bromobenzoyl)piperidin-1-yl)ethanone (43). 64% yield from **42** and bromobenzene. ^1H NMR (CDCl_3) δ (ppm): 1.60–1.70 (m, 1H), 1.74–1.96 (m, 3H), 2.11 (s, 3H), 2.77–2.88 (m, 1H), 3.17–3.27 (m, 1H), 3.43 (tt, 1H, $J = 10.8, 4.0$ Hz), 3.86–3.95 (m, 1H), 4.53–4.62 (m, 1H), 7.63 (AA'XX', 2H, $J_{\text{AX}} = 8.7$ Hz, $J_{\text{AA'XX'}} = 2.1$ Hz), 7.80 (AA'XX', 2H, $J_{\text{AX}} = 8.6$ Hz, $J_{\text{AA'XX'}} = 2.1$ Hz).

4.1.17.36. 1-(4-(4-Cyclopropylbenzoyl)piperidin-1-yl)ethanone (44). 92% yield from **43**. ^1H NMR (CDCl_3) δ (ppm): 0.75–0.81 (m, 2H), 1.03–1.11 (m, 2H), 1.57–1.91 (bm, 4H), 1.91–1.99 (m, 1H), 2.11 (s, 3H), 2.74–2.92 (bm, 1H), 3.11–3.29 (bm, 1H), 3.41–3.51 (m, 1H), 3.80–3.98 (bm, 1H), 4.47–4.64 (bm, 1H), 7.13 (d, 2H, $J = 8.3$ Hz), 7.83 (d, 2H, $J = 8.4$ Hz).

4.1.17.37. (4-Cyclopropylphenyl)(piperidin-4-yl)methanone (45). 86% yield from **44**. ^1H NMR (CDCl_3) δ (ppm): 0.75–0.81 (m, 2H), 1.03–1.10 (m, 2H), 1.67–1.80 (m, 2H), 1.83–1.92 (m, 2H), 1.92–1.99 (m, 1H), 2.44 (bs, 1H), 2.81 (td, 2H, $J = 12.1, 2.6$ Hz), 3.22 (dt, 2H, $J = 12.8, 3.6$ Hz), 3.39 (tt, 1H, $J = 10.9, 3.8$ Hz), 7.12 (AA'XX', 2H, $J_{AX} = 8.3$ Hz, $J_{AA'XX'} = 1.9$ Hz), 7.83 (AA'XX', 2H, $J_{AX} = 8.4$ Hz, $J_{AA'XX'} = 1.9$ Hz).

4.1.17.38. (4-(4-Cyclopropylbenzoyl)piperidin-1-yl)(3-methoxyphenyl)methanone (46). 75% yield from **45** and 3-methoxybenzoic acid. ^1H NMR (CDCl_3) δ (ppm): 0.75–0.81 (m, 2H), 1.04–1.11 (m, 2H), 1.72–1.87 (bm, 3H), 1.90–2.01 (m, 2H), 2.95–3.23 (bm, 2H), 3.45–3.57 (bm, 1H), 3.74–3.97 (bm, 1H), 3.82 (s, 3H), 4.56–4.78 (bm, 1H), 6.92–6.99 (m, 3H), 7.14 (d, 2H, $J = 8.3$ Hz), 7.31 (dd, 1H, $J = 9.0, 7.5$ Hz), 7.84 (AA'XX', 2H, $J_{AX} = 8.4$ Hz, $J_{AA'XX'} = 1.8$ Hz).

4.1.17.39. 1-(4-(4-Cyclohexylbenzoyl)piperidin-1-yl)ethanone (47). 40% yield from **42** and phenylcyclohexane. ^1H NMR (CDCl_3) δ (ppm): 1.34–1.50 (bm, 4H), 1.56–1.98 (bm, 10H), 2.13 (s, 3H), 2.47–2.64 (m, 1H), 2.72–3.03 (bm, 1H), 3.07–3.33 (bm, 1H), 3.43–3.54 (m, 1H), 3.77–4.02 (bm, 1H), 4.45–4.65 (bm, 1H), 7.31 (d, 2H, $J = 8.2$ Hz), 7.87 (AA'XX', 2H, $J_{AX} = 8.4$ Hz, $J_{AA'XX'} = 1.8$ Hz).

4.1.17.40. (4-Cyclohexylphenyl)(piperidin-4-yl)methanone (48). 81% yield from **47**. ^1H NMR (CDCl_3) δ (ppm): 1.33–1.50 (bm, 4H), 1.65–1.95 (bm, 10H), 2.24 (bs, 1H), 2.51–2.61 (bm, 1H), 2.80 (td, 2H, $J = 12.1, 2.1$ Hz), 3.15–3.27 (m, 2H), 3.40 (tt, 1H, $J = 10.9, 3.7$ Hz), 7.29 (d, 2H, $J = 8.2$ Hz), 7.87 (d, 2H, $J = 8.4$ Hz).

4.1.17.41. (4-(4-Cyclohexylbenzoyl)piperidin-1-yl)(3-methoxyphenyl)methanone (49). 68% yield from **48** and 3-methoxybenzoic acid. ^1H NMR (CDCl_3) δ (ppm): 1.43–1.50 (bm, 5H), 1.70–2.03 (bm, 9H), 2.51–2.62 (bm, 1H), 2.98–3.20 (bm, 2H), 3.47–3.58 (bm, 1H), 3.77–4.00 (bm, 1H), 3.82 (s, 3H), 4.57–4.80 (bm, 1H), 6.91–7.00 (m, 3H), 7.27–7.34 (m, 3H), 7.87 (d, 2H, $J = 8.4$ Hz).

4.1.17.42. 1-(4-(4-Benzylbenzoyl)piperidin-1-yl)ethanone (50). 49% yield from **42** and diphenylmethane. ^1H NMR (CDCl_3) δ (ppm): 1.68–1.80 (bm, 2H), 1.85–1.93 (bm, 2H), 2.13 (s, 3H), 2.77–3.28 (bm, 2H), 3.42–3.51 (m, 1H), 3.83–4.00 (bm, 1H), 4.04 (s, 2H), 4.42–4.62 (bm, 1H), 7.16–7.20 (m, 2H), 7.23 (tt, 1H, $J = 7.3, 2.2$ Hz), 7.27–7.33 (m, 4H), 7.86–7.89 (m, 2H).

4.1.17.43. (4-Benzylphenyl)(piperidin-4-yl)methanone (51). 91% yield from **50**. ^1H NMR (CDCl_3) δ (ppm): 1.66–1.78 (m, 2H), 1.82–1.91 (m, 1H), 2.80 (td, 2H, $J = 12.2, 2.7$ Hz), 3.21 (dt, 2H, $J = 12.7, 3.6$ Hz), 3.38 (tt, 1H, $J = 10.8, 3.7$ Hz), 4.03 (s, 2H), 7.15–7.20 (m, 2H), 7.20–7.26 (m, 1H), 7.26–7.33 (m, 4H), 7.86 (AA'XX', 2H, $J_{AX} = 8.3$ Hz, $J_{AA'XX'} = 1.8$ Hz).

4.1.17.44. (4-(4-Benzylbenzoyl)piperidin-1-yl)(3-methoxyphenyl)methanone (52). 80% yield from **51** and 3-methoxybenzoic acid. ^1H NMR (CDCl_3) δ (ppm): 1.72–2.06 (bm, 4H), 3.00–3.17 (bm, 2H), 3.46–3.55 (m, 1H), 3.78–3.92 (bm, 1H), 3.82 (s, 3H), 4.04 (s, 2H), 4.61–4.74 (bm, 1H), 6.92–6.98 (m, 3H), 7.15–7.20 (m, 2H), 7.22 (tt, 1H, $J = 7.4, 2.2$ Hz), 7.27–7.34 (m, 5H), 7.87 (d, 2H, $J = 8.2$ Hz).

4.1.17.45. (4-(4-Benzylbenzoyl)piperidin-1-yl)(2-fluoro-5-methoxyphenyl)methanone (53). 77% yield from **51** and 2-fluoro-5-methoxybenzoic acid. ^1H NMR (CDCl_3) δ (ppm): 1.74–1.86 (bm, 3H), 1.97–2.04 (m, 1H), 3.02–3.12 (m, 1H), 3.313–3.30 (bm, 1H), 3.44–3.54 (bm, 1H), 3.65–3.74 (m, 1H), 3.80 (s, 3H), 4.04 (s, 2H), 4.64–4.74 (m, 1H), 6.85–6.92 (m, 2H), 7.00 (t, 1H, $J = 8.6$ Hz), 7.15–7.20 (m, 2H), 7.23 (tt, 1H, $J = 7.3, 2.2$ Hz), 7.27–7.33 (m, 4H),

7.88 (d, 2H, $J = 8.3$ Hz).

4.1.17.46. (4-(4-Benzylbenzoyl)piperidin-1-yl)(2,4-difluoro-5-methoxyphenyl)methanone (54). 73% yield from **51** to 2,4-difluoro-5-methoxybenzoic acid **24**. ^1H NMR (CDCl_3) δ (ppm): 1.75–1.87 (bm, 3H), 1.97–2.06 (bm, 1H), 3.01–3.13 (m, 1H), 3.14–3.31 (m, 1H), 3.45–3.57 (bm, 1H), 3.64–3.74 (m, 1H), 3.89 (s, 3H), 4.04 (s, 2H), 4.63–4.73 (m, 1H), 6.88 (dd, 1H, $J = 10.7, 8.7$ Hz), 6.99 (dd, 1H, $J = 9.1, 6.1$ Hz), 7.15–7.20 (m, 2H), 7.23 (tt, 1H, $J = 7.3, 1.8$ Hz), 7.27–7.34 (m, 4H), 7.87 (d, 2H, $J = 8.4$ Hz).

4.1.17.47. 1-(4-(4-Phenylamino)benzoyl)piperidin-1-yl)ethanone (55). 99% yield from **43** and aniline. ^1H NMR (CDCl_3) δ (ppm): 1.64–1.93 (bm, 4H), 2.13 (s, 3H), 2.77–2.93 (bm, 1H), 3.12–3.29 (bm, 1H), 3.39–3.49 (m, 1H), 3.84–3.99 (bm, 1H), 4.49–4.64 (bm, 1H), 7.01 (AA'XX', 2H, $J_{AX} = 8.8$ Hz, $J_{AA'XX'} = 2.3$ Hz), 7.10 (tt, 1H, $J = 7.4, 1.1$ Hz), 7.16–7.22 (m, 2H), 7.32–7.39 (m, 2H), 7.87 (AA'XX', 2H, $J_{AX} = 8.8$ Hz, $J_{AA'XX'} = 2.3$ Hz).

4.1.17.48. 1-(4-(4-Phenoxybenzoyl)piperidin-1-yl)ethanone (56). 84% yield from **43** and phenol. ^1H NMR (CDCl_3) δ (ppm): 1.59–1.95 (bm, 4H), 2.12 (s, 3H), 2.77–2.90 (bm, 1H), 3.15–3.28 (bm, 1H), 3.45 (tt, 1H, $J = 10.4, 3.9$ Hz), 3.85–3.97 (bm, 1H), 4.50–4.63 (bm, 1H), 7.02 (AA'XX', 2H, $J_{AX} = 8.9$ Hz, $J_{AA'XX'} = 2.4$ Hz), 7.05–7.10 (m, 2H), 7.21 (tt, 1H, $J = 7.4, 1.1$ Hz), 7.37–7.44 (m, 2H), 7.93 (AA'XX', 2H, $J_{AX} = 8.9$ Hz, $J_{AA'XX'} = 2.4$ Hz).

4.1.17.49. (4-(Phenylamino)phenyl)(piperidin-4-yl)methanone (57). 99% yield from **55**. ^1H NMR (CDCl_3) δ (ppm): 1.63–1.90 (m, 4H), 2.77 (td, 2H, $J = 12.1, 2.6$ Hz), 3.14–3.24 (m, 2H), 3.34 (tt, 1H, $J = 11.3, 3.6$ Hz), 6.10 (exchangeable s, 1H), 7.00 (AA'XX', 2H, $J_{AX} = 8.8$ Hz, $J_{AA'XX'} = 2.3$ Hz), 7.08 (tt, 1H, $J = 7.4, 1.1$ Hz), 7.15–7.21 (m, 2H), 7.31–7.38 (m, 2H), 7.87 (AA'XX', 2H, $J_{AX} = 8.8$ Hz, $J_{AA'XX'} = 2.3$ Hz).

4.1.17.50. (4-Phenoxyphenyl)(piperidin-4-yl)methanone (58). 93% yield from **56**. ^1H NMR (CDCl_3) δ (ppm): 1.61–1.74 (m, 2H), 1.75–1.92 (m, 2H), 2.76 (td, 2H, $J = 12.3, 2.7$ Hz), 3.19 (dt, 2H, $J = 12.5, 3.4$ Hz), 3.35 (tt, 1H, $J = 11.4, 3.6$ Hz), 7.00 (AA'XX', 2H, $J_{AX} = 8.9$ Hz, $J_{AA'XX'} = 2.4$ Hz), 7.04–7.10 (m, 2H), 7.20 (tt, 1H, $J = 7.4, 1.1$ Hz), 7.36–7.43 (m, 2H), 7.93 (AA'XX', 2H, $J_{AX} = 8.9$ Hz, $J_{AA'XX'} = 2.4$ Hz).

4.1.17.51. (1-(3-Methoxybenzoyl)piperidin-4-yl)(4-(phenylamino)phenyl)methanone (59). 65% yield from **57** and 3-methoxybenzoic acid. ^1H NMR (CDCl_3) δ (ppm): 1.72–2.07 (bm, 4H), 2.94–3.22 (bm, 2H), 3.43–3.52 (bm, 1H), 3.78–3.95 (bm, 1H), 3.82 (s, 3H), 4.60–4.80 (bm, 1H), 6.92–7.03 (m, 5H), 7.10 (t, 1H, $J = 7.4$ Hz), 7.16–7.22 (m, 2H), 7.27–7.39 (m, 3H), 7.87 (d, 2H, $J = 8.8$ Hz).

4.1.17.52. (1-(3-Methoxybenzoyl)piperidin-4-yl)(4-phenoxyphenyl)methanone (60). 85% yield from **58** and 3-methoxybenzoic acid. ^1H NMR (CDCl_3) δ (ppm): 1.73–2.10 (m, 4H), 2.96–3.21 (bm, 2H), 3.45–3.55 (m, 1H), 3.80–3.95 (bm, 1H), 3.82 (s, 3H), 4.63–4.76 (bm, 1H), 6.92–6.99 (m, 3H), 7.02 (AA'XX', 2H, $J_{AX} = 8.9$ Hz, $J_{AA'XX'} = 2.4$ Hz), 7.05–7.10 (m, 2H), 7.21 (tt, 1H, $J = 7.4, 1.1$ Hz), 7.31 (dd, 1H, $J = 9.0, 7.5$ Hz), 7.37–7.44 (m, 2H), 7.94 (AA'XX', 2H, $J_{AX} = 8.9$ Hz, $J_{AA'XX'} = 2.4$ Hz).

4.1.17.53. 1-(4-(4-(phenylthio)benzoyl)piperidin-1-yl)ethanone (61). 97% yield from **43** and thiophenol. ^1H NMR (CDCl_3) δ (ppm): 1.63–1.69 (m, 1H), 1.73–1.93 (m, 3H), 2.11 (s, 3H), 2.75–2.85 (m, 1H), 3.15–3.25 (m, 1H), 3.41 (tt, 1H, $J = 10.6, 4.1$ Hz), 3.85–3.94 (m, 1H), 4.51–4.60 (m, 1H), 7.21 (AA'XX', 2H, $J_{AX} = 8.7$ Hz, $J_{AA'XX'} = 2.0$ Hz), 7.39–7.43 (m, 3H), 7.48–7.53 (m, 2H), 7.80 (AA'XX', 2H, $J_{AX} = 8.7$ Hz, $J_{AA'XX'} = 2.0$ Hz).

4.1.17.54. (4-(phenylthio)phenyl)(piperidin-4-yl)methanone (62). 99% yield from **61**. ^1H NMR (CDCl_3) δ (ppm): 1.57–1.87 (m, 4H), 2.67–2.80 (m, 2H), 2.95–3.22 (m, 2H), 3.29 (tt, 1H, $J = 11.4, 3.8$ Hz), 7.21 (AA'XX', 2H, $J_{AX} = 8.6$ Hz, $J_{AA'/XX'} = 2.0$ Hz), 7.37–7.43 (m, 3H), 7.47–7.53 (m, 2H), 7.81 (AA'XX', 2H, $J_{AX} = 8.6$ Hz, $J_{AA'/XX'} = 2.0$ Hz).

4.1.17.55. (1-(3-Methoxybenzoyl)piperidin-4-yl)(4-(phenylthio)phenyl)methanone (63). 73% yield from **62** and 3-methoxybenzoic acid. ^1H NMR (CDCl_3) δ (ppm): 1.72–2.04 (m, 4H), 2.95–3.20 (bm, 2H), 3.39–3.52 (m, 1H), 3.76–3.96 (bm, 1H), 3.82 (s, 3H), 4.58–4.76 (bm, 1H), 6.92–6.98 (m, 2H), 7.22 (AA'XX', 2H, $J_{AX} = 8.6$ Hz, $J_{AA'/XX'} = 2.0$ Hz), 7.30 (dd, 1H, $J = 8.9, 7.5$ Hz), 7.38–7.44 (m, 4H), 7.48–7.54 (m, 2H), 7.78–7.84 (m, 2H).

4.1.17.56. (1-(2-Fluoro-5-methoxybenzoyl)piperidin-4-yl)(4-(phenylthio)phenyl)methanone (64). 85% yield from **62** and 2-fluoro-5-methoxybenzoic acid. ^1H NMR (CDCl_3) δ (ppm): 1.72–1.86 (m, 3H), 1.95–2.03 (m, 1H), 2.98–3.10 (m, 1H), 3.11–3.27 (bm, 1H), 3.41–3.50 (bm, 1H), 3.65–3.74 (m, 1H), 3.79 (s, 3H), 4.65–4.73 (m, 1H), 6.84–6.91 (m, 2H), 7.00 (t, 1H, $J = 8.7$ Hz), 7.21 (AA'XX', 2H, $J_{AX} = 8.5$ Hz, $J_{AA'/XX'} = 2.0$ Hz), 7.38–7.44 (m, 3H), 7.48–7.53 (m, 2H), 7.81 (AA'XX', 2H, $J_{AX} = 8.6$ Hz, $J_{AA'/XX'} = 2.0$ Hz).

4.1.17.57. (1-(2,4-Difluoro-5-methoxybenzoyl)piperidin-4-yl)(4-(phenylthio)phenyl)methanone (65). 77% yield from **62** to 2,4-difluoro-5-methoxybenzoic acid **24**. ^1H NMR (CDCl_3) δ (ppm): 1.72–1.86 (m, 3H), 1.95–2.04 (bm, 1H), 2.99–3.12 (bm, 1H), 3.12–3.30 (bm, 1H), 3.41–3.52 (bm, 1H), 3.64–3.74 (m, 1H), 3.89 (s, 3H), 4.62–4.73 (m, 1H), 6.88 (dd, 1H, $J = 10.5, 8.7$ Hz), 6.95–7.02 (m, 1H), 7.21 (d, 2H, $J = 8.4$ Hz), 7.38–7.44 (m, 3H), 7.47–7.54 (m, 2H), 7.81 (d, 2H, $J = 8.5$ Hz).

4.1.17.58. 1-(4-(4-(Phenylsulfonyl)benzoyl)piperidin-1-yl)ethanone (66). 99% yield from **61**. ^1H NMR (CDCl_3) δ (ppm): 1.57–1.92 (bm, 4H), 2.11 (s, 3H), 2.78–2.89 (bm, 1H), 3.15–3.28 (bm, 1H), 3.44 (tt, 1H, $J = 10.7, 4.0$ Hz), 3.83–3.96 (bm, 1H), 4.48–4.60 (bm, 1H), 7.51–7.56 (m, 2H), 7.61 (tt, 1H, $J = 7.3, 1.6$ Hz), 7.94–7.99 (m, 2H), 8.00–8.07 (m, 4H).

4.1.17.59. (4-(Phenylsulfonyl)phenyl)(piperidin-4-yl)methanone (67). 81% yield from **66**. ^1H NMR (CDCl_3) δ (ppm): 1.60–1.73 (m, 4H), 1.77–1.85 (m, 2H), 2.75 (td, 1H, $J = 12.4, 2.4$ Hz), 3.17 (dt, 1H, $J = 12.5, 3.2$ Hz), 3.33 (tt, 1H, $J = 11.4, 3.6$ Hz), 7.50–7.56 (m, 2H), 7.60 (tt, 1H, $J = 7.4, 1.9$ Hz), 7.93–7.99 (m, 2H), 7.99–8.06 (m, 4H).

4.1.17.60. (1-(3-Methoxybenzoyl)piperidin-4-yl)(4-(phenylsulfonyl)phenyl)methanone (68). 49% yield from **67** and 3-methoxybenzoic acid. ^1H NMR (CDCl_3) δ (ppm): 1.70–2.01 (m, 4H), 2.89–3.19 (bm, 2H), 3.44–3.54 (m, 1H), 3.76–3.96 (bm, 1H), 3.82 (s, 3H), 4.56–4.74 (bm, 1H), 6.91–6.97 (m, 3H), 7.30 (t, 1H, $J = 8.1$ Hz), 7.50–7.57 (m, 2H), 7.61 (tt, 1H, $J = 7.5, 2.3$ Hz), 7.94–7.99 (m, 2H), 8.00–8.08 (m, 4H).

4.1.17.61. 1-(4-(4-(3-Hydroxy-3-methylbut-1-yn-1-yl)benzoyl)piperidin-1-yl)ethanone (69). 99% yield from **43**. ^1H NMR (CDCl_3) δ (ppm): 1.63 (s, 6H), 1.75–1.95 (bm, 4H), 2.11 (s, 3H), 2.78–2.88 (m, 1H), 3.17–3.27 (m, 1H), 3.46 (tt, 1H, $J = 10.9, 3.9$ Hz), 3.86–3.95 (m, 1H), 4.53–4.63 (m, 1H), 7.51 (d, 2H, $J = 8.6$ Hz), 7.88 (d, 2H, $J = 8.6$ Hz).

4.1.17.62. 1-(4-(4-Ethynylbenzoyl)piperidin-1-yl)ethanone (70). 82% yield from **69**. ^1H NMR (CDCl_3) δ (ppm): 1.62–1.95 (bm, 4H), 2.12 (s, 3H), 2.77–2.91 (bm, 1H), 3.14–3.30 (bm, 1H), 3.26 (s, 1H), 3.47 (tt, 1H, $J = 10.8, 3.9$ Hz), 3.84–3.97 (bm, 1H), 4.51–4.63 (bm, 1H), 7.59 (AA'XX', 2H, $J_{AX} = 8.4$ Hz, $J_{AA'/XX'} = 1.7$ Hz), 7.89 (AA'XX', 2H,

$J_{AX} = 8.6$ Hz, $J_{AA'/XX'} = 1.8$ Hz).

4.1.17.63. Azidobenzene (74). 70% yield from **71**. ^1H NMR (CDCl_3) δ (ppm): 7.01–7.06 (m, 2H), 7.14 (tt, 1H, $J = 7.4, 1.1$ Hz), 7.32–7.39 (m, 2H).

4.1.17.64. (Azidomethyl)benzene (75). 61% yield from **72**. ^1H NMR (CDCl_3) δ (ppm): 4.34 (s, 2H), 7.30–7.42 (m, 5H).

4.1.17.65. (3-Azidopropyl)benzene (76). 77% yield from **73**. ^1H NMR (CDCl_3) δ (ppm): 1.92 (quint, 2H, $J = 6.7$ Hz), 2.71 (t, 2H, $J = 7.6$ Hz), 3.29 (t, 2H, $J = 6.8$ Hz), 7.17–7.24 (m, 3H), 7.27–7.33 (m, 2H).

4.1.17.66. 1-(4-(4-(1-Phenyl-1H-1,2,3-triazol-4-yl)benzoyl)piperidin-1-yl)ethanone (77). 79% yield from **70** and **74**. ^1H NMR (CDCl_3) δ (ppm): 1.73–2.00 (bm, 4H), 2.14 (s, 3H), 2.81–2.96 (bm, 1H), 3.17–3.32 (bm, 1H), 3.54 (tt, 1H, $J = 10.6, 4.0$ Hz), 3.86–4.00 (bm, 1H), 4.51–4.67 (bm, 1H), 7.49 (tt, 1H, $J = 7.5, 1.2$ Hz), 7.54–7.61 (m, 2H), 7.78–7.83 (m, 2H), 8.05 (s, 4H), 8.30 (s, 1H).

4.1.17.67. 1-(4-(4-(1-Benzyl-1H-1,2,3-triazol-4-yl)benzoyl)piperidin-1-yl)ethanone (78). 66% yield from **70** and **75**. ^1H NMR (CDCl_3) δ (ppm): 1.63–1.72 (bm, 1H), 1.77–1.96 (bm, 3H), 2.11 (s, 3H), 2.80–2.90 (m, 1H), 3.18–3.29 (m, 1H), 3.50 (tt, 1H, $J = 10.7, 4.1$ Hz), 3.86–3.96 (m, 1H), 4.52–4.62 (m, 1H), 5.60 (s, 2H), 7.31–7.35 (m, 2H), 7.37–7.44 (m, 3H), 7.75 (s, 1H), 7.92 (d, 2H, $J = 8.6$ Hz), 7.98 (d, 2H, $J = 8.6$ Hz).

4.1.17.68. 1-(4-(4-(1-(3-Phenylpropyl)-1H-1,2,3-triazol-4-yl)benzoyl)piperidin-1-yl)ethanone (79). 97% yield from **70** and **76**. ^1H NMR (CDCl_3) δ (ppm): 1.61–1.73 (bm, 1H), 1.77–1.99 (bm, 3H), 2.12 (s, 3H), 2.32 (quint, 2H, $J = 7.3$ Hz), 2.71 (t, 2H, $J = 7.4$ Hz), 2.81–2.90 (bm, 1H), 3.20–3.30 (m, 1H), 3.52 (tt, 1H, $J = 10.6, 3.9$ Hz), 3.89–3.96 (m, 1H), 4.43 (t, 2H, $J = 7.1$ Hz), 4.57–4.64 (m, 1H), 7.17–7.25 (m, 3H), 7.28–7.35 (m, 2H), 7.81 (s, 1H), 7.95 (d, 2H, $J = 8.6$ Hz), 8.01 (d, 2H, $J = 8.6$ Hz).

4.1.17.69. (4-(1-Phenyl-1H-1,2,3-triazol-4-yl)phenyl)(piperidin-4-yl)methanone (80). 82% yield from **77**. ^1H NMR ($\text{DMSO}-d_6$) δ (ppm): 1.59–1.73 (m, 2H), 1.80–1.93 (m, 2H), 2.85–2.96 (m, 2H), 3.14–3.26 (m, 2H), 3.65–3.77 (bm, 1H), 7.51–7.58 (m, 1H), 7.62–7.71 (m, 2H), 7.93–8.02 (m, 2H), 8.13 (s, 4H), 9.50 (s, 1H).

4.1.17.70. (4-(1-Benzyl-1H-1,2,3-triazol-4-yl)phenyl)(piperidin-4-yl)methanone (81). 88% yield from **78**. ^1H NMR (CDCl_3) δ (ppm): 1.70 (td, 2H, $J = 11.7, 3.6$ Hz), 1.81–1.89 (m, 2H), 2.77 (td, 2H, $J = 12.4, 2.7$ Hz), 3.19 (dt, 2H, $J = 9.6, 3.3$ Hz), 3.39 (tt, 1H, $J = 11.3, 3.6$ Hz), 5.60 (s, 2H), 7.31–7.35 (m, 2H), 7.37–7.44 (m, 3H), 7.42 (s, 1H), 7.90 (d, 2H, $J = 8.4$ Hz), 7.98 (d, 2H, $J = 8.5$ Hz).

4.1.17.71. (4-(1-(3-Phenylpropyl)-1H-1,2,3-triazol-4-yl)phenyl)(piperidin-4-yl)methanone (82). 69% yield from **79**. ^1H NMR (CDCl_3) δ (ppm): 1.63–1.76 (m, 2H), 1.82–1.91 (m, 2H), 2.32 (quint, 2H, $J = 7.3$ Hz), 2.71 (t, 2H, $J = 7.4$ Hz), 2.79 (td, 2H, $J = 12.4, 2.4$ Hz), 3.16–3.24 (m, 2H), 3.42 (tt, 1H, $J = 11.0, 3.6$ Hz), 4.42 (t, 2H, $J = 7.1$ Hz), 7.17–7.25 (m, 3H), 7.28–7.34 (m, 2H), 7.80 (s, 1H), 7.93 (d, 2H, $J = 8.6$ Hz), 8.01 (d, 2H, $J = 8.6$ Hz).

4.1.17.72. (1-(3-Methoxybenzoyl)piperidin-4-yl)(4-(1-phenyl-1H-1,2,3-triazol-4-yl)phenyl)methanone (83). 98% yield from **80** and 3-methoxybenzoic acid. ^1H NMR (CDCl_3) δ (ppm): 1.78–2.13 (m, 4H), 3.03–3.24 (bm, 2H), 3.54–3.64 (bm, 1H), 3.81–3.98 (bm, 1H), 3.83 (s, 3H), 4.63–4.80 (bm, 1H), 6.93–7.01 (m, 3H), 7.28–7.35 (m, 1H), 7.46–7.52 (m, 1H), 7.54–7.61 (m, 2H), 7.81 (d, 2H, $J = 8.0$ Hz), 8.05 (s, 4H), 8.30 (s, 1H).

4.1.17.73. (4-(4-(1-Benzyl-1H-1,2,3-triazol-4-yl)benzoyl)piperidin-1-yl)(3-methoxyphenyl)methanone (**84**). 87% yield from **81** and 3-methoxybenzoic acid. ^1H NMR (CDCl_3) δ (ppm): 1.73–2.10 (bm, 4H), 3.00–3.24 (bm, 2H), 3.50–3.60 (bm, 1H), 3.82 (s, 3H), 3.84–3.99 (bm, 1H), 4.57–4.79 (bm, 1H), 5.60 (s, 2H), 6.92–6.99 (m, 3H), 7.28–7.35 (m, 3H), 7.37–7.44 (m, 3H), 7.76 (s, 1H), 7.92 (d, 2H, $J = 8.6$ Hz), 7.98 (d, 2H, $J = 8.6$ Hz).

4.1.17.74. (1-(3-Methoxybenzoyl)piperidin-4-yl)(4-(1-(3-phenylpropyl)-1H-1,2,3-triazol-4-yl)phenyl)methanone (**85**). 99% yield from **82** and 3-methoxybenzoic acid. ^1H NMR (CDCl_3) δ (ppm): 1.76–1.89 (bm, 3H), 1.92–2.10 (bm, 1H), 2.33 (quint, 2H, $J = 7.3$ Hz), 2.71 (t, 2H, $J = 7.5$ Hz), 3.00–3.23 (bm, 2H), 3.52–3.62 (bm, 1H), 3.83 (s, 3H), 3.84–3.95 (bm, 1H), 4.43 (t, 2H, $J = 7.1$ Hz), 4.62–4.80 (bm, 1H), 6.93–7.00 (m, 3H), 7.17–7.25 (m, 3H), 7.28–7.34 (m, 3H), 7.81 (s, 1H), 7.95 (d, 2H, $J = 8.6$ Hz), 8.02 (d, 2H, $J = 8.6$ Hz).

4.2. Docking calculations

The X-ray structure of MAGL (PDB code 3PE6) [48] was downloaded from the Protein Data Bank [49]. Hydrogen atoms were added to the ligand-protein complex, which was then minimized using Amber16 software [50] and ff14SB force field at 300 K. The complex was placed at the center of a rectangular parallelepiped box and solvated with a 20 Å water cap, generated using TIP3P explicit solvent model. Sodium ions were then added to neutralize the system, which was then energy minimized using a two-step protocol. In the first step, only the minimization of the solvent was performed, since a position restraint of 500 kcal/mol·Å² was applied on all solute atoms. In the second step, 5000 cycles of steepest descent followed by conjugate gradient (CG) were used to minimize the whole system, until a convergence of 0.05 kcal/Å·mol. The ligand was built with Maestro [51] and then subjected to energy minimization performed with MacroModel [52] until a convergence value of 0.05 kcal/Å·mol, by employing the CG algorithm, MMFFs force field and a distance-dependent dielectric constant of 1.0. Docking calculations were performed using AUTODOCK 4.0 software [53]. Autodock Tools was used to automatically identify the torsion angles in the ligand, add the solvent model and determine ligand and protein atomic charges. Gasteiger and Kollmann charges were assigned for ligand and protein, respectively. A grid box of 82, 40, and 30 points in the x, y, and z directions centered on the bound inhibitor ZYH was used as the docking site, in which the energetic maps were calculated using a grid spacing of 0.375 Å and a distance-dependent function of the dielectric constant. The ligand was docked performing 200 runs of Autodock search with the Lamarckian Genetic Algorithm, following a robust protocol [54,55]. For each docking run, 10 000 000 steps of energy evaluations were performed, the number of individuals in the initial population was set to 500 and a maximum of 10 000 000 generations were simulated. An RMS cut-off 2.0 Å was used for pose clustering.

4.3. MD simulations

Molecular dynamics (MD) simulations were performed using AMBER, version 16 [50], using the ff14SB force field. General Amber force field (GAFF) parameters were used for the ligand, whose partial charges were assigned using the Antechamber suite of AMBER 16, based on the AM1-BCC method. The complex was placed at the center of a rectangular parallelepiped box and solvated with a 20 Å water cap, generated using TIP3P explicit solvent model. Sodium ions were then added to neutralize the system, which was then energy minimized following the same procedure

described above. The minimized complexes were used as input structures for the MD simulations, which were run using Particle Mesh Ewald (PME) electrostatics, a cutoff of 10 Å for the non-bonded interactions and periodic boundary conditions. SHAKE algorithm was used to constrain all bonds involving hydrogen atoms and a time step of 2.0 fs was thus used for the simulation. Initially, an MD step of 0.5 ns in which the temperature of the system was raised from 0 to 300 K was performed using constant-volume periodic boundary conditions. An equilibration step of constant pressure periodic boundary MD was run for 3 ns, keeping the temperature of the system at the constant value of 300 K with Langevin thermostat. Finally, a further MD step with constant pressure conditions was run for 246.5 ns. All α carbons of the protein were subjected to a harmonic potential of 10 kcal/mol·Å² during the three MD steps, for a total of 250 ns of simulation. The final structure of **22a**-MAGL complex corresponded to the average of the last 200.0 ns of MD minimized by the CG method until a convergence of 0.05 kcal/mol·Å². The average structure was obtained using the Cpptraj program [56] implemented in AMBER 16.

4.4. SMD simulations

Steered molecular dynamics (SMD) simulations were performed using AMBER16 [50]. The final MD frame obtained from the simulation of **22a**-MAGL complex was used as the starting structure for the SMD simulations, which were thus performed at the same constant-pressure periodic boundary conditions and at the constant temperature of 300 K. However, no position restraint was applied on the protein α carbons during the simulations. Three different SMD simulations using three different initial pulling directions were performed. Each pulling direction was imposed by selecting a couple of atoms, one belonging to the protein and one belonging to the ligand, which set the initial distance to be stretched during the SMD: a) the α carbon of S48 and the C47 atom of the ligand; b) the α carbon of M123 and the C47 atom of the ligand; c) the α carbon of A126 and the C47 atom of the ligand. In all simulation, the ligand was pulled out from the protein binding site by increasing the initial distance between the selected couple of atoms by 30 Å, through the application of a spring constant of 5 kcal/mol·Å². Each SMD simulation was performed at the constant velocity of 0.1 Å/ns by setting the simulation length to 300 ns; this allowed us to consider the simulated ligand unbinding process as reversible, and the pulling work associated to the process as the exact free energy [29,30].

4.5. Binding energy evaluations

The total and per-frame ligand-protein binding affinity of the **22a**-MAGL complex were calculated with AMBER 16 using the MM-GBSA method. The trajectories corresponding to the last 200 ns of the classic MD simulation and the full trajectory of the SMD simulation (300 ns) were used for the evaluation, which was thus performed on a total of 200 and 300 MD frames (1 per ns), respectively. MOLSURF program and the MM-PBSA module of AMBER 16 were used to calculate nonpolar and polar energies, respectively, while van der Waals, electrostatic and internal contributions were estimated with SANDER module [57,58]. The ligand's entropy was not taken into account in the calculation.

4.6. MAGL inhibition assay

Human recombinant MAGL, **2** and 4-nitrophenylacetate (4-NPA) substrate were purchased from Cayman Chemical. The IC₅₀ values were generated in 96-well microtiter plates. The MAGL reaction was carried out at room temperature, at a final volume of 200 µL in

10 mM Tris buffer, pH 7.2, containing 1 mM EDTA and BSA 0.1 mg/mL. A total of 150 μ L of 4-NPA 133.3 μ M was added to 10 μ L of DMSO containing the suitable amount of compound. The reaction was initiated by the addition of 40 μ L of MAGL (11 ng/well) in such a way that the assay was linear over 30 min. After the reaction had proceeded for 30 min, absorbance values were then measured by using a Victor X3 Microplates Reader (PerkinElmer®) at 405 nm.⁵³ Two reactions were also run: one reaction containing no compounds and the second one containing neither compound nor MAGL. IC₅₀ values were derived from experimental data using the Sigmoidal dose–response fitting of GraphPad Prism software. Final values were obtained from duplicates of three independent experiments. To remove possible false-positive results, for each compound concentration a blank analysis was carried out, and the final absorbance results were obtained subtracting the absorbance produced by the presence of all the components except MAGL in the same conditions. In the enzyme kinetics experiments, compounds **21a,b**, **22a,b** were tested in the presence of scalar concentrations of 4-NPA. They were added in scalar amounts (concentration range = 1–0.125 μ M for compounds **21a,b**, **22b** and 0.5–0.0625 μ M for **22a**) to a reaction mixture containing scalar concentrations of 4-NPA (15–1400 μ M). Finally, MAGL solution was added (11 ng/well). The MAGL activity was measured by recording the increase in 4-nitrophenol absorbance using the Victor X3 Microplates Reader (PerkinElmer®). The experimental data were analyzed by non-linear regression analysis with GraphPad Prism software, using a second order polynomial regression analysis, and by applying the mixed-model inhibition fit.

4.7. MAGL preincubation assay

The MAGL reaction was conducted in the same conditions reported above. A total of 150 μ L of MAGL (11 ng/well) was added to 10 μ L of DMSO containing the appropriate amount of compound. After 0 min, 30 min, and 60 min of incubation time the reaction was initiated by the addition of 40 μ L of 4-NPA 500 μ M. The enzyme activity was then measured according to the procedure described above. Final values were obtained from triplicates of two independent experiments.

4.8. MAGL dilution assay

The enzyme (880 ng in 75 μ L of Tris buffer, pH 7.2) was incubated during 60 min at room temperature with 5 μ L of compounds **21a,b**, **22a,b** (concentration of 2 μ M in the mixture) dissolved in DMSO. The MAGL-inhibitor mixture was then diluted 40-fold with the buffer. After 15 min of incubation, the reaction was initiated on a 160 μ L aliquot by the addition of 40 μ L of 4-NPA 500 μ M and the enzyme activity was measured according to the procedure described above. Final values were obtained from triplicates of two independent experiments.

4.9. Enzyme activity assays

Enzyme activity assays were performed as previously described using cell homogenates HEK-293 cells stably transfected with ABHD6 and ABHD12 (ABHD6 and ABHD12), and intact U937 cells (FAAH and MAGL) [24]. Briefly, *h*ABHD6 and *h*ABHD12 activity assays were performed using cell homogenates from *h*ABHD6 and *h*ABHD12 stably transfected HEK293 cells. Compounds at the screening concentration of 10 μ M were pre-incubated with 40 μ g of cell homogenate for 30 min at 37 °C in assay buffer (Tris 1 mM, EDTA 10 mM plus fatty acid-free 0.1% BSA, pH 7.6). WWL70 10 μ M or THL 20 μ M were used as positive controls, while DMSO as vehicle control. Then, 10 μ M of 2-OG was added and incubated for 5 min at

37 °C. The reaction was stopped by the addition of 400 μ L of ice-cold CHCl₃:MeOH (1:1) and samples were vortexed and centrifuged (16 000 \times g, 10 min, 4 °C). Aliquots (200 μ L) of the aqueous phase were assayed for tritium content by liquid scintillation spectroscopy. Blank values were recovered from tubes containing no enzyme, whereas basal 2-OG hydrolysis occurring in non-transfected HEK293 cells was subtracted. For FAAH and MAGL activity assay 1.0 \times 10⁶ of intact U937 cells were suspended in 400 μ L of assay buffer (Tris-HCl 10 mM, EDTA 1 mM plus fatty acid-free 0.1% BSA, pH 8) in plastic tubes and incubated with different concentrations of the screening compounds at 37 °C (co-incubation). Then, 10 μ M of nonradioactive (2-OG) and a small tracer (0.5 nM) of [1,2,3-³H]2-OG or 1 μ M of AEA containing 2 nM of [ethanolamine-1-³H]AEA were added and cells were incubated for 15 min at 37 °C with shaking. The reaction was stopped by the addition of 800 μ L of a methanol chloroform ice-cold mixture 1:1 (v/v) and, after vigorous vortexing, aqueous and organic phases were separated by centrifugation at 10 000 \times g, for 10 min, at 4 °C. Aliquots (400 μ L) of both the aqueous and organic phases were transferred in scintillation tubes and mixed with 3 mL of Ultima Gold scintillation liquid. The radioactivity associated with the [³H]glycerol or [³H]ethanolamine formation for the aqueous phase was measured for tritium content by liquid scintillation spectroscopy. Compounds were tested in three independent experiments, each performed in triplicates.

4.10. CB1 and CB2 binding assay

Binding assay to cannabinoid receptor 1 and 2 (CB1 and CB2) were performed as previously described.⁶ Briefly, clean membranes expressing *h*CB1 or *h*CB2 were resuspended in binding buffer (50 mM Tris-HCl, 2.5 mM EDTA, 5 mM MgCl₂, 0.5% fatty acid-free bovine serum albumin (BSA), pH 7.4) and incubated with vehicle or compounds and 0.5 nM of [³H]CP55,940 for 90 min at 30 °C. Non-specific binding was determined in the presence of 10 μ M of WIN55,512. After incubation, membranes were filtered through a pre-soaked 96-well microplate bonded with GF/B filters under vacuum and washed twelve times with 150 μ L of ice-cold binding buffer. The radioactivity was measured and the results expressed as [³H]CP55,940 binding. Compounds were tested, at a screening concentration of 10 μ M, in two independent experiments, each performed in triplicates.

4.11. Competitive activity-based protein profiling (ABPP)

Activity-based protein profiling (ABPP) experiments were performed using mouse brain membrane preparations at a final concentration of 4 mg/mL in PBS. Sample preparation was performed as previously described.⁶ Samples (19.5 μ L) were preincubated with either DMSO (vehicle control), URB597 (4 μ M), JZL184 (1 μ M), WWL70 (10 μ M), THL (20 μ M), DO264 (5 μ M) or compound **21a**, **21b**, **22a**, **22b** (different concentrations) for 25 min at 25 °C under shaking and then added with TAMRA-FP probe (125 nM final concentration) and incubated for 5 min at 25 °C under shaking. URB597, JZL184, WWL70 and THL/DO264 were used as positive controls for FAAH, MAGL, ABHD6 and ABHD12 inhibition, respectively. The reaction was stopped by adding 10 μ L of 3 \times Laemmli buffer and the samples kept for 3 min at room temperature, boiled for 10 min at 90 °C, cooled down to room temperature and centrifuged at 10'000 g for 1 min. The samples were loaded on an 11% SDS-PAGE gel and resolved by electrophoresis at 120 V for 180 min. The gel was scanned with a Typhoon FLA 9500 using TAMRA settings at the excitation wavelength of 542 nm and emission light wavelength 568 nm. After coomassie staining and destaining, the gels were scanned in Cy5 settings.

4.12. Cell viability assay

Human breast MDA-MB-231, colorectal HCT116 and ovarian CAOV3, OVCAR3 and SKOV3 cancer cell lines (from ATCC) were maintained at 37 °C in a humidified atmosphere containing 5% CO₂ according to the supplier. Cells (5×10^2) were plated in 96-well culture plates. The day after seeding, vehicle or compounds were added at different concentrations to the medium. Compounds were added to the cell culture at a concentration ranging from 200 to 0.02 μ M. Cell viability was measured after 96 h according to the supplier (CellTiter-Glo® luminescence assay, Promega G7571) with a Tecan M1000 PRO instrument. IC₅₀ values were calculated from logistical dose-response curves and performed in triplicates. Error bars are standard deviations.

4.13. Human cancer organoids

Patient-derived organoids (PDO) were obtained from totally anonymized surgical specimens. However, biobank informed consent for research purposes was available to collect the samples. Tissues were processed and cultured using the protocol described by Stappenbeck [59]. Summarizing, a piece of tissue was dissected and incubated with 2 mg/mL of collagenase for 30'. After the enzymatic digestion, the tissue was transferred into a clean 15 mL tube with 10 mL of washing medium and centrifugated at 0.5×g. Supernatant was discarded, the pellet was resuspended in 10 μ L of Cultrex® BME (Trevigen, MD, US) and plated in a 24 mw. After solidification of the matrix, 500 μ L of medium derived from Hill et al. [39], was added to each well. Cell viability was done utilizing the CellTiter-Glo® luminescence assay as previously described.

4.14. PDAC cells viability assay

The newly synthesized benzoylpiperidines **21a,b** and **22a,b** were dissolved in DMSO. RPMI medium was from Gibco (Gaithersburg, MD, USA), sterile filtered Newborn Calf Serum (NBCS) was from Biowest, Pen – Strep (10.000 U Penicillin/mL, 10.000 Streptomycin/mL) was from Lonza (Verviers, Belgium). All other chemicals were from Sigma (Zwijndrecht, theNetherlands). The HPDE immortalized pancreatic ductal cell line was kindly supplied by Dr. Tsao, Ontario, Canada) and cultured in supplemented KGM medium (Lonza). PDAC-3 cells were isolated from a patient at Pisa University Hospital as described previously [47]. The cells were cultured in RPMI-1640 (Roswell Park Memorial Institute 1640) supplemented with 10% sterile filtered NBCS and 1% penicillin/streptomycin. The cells were kept in a humidified atmosphere of 5% CO₂ and 95% air at 37 °C and harvested with Trypsin–EDTA solution (Sigma, Zwijndrecht, theNetherlands). The *in vitro* anti-proliferative activity of the compounds **21a,b** and **22a,b** was evaluated on PDAC-3 cells using a properly optimized Sulforhodamine-B (SRB) protocol, as previously described [60]. Cells were seeded into flat bottomed 96-well plates (VWR, Dublin, Ireland) in triplicate in a volume of 100 μ L (3×10^3 cells/well for SUIT-2-28 and 5×10^3 cells/well for PDAC-3 cells) and incubated for 24 h at 37 °C to create a confluent monolayer. Then, the cells were treated with 100 μ L of the compounds **21a,b** and **22a,b** dissolved in DMSO at different concentration ranging from 156.25 to 20 000 nM. After 72 h of treatment, the cells were fixed with 25 μ L of 50% cold trichloroacetic acid and kept for at least 60 min at 4 °C. Later, the plates were washed gently with deionized water, dried at RT overnight and stained with 50 μ L of 0.4% SRB solution in 1% acetic acid for 15 min at RT. The excess of SRB stain was removed on dried tissues and the plates were washed with a 1% acetic acid solution and dried at RT overnight. The SRB staining was dissolved in 150 μ L of tris(hydroxymethyl)aminomethane solution pH = 8.8

(TRIS buffer), and the optical density (OD) was measured at wavelengths of 490 nm and 540 nm. Cell growth inhibition was calculated as the percentage of drug treated cells versus vehicle-treated cells (“control”) OD (corrected for OD before drug addition, “day-0”). The SRB assays were carried out in triplicate and repeated at least three times. The data were evaluated using GraphPad Prism 8.2.1 (Intuitive Software for Science, San Diego, CA, USA).

4.15. RNA-sequencing data analysis

Sample preparation of primary PDAC cells and normal cells HPDE was performed as described previously [60] and sequenced using 100 bp SE with Illumina Platform. Raw data were pre-processed for quality filtering and adapter trimming using FASTX Toolkit (version 0.7) and subsequently mapped to the Human genome (GRCh38) using STAR alignment tool (version 2.5.3a) [61]. We obtained ~90% of reads mapped to the Human Genome per sample. Gene counts were normalized to FPKM through CuffLinks algorithm [62] and plots were generated in R Studio with R version 3.5.0.

Declaration of competing interest

The authors declare that they have no known competing financial interests or personal relationships that could have appeared to influence the work reported in this paper.

Acknowledgments

We are grateful to the University of Pisa (Progetti di Ricerca di Ateneo, prog. PRA-2018-18), MIUR (PRIN 2017, project 2017SA5837) and the Italian Ministry of Health – Ricerca Finalizzata 2016 - NET-2016-02363765 for funding.

Appendix A. Supplementary data

Supplementary data to this article can be found online at <https://doi.org/10.1016/j.ejmech.2020.112857>.

References

- [1] R.G. Pertwee, A.C. Howlett, M.E. Abood, S.P.H. Alexander, V. Di Marzo, M.R. Elphick, P.J. Greasley, H.S. Hansen, G. Kunos, K. Mackie, R. Mechoulam, R.A. Ross, International union of basic and clinical pharmacology. LXXIX. Cannabinoid receptors and their ligands: beyond CB 1 and CB 2, *Pharmacol. Rev.* 62 (2010) 588–631, <https://doi.org/10.1124/pr.110.003004>.
- [2] A. Chicca, J. Marazzi, S. Nicolussi, J. Gertsch, Evidence for bidirectional endocannabinoid transport across cell membranes, *J. Biol. Chem.* 287 (2012) 34660–34682, <https://doi.org/10.1074/jbc.M112.373241>.
- [3] A. Chicca, S. Nicolussi, R. Bartholomäus, M. Blunder, A. Aparisi Rey, V. Petrucci, I. del C. Reynoso-Moreno, J.M. Viveros-Paredes, M. Dalghi Gens, B. Lutz, H.B. Schiöth, M. Soeberdt, C. Abels, R.-P. Charles, K.-H. Altmann, J. Gertsch, Chemical probes to potently and selectively inhibit endocannabinoid cellular reuptake, *Proc. Natl. Acad. Sci. Unit. States Am.* 114 (2017) E5006–E5015, <https://doi.org/10.1073/pnas.1704065114>.
- [4] A. Chicca, C. Arena, C. Manera, Beyond the direct activation of cannabinoid receptors: new strategies to modulate the endocannabinoid system in CNS-related diseases, *Recent Pat. CNS Drug Discov.* 10 (2016) 122–141, <https://doi.org/10.2174/1574889810999160603185126>.
- [5] P. Pacher, S. Bátkai, G. Kunos, The endocannabinoid system as an emerging target of pharmacotherapy, *Pharmacol. Rev.* 58 (2006) 389–462, <https://doi.org/10.1124/pr.58.3.2>.
- [6] H. Deng, W. Li, Monoacylglycerol lipase inhibitors: modulators for lipid metabolism in cancer malignancy, neurological and metabolic disorders, *Acta Pharm. Sin. B.* 10 (2020) 582–602, <https://doi.org/10.1016/j.apsb.2019.10.006>.
- [7] M. De Leo, L. Peruzzi, C. Granchi, T. Tuccinardi, F. Minutolo, N. De Tommasi, A. Braca, Constituents of *polygala flavescens* ssp. *flavescens* and their activity as inhibitors of human lactate dehydrogenase, *J. Nat. Prod.* 80 (2017) 2077–2087, <https://doi.org/10.1021/acs.jnatprod.7b00295>.
- [8] J.Z. Long, W. Li, L. Booker, J.J. Burston, S.G. Kinsey, J.E. Schlosburg, F.J. Pavón, A.M. Serrano, D.E. Selley, L.H. Parsons, A.H. Lichtman, B.F. Cravatt, Selective

- blockade of 2-arachidonoylglycerol hydrolysis produces cannabinoid behavioral effects, *Nat. Chem. Biol.* 5 (2009) 37–44, <https://doi.org/10.1038/nchembio.129>.
- [9] G.G. Muccioli, G. Labar, D.M. Lambert, CAY10499, a novel monoglyceride lipase inhibitor evidenced by an expeditious MGL assay, *Chembiochem* 9 (2008) 2704–2710, <https://doi.org/10.1002/cbic.200800428>.
 - [10] J.S. Cisar, O.D. Weber, J.R. Clapper, J.L. Blankman, C.L. Henry, G.M. Simon, J.P. Alexander, T.K. Jones, R.A.B. Ezekowitz, G.P. O'Neill, C.A. Grice, Identification of ABX-1431, a selective inhibitor of monoacylglycerol lipase and clinical candidate for treatment of neurological disorders, *J. Med. Chem.* 61 (2018) 9062–9084, <https://doi.org/10.1021/acs.jmedchem.8b00951>.
 - [11] J.E. Schlosburg, J.L. Blankman, J.Z. Long, D.K. Nomura, B. Pan, S.G. Kinsey, P.T. Nguyen, D. Ramesh, L. Booker, J.J. Burston, E.A. Thomas, D.E. Selley, L.J. Sim-Selley, Q.S. Liu, A.H. Lichtman, B.F. Cravatt, Chronic monoacylglycerol lipase blockade causes functional antagonism of the endocannabinoid system, *Nat. Neurosci.* 13 (2010) 1113–1119, <https://doi.org/10.1038/nn.2616>.
 - [12] P.K. Chanda, Y. Gao, L. Mark, J. Btsh, B.W. Strassle, P. Lu, M.J. Piesla, M.-Y. Zhang, B. Bingham, A. Uveges, D. Kowal, D. Garbe, E.V. Kouranova, R.H. Ring, B. Bates, M.N. Pangalos, J.D. Kennedy, G.T. Whiteside, T.A. Samad, Monoacylglycerol lipase activity is a critical modulator of the tone and integrity of the endocannabinoid system, *Mol. Pharmacol.* 78 (2010) 996–1003, <https://doi.org/10.1124/mol.110.068304>.
 - [13] U. Taschler, F.P.W. Radner, C. Heier, R. Schreiber, M. Schweiger, G. Schoiswohl, K. Preiss-Landl, D. Jaeger, B. Reiter, H.C. Koefeler, J. Wojciechowski, C. Theussl, J.M. Penninger, A. Lass, G. Haemmerle, R. Zechner, R. Zimmermann, Monoacylglycerol lipase deficiency in mice impairs lipolysis and attenuates diet-induced insulin resistance, *J. Biol. Chem.* 286 (2011) 17467–17477, <https://doi.org/10.1074/jbc.M110.215434>.
 - [14] S. Ghosh, L.E. Wise, Y. Chen, R. Gujjar, A. Mahadevan, B.F. Cravatt, A.H. Lichtman, The monoacylglycerol lipase inhibitor JZL184 suppresses inflammatory pain in the mouse carrageenan model, *Life Sci.* 92 (2013) 498–505, <https://doi.org/10.1016/j.lfs.2012.06.020>.
 - [15] J.E. Schlosburg, S.G. Kinsey, B. Ignatowska-Jankowska, D. Ramesh, R.A. Abdullah, Q. Tao, L. Booker, J.Z. Long, D.E. Selley, B.F. Cravatt, A.H. Lichtman, Prolonged monoacylglycerol lipase blockade causes equivalent cannabinoid receptor type 1 receptor-mediated adaptations in fatty acid amide hydrolase wild-type and knockout mice, *J. Pharmacol. Exp. Therapeut.* 350 (2014) 196–204, <https://doi.org/10.1124/jpet.114.212753>.
 - [16] A.R. King, E.Y. Dotsey, A. Lodola, K.M. Jung, A. Ghomian, Y. Qiu, J. Fu, M. Mor, D. Piomelli, Discovery of potent and reversible monoacylglycerol lipase inhibitors, *Chem. Biol.* 16 (2009) 1045–1052, <https://doi.org/10.1016/j.chembiol.2009.09.012>.
 - [17] A. Chicca, J. Marazzi, J. Gertsch, The antinociceptive triterpene β -amyrin inhibits 2-arachidonoylglycerol (2-AG) hydrolysis without directly targeting cannabinoid receptors, *Br. J. Pharmacol.* 167 (2012) 1596–1608, <https://doi.org/10.1111/j.1476-5381.2012.02059.x>.
 - [18] L. Wang, G. Wang, D. Yang, X. Guo, Y. Xu, B. Feng, J. Kang, Euphorbia arrests breast cancer cells at the G1 phase through the modulation of cyclin D1, p21 and p27 expression, *Mol. Med. Rep.* 8 (2013) 1279–1285, <https://doi.org/10.3892/mmr.2013.1650>.
 - [19] G. Hernández-Torres, M. Cipriano, E. Hedén, E. Björklund, A. Canales, D. Zian, A. Feliú, M. Mecha, C. Guaza, C.J. Fowler, S. Ortega-Gutiérrez, M.L. López-Rodríguez, A reversible and selective inhibitor of monoacylglycerol lipase ameliorates multiple sclerosis, *Angew. Chem. Int. Ed.* 53 (2014) 13765–13770, <https://doi.org/10.1002/anie.201407807>.
 - [20] M. Aghazadeh Tabrizi, P.G. Baraldi, S. Baraldi, E. Ruggiero, L. De Stefano, F. Rizzolio, L. Di Cesare Mannelli, C. Ghelardini, A. Chicca, M. Lapillo, J. Gertsch, C. Manera, M. Macchia, A. Martinelli, C. Granchi, F. Minutolo, T. Tuccinardi, Discovery of 1,5-diphenylpyrazole-3-carboxamide derivatives as potent, reversible, and selective monoacylglycerol lipase (MAGL) inhibitors, *J. Med. Chem.* 61 (2018) 1340–1354, <https://doi.org/10.1021/acs.jmedchem.7b01845>.
 - [21] G. Bononi, C. Granchi, M. Lapillo, M. Giannotti, D. Nieri, S. Fortunato, M. El Boustani, I. Caligiuri, G. Poli, K.E. Carlson, S.H. Kim, M. Macchia, A. Martinelli, F. Rizzolio, A. Chicca, J.A. Katzenellenbogen, F. Minutolo, T. Tuccinardi, Discovery of long-chain salicylketoxime derivatives as monoacylglycerol lipase (MAGL) inhibitors, *Eur. J. Med. Chem.* 157 (2018) 817–836, <https://doi.org/10.1016/j.ejmech.2018.08.038>.
 - [22] J. Aida, M. Fushimi, T. Kusumoto, H. Sugiyama, N. Arimura, S. Ikeda, M. Sasaki, S. Sogabe, K. Aoyama, T. Koike, Design, synthesis, and evaluation of piperazinyl pyrrolidin-2-ones as a novel series of reversible monoacylglycerol lipase inhibitors, *J. Med. Chem.* 61 (2018) 9205–9217, <https://doi.org/10.1021/acs.jmedchem.8b00824>.
 - [23] C. Granchi, F. Rizzolio, S. Palazzolo, S. Carmignani, M. Macchia, G. Saccomanni, C. Manera, A. Martinelli, F. Minutolo, T. Tuccinardi, Structural optimization of 4-chlorobenzoylpiperidine derivatives for the development of potent, reversible, and selective monoacylglycerol lipase (MAGL) inhibitors, *J. Med. Chem.* 59 (2016) 10299–10314, <https://doi.org/10.1021/acs.jmedchem.6b01459>.
 - [24] C. Granchi, M. Lapillo, S. Glasmacher, G. Bononi, C. Licari, G. Poli, M. El Boustani, I. Caligiuri, F. Rizzolio, J. Gertsch, M. Macchia, F. Minutolo, T. Tuccinardi, A. Chicca, Optimization of a benzoylpiperidine class identifies a highly potent and selective reversible monoacylglycerol lipase (MAGL) inhibitor, *J. Med. Chem.* 62 (2019) 1932–1958, <https://doi.org/10.1021/acs.jmedchem.8b01483>.
 - [25] T. Tuccinardi, C. Granchi, F. Rizzolio, I. Caligiuri, V. Battistello, G. Toffoli, F. Minutolo, M. Macchia, A. Martinelli, Identification and characterization of a new reversible MAGL inhibitor, *Bioorg. Med. Chem.* 22 (2014) 3285–3291, <https://doi.org/10.1016/j.bmc.2014.04.057>.
 - [26] C. Granchi, S. Roy, C. Del Fiandra, T. Tuccinardi, M. Lanza, L. Betti, G. Giannaccini, A. Lucacchini, A. Martinelli, M. Macchia, F. Minutolo, Triazole-substituted N-hydroxyindol-2-carboxylates as inhibitors of isoform 5 of human lactate dehydrogenase (hLDH5), *Medchemcomm* 2 (2011) 638–643, <https://doi.org/10.1039/c1md00071c>.
 - [27] F. Musumeci, S. Schenone, A. Desogus, E. Nieddu, D. Deodato, L. Botta, Click chemistry, A potent tool in medicinal sciences, *Curr. Med. Chem.* 22 (2015) 2022–2050, <https://doi.org/10.2174/0929867322666150421110819>.
 - [28] E.D. Goddard-Borger, R.V. Stick, An efficient, inexpensive, and shelf-stable diazotransfer reagent: imidazole-1-sulfonyl azide hydrochloride, *Org. Lett.* 9 (2007) 3797–3800, <https://doi.org/10.1021/ol701581g>.
 - [29] S. Park, F. Khalili-Araghi, E. Tajkhorshid, K. Schulten, Free energy calculation from steered molecular dynamics simulations using Jarzynski's equality, *J. Chem. Phys.* 119 (2003) 3559–3566, <https://doi.org/10.1063/1.1590311>.
 - [30] F. Célerse, L. Lagardère, E. Derat, J.P. Piquemal, Massively parallel implementation of steered molecular dynamics in tinker-HP: comparisons of polarizable and non-polarizable simulations of realistic systems, *J. Chem. Theor. Comput.* 15 (2019) 3694–3709, <https://doi.org/10.1021/acs.jctc.9b00199>.
 - [31] M.J. Niphakis, B.F. Cravatt, Enzyme inhibitor discovery by activity-based protein profiling, *Annu. Rev. Biochem.* 83 (2014) 341–377, <https://doi.org/10.1146/annurev-biochem-060713-035708>.
 - [32] J.L. Blankman, B.F. Cravatt, Chemical probes of endocannabinoid metabolism, *Pharmacol. Rev.* 65 (2013) 849–871, <https://doi.org/10.1124/pr.112.006387>.
 - [33] M.P. Baggelaar, F.J. Janssen, A.C.M. van Esbroeck, H. den Dulk, M. Allarà, S. Hoogendoorn, R. McGuire, B.I. Florea, N. Meeuwenoord, H. van den Elst, G.A. van der Marel, J. Brouwer, V. Di Marzo, H.S. Overkleef, M. van der Stelt, Development of an activity-based probe and in silico design reveal highly selective inhibitors for diacylglycerol lipase- α in brain, *Angew. Chem. Int. Ed.* 52 (2013) 12081–12085, <https://doi.org/10.1002/anie.201306295>.
 - [34] D.K. Nomura, J.Z. Long, S. Niessen, H.S. Hoover, S.W. Ng, B.F. Cravatt, Monoacylglycerol lipase regulates a fatty acid network that promotes cancer pathogenesis, *Cell* 140 (2010) 49–61, <https://doi.org/10.1016/j.cell.2009.11.027>.
 - [35] Y.Y. Wang, C. Attané, D. Milhas, B. Dirat, S. Dauvillier, A. Guerard, J. Gilhodes, I. Lazar, N. Alet, V. Laurent, S. Le Gonidec, D. Biard, C. Hervé, F. Bost, G.S. Ren, F. Bono, G. Escourrou, M. Prentki, L. Nieto, P. Valet, C. Muller, Mammary adipocytes stimulate breast cancer invasion through metabolic remodeling of tumor cells, *JCI Insight* 2 (2017), e87489, <https://doi.org/10.1172/jci.insight.87489>.
 - [36] M. Ma, J. Bai, Y. Ling, W. Chang, G. Xie, R. Li, G. Wang, K. Tao, Monoacylglycerol lipase inhibitor JZL184 regulates apoptosis and migration of colorectal cancer cells, *Mol. Med. Rep.* 13 (2016) 2850–2856, <https://doi.org/10.3892/mmr.2016.4829>.
 - [37] A.T. Byrne, D.G. Alferez, F. Amant, D. Annibali, J. Arribas, A.V. Biankin, A. Bruna, E. Budinská, C. Caldas, D.K. Chang, R.B. Clarke, H. Clevers, G. Coukos, V. Dangles-Marie, S.G. Eckhardt, E. Gonzalez-Suarez, E. Hermans, M. Hidalgo, M.A. Jarzabek, S. de Jong, J. Jonkers, K. Kemper, L. Lanfranccone, G.M. Mølandsmo, E. Marangoni, J.-C. Marine, E. Medico, J.H. Norum, H.G. Palmer, D.S. Peeper, P.G. Pelicci, A. Piris-Gimenez, S. Roman-Roman, O.M. Rueda, J. Seoane, V. Serra, L. Soucek, D. Vanhecke, A. Villanueva, E. Vinolo, A. Bertotti, L. Trusolino, Interrogating open issues in cancer precision medicine with patient-derived xenografts, *Nat. Rev. Canc.* 17 (2017) 254–268, <https://doi.org/10.1038/nrc.2016.140>.
 - [38] H. Fan, U. Demirci, P. Chen, Emerging organoid models: leaping forward in cancer research, *J. Hematol. Oncol.* 12 (2019) 142, <https://doi.org/10.1186/s13045-019-0832-4>.
 - [39] S.J. Hill, B. Decker, E.A. Roberts, N.S. Horowitz, M.G. Muto, M.J. Worley, C.M. Feltmate, M.R. Nucci, E.M. Swisher, H. Nguyen, C. Yang, R. Morizane, B.S. Kochupurakkal, K.T. Do, P.A. Konstantinopoulos, J.F. Liu, J.V. Bonventre, U.A. Matulonis, G.I. Shapiro, R.S. Berkowitz, C.P. Crum, A.D. D'Andrea, Prediction of DNA repair inhibitor response in short-term patient-derived ovarian cancer organoids, *Canc. Discov.* 8 (2018) 1404–1421, <https://doi.org/10.1158/2159-8290.CD-18-0474>.
 - [40] O. Kopper, C.J. de Witte, K. Löhmussaar, J.E. Valle-Inclán, N. Hani, L. Kester, A.V. Balgobind, J. Korving, N. Proost, H. Begthel, L.M. van Wijk, S.A. Revilla, R. Theeuwens, M. van de Ven, M.J. van Roosmalen, B. Ponsioen, V.W.H. Ho, B.G. Neel, T. Bosse, K.N. Gaarenstroom, H. Vrieling, M.P.G. Vreeswijk, P.J. van Diest, P.O. Witteveen, T. Jonges, J.L. Bos, A. van Oudenaarden, R.P. Zweemer, H.J.G. Snijper, W.P. Kloosterman, H. Clevers, An organoid platform for ovarian cancer captures intra- and interpatient heterogeneity, *Nat. Med.* 25 (2019) 838–849, <https://doi.org/10.1038/s41591-019-0422-6>.
 - [41] S. Palazzolo, M. Hadla, C. Russo Spena, I. Caligiuri, R. Rotondo, M. Adeel, V. Kumar, G. Corona, V. Canzonieri, G. Toffoli, F. Rizzolio, An effective multi-stage liposomal DNA origami nanosystem for in vivo cancer therapy, *Cancers* 11 (2019) 1997, <https://doi.org/10.3390/cancers11121997>.
 - [42] F. Visentin, T. Scattolin, E. Bortolamiol, I. Caligiuri, T. Perin, V. Canzonieri, S. Pluda, A. Angelini, N. Demitri, F. Rizzolio, A. Togni, S. Palazzolo, Palladium(II)- η^3 -allyl complexes bearing N-trifluoromethyl N-heterocyclic carbenes: a new generation of anticancer agents which restrain the growth of high grade serous ovarian cancer tumors, *Chem. Eur J.* (2020), <https://doi.org/10.1002/chem.202002199>.
 - [43] F. Bray, J. Ferlay, I. Soerjomataram, R.L. Siegel, L.A. Torre, A. Jemal, Global

- cancer statistics 2018: GLOBOCAN estimates of incidence and mortality worldwide for 36 cancers in 185 countries, *CA, Cancer J. Clin.* 68 (2018) 394–424, <https://doi.org/10.3322/caac.21492>.
- [44] R.L. Siegel, K.D. Miller, A. Jemal, Cancer statistics, 2020, *CA, Cancer J. Clin.* 70 (2020) 7–30, <https://doi.org/10.3322/caac.21590>.
- [45] E. Giovannetti, C.L. van der Borden, A.E. Frampton, A. Ali, O. Firuzi, G.J. Peters, Never let it go: stopping key mechanisms underlying metastasis to fight pancreatic cancer, *Semin. Canc. Biol.* 44 (2017) 43–59, <https://doi.org/10.1016/j.semcancer.2017.04.006>.
- [46] A.J. Grossberg, L.C. Chu, C.R. Deig, E.K. Fishman, W.L. Hwang, A. Maitra, D.L. Marks, A. Mehta, N. Nabavizadeh, D.M. Simeone, C.D. Weekes, C.R. Thomas, Multidisciplinary standards of care and recent progress in pancreatic ductal adenocarcinoma, *CA, Cancer J. Clin.* (2020), <https://doi.org/10.3322/caac.21626>.
- [47] A. Avan, V. Caretti, N. Funel, E. Galvani, M. Maftouh, R.J. Honeywell, T. Lagerweij, O. Van Tellingen, D. Campani, D. Fuchs, H.M. Verheul, G.-J. Schuurhuis, U. Boggi, G.J. Peters, T. Würdinger, E. Giovannetti, Crizotinib inhibits metabolic inactivation of gemcitabine in c-Met–driven pancreatic carcinoma, *Canc. Res.* 73 (2013) 6745–6756, <https://doi.org/10.1158/0008-5472.CAN-13-0837>.
- [48] C. Schalk-Hihi, C. Schubert, R. Alexander, S. Bayoumy, J.C. Clemente, I. Deckman, R.L. Desjarlais, K.C. Dzordzorme, C.M. Flores, B. Grasberger, J.K. Kranz, F. Lewandowski, L. Liu, H. Ma, D. Maguire, M.J. Macielag, M.E. McDonnell, T.M. Haarlander, R. Miller, C. Milligan, C. Reynolds, L.C. Kuo, Crystal structure of a soluble form of human monoglyceride lipase in complex with an inhibitor at 1.35 Å resolution, *Protein Sci.* 20 (2011) 670–683, <https://doi.org/10.1002/pro.596>.
- [49] H.M. Berman, T. Battistuz, T.N. Bhat, W.F. Bluhm, P.E. Bourne, K. Burkhardt, Z. Feng, G.L. Gilliland, L. Iype, S. Jain, P. Fagan, J. Marvin, D. Padilla, V. Ravichandran, B. Schneider, N. Thanki, H. Weissig, J.D. Westbrook, C. Zardecki, The protein data bank, *Acta Crystallogr. Sect. D Biol. Crystallogr.* 58 (2002) 899–907, <https://doi.org/10.1107/S0907444902003451>.
- [50] D.A. Case, R.M. Betz, D.S. Cerutti, C.I. T.E., T.A. Darden, R.E. Duke, T.J. Giese, H. Gohlke, A.W. Goetz, N. Homeyer, S. Izadi, P. Janowski, J. Kaus, A. Kovalenko, T.S. Lee, S. LeGrand, P. Li, C. Lin, T. Luchko, R. Luo, B. Madej, D. Mermelstein, K.M. Merz, G. Monard, H. Nguyen, H.T. Nguyen, I. Omelyan, A. Onufriev, D.R. Roe, A. Roitberg, C. Sagui, C.L. Simmerling, W.M. Botello-Smith, J. Swails, R.C. Walker, J. Wang, R.M. Wolf, X. Wu, L. Xiao, P.A. Kollman, *Amber* (2016). Univ. California, San Fr. (2016).
- [51] Maestro, Schrödinger, Inc., New York (2016) version 10.6.
- [52] Macromodel, Schrödinger, Inc., New York (2009) version 9.7.
- [53] G.M. Morris, R. Huey, W. Lindstrom, M.F. Sanner, R.K. Belew, D.S. Goodsell, A.J. Olson, AutoDock4 and AutoDockTools4: automated docking with selective receptor flexibility, *J. Comput. Chem.* 30 (2009) 2785–2791, <https://doi.org/10.1002/jcc.21256>.
- [54] G. Poli, A. Gelain, F. Porta, A. Asai, A. Martinelli, T. Tuccinardi, Identification of a new STAT3 dimerization inhibitor through a pharmacophore-based virtual screening approach, *J. Enzym. Inhib. Med. Chem.* 31 (2016) 1011–1017, <https://doi.org/10.3109/14756366.2015.1079184>.
- [55] M. De Leo, C.G. Huallpa, B. Alvarado, C. Granchi, G. Poli, N. De Tommasi, A. Braca, New diterpenes from *Salvia pseudorosmarinus* and their activity as inhibitors of monoacylglycerol lipase (MAGL), *Fitoterapia* 130 (2018) 251–258, <https://doi.org/10.1016/j.fitote.2018.09.010>.
- [56] D.R. Roe, T.E. Cheatham, PTRAJ and CPPTRAJ: software for processing and analysis of molecular dynamics trajectory data, *J. Chem. Theor. Comput.* 9 (2013) 3084–3095, <https://doi.org/10.1021/ct400341p>.
- [57] G. Poli, M. Lapillo, V. Jha, N. Mouawad, I. Caligiuri, M. Macchia, F. Minutolo, F. Rizzolio, T. Tuccinardi, C. Granchi, Computationally driven discovery of phenyl(piperazin-1-yl)methanone derivatives as reversible monoacylglycerol lipase (MAGL) inhibitors, *J. Enzym. Inhib. Med. Chem.* 34 (2019) 589–596, <https://doi.org/10.1080/14756366.2019.1571271>.
- [58] G. Poli, M. Lapillo, C. Granchi, J. Caciolla, N. Mouawad, I. Caligiuri, F. Rizzolio, T. Langer, F. Minutolo, T. Tuccinardi, Binding investigation and preliminary optimisation of the 3-amino-1,2,4-triazin-5(2H)-one core for the development of new Fyn inhibitors, *J. Enzym. Inhib. Med. Chem.* 33 (2018) 956–961, <https://doi.org/10.1080/14756366.2018.1469017>.
- [59] H. Miyoshi, T.S. Stappenbeck, In vitro expansion and genetic modification of gastrointestinal stem cells in spheroid culture, *Nat. Protoc.* 8 (2013) 2471–2482, <https://doi.org/10.1038/nprot.2013.153>.
- [60] R. Sciarillo, A. Wojtuszkiewicz, I.E. Kooi, V.E. Gómez, U. Boggi, G. Jansen, G.-J. Kaspers, J. Cloos, E. Giovannetti, Using RNA-sequencing to detect novel splice variants related to drug resistance in in vitro cancer models, *JoVE* (2016) 54714, <https://doi.org/10.3791/54714>.
- [61] A. Dobin, C.A. Davis, F. Schlesinger, J. Drenkow, C. Zaleski, S. Jha, P. Batut, M. Chaisson, T.R. Gingeras, STAR: ultrafast universal RNA-seq aligner, *Bioinformatics* 29 (2013) 15–21, <https://doi.org/10.1093/bioinformatics/bts635>.
- [62] C. Trapnell, A. Roberts, L. Goff, G. Pertea, D. Kim, D.R. Kelley, H. Pimentel, S.L. Salzberg, J.L. Rinn, L. Pachter, Differential gene and transcript expression analysis of RNA-seq experiments with TopHat and Cufflinks, *Nat. Protoc.* 7 (2012) 562–578, <https://doi.org/10.1038/nprot.2012.016>.